Forschungszentrum Karlsruhe

Technik und Umwelt

Wissenschaftliche Berichte

FZKA 6291

Mineral/water interactions close to equilibrium

Workshop of the Forschungszentrum Karlsruhe held at Speyer

at 25th and 26th of March 1999

Editors:
W. Schüßler, A. Bauer

Institut für Nukleare Entsorgungstechnik

Forschungszentrum Karlsruhe GmbH, Karlsruhe
1999

Content

Preface

The second Karlsruhe Geochemical Workshop is dedicated to the improved understanding of water/solid interactions and, in particular, dissolution/precipitation reactions at the close to equilibrium conditions typical of natural systems. This topic is of widespread interest at present because these reactions are fundamental to a large number of geochemical processes at both low and high temperatures. For example, at the surface of the earth the dissolution and precipitation of carbonate minerals contribute significantly to the CO_2 content of the atmosphere, and thereby effects climate. Another fundamental topic involves long term stability of radioactive waste contained within glass in the near-subsurface because the stability is controlled by the dissolution rates of these glasses. The porosity and permeability of petroleum reservoirs is intimately linked to the precipitation of quartz cements and clay minerals, respectively, at close to equilibrium conditions. At elevated temperatures, the deposition of hydrothermal ore deposits is the result of precipitation and dissolution reactions among fluids circulating in fractures and their host rocks.

Over the past several years we have been witnesses to a dramatic increase in our understanding of processes that occur at the solid-water interface. This is, in large, partly due to the application of new and/or improved experimental techniques. Many of these techniques are detailed in this proceedings volume including: flow-through hydrothermal reactors that allow the measurement of dissolution and precipitation rates at independently controlled solution compositions, use of synchrotron radiation sources that enable in-situ identification of the species at mineral surfaces in the presence of reacting solutions, and atomic force microscopy which permits in-situ characterization of surface structures while fluid-mineral surface reactions occur.

The second Karlsruhe Geochemical Workshop strives to provide a comfortable forum for the informal and free exchange of ideas among the international geochemical community. Such discussions will lead to new insight and potentially facilitate further exciting advances in the near future. The organizing committee would like to thank all participants for their efforts towards this goal.

The organization of any workshop such as this one requires the efforts of numerous behind the scenes contributions from various people. The organizing committee would especially like to thank several of these persons including Professor Hennies and Professor Kim for continues encouragement of undertaking this workshop. Thanks are also due to Ms. Stein, Ms. Endress, and Ms. Lukas for their administrative assistance.

High-pH alteration of argillaceous rocks: An experimental and modeling study

Michael Adler,Urs K. Mäder

Water-Rock Interaction Group, Institute of Geology and Institute of Mineralogy and Petrology, University of Bern, Baltzerstrasse 1, CH-3012 Bern, Switzerland
adler@mpi.unibe.ch

Introduction

Disposal strategies for high-level radioactive waste in several countries envisage cementiceous repositories in argillaceous rock (e.g. Opalinus Clay in Switzerland). Current knowledge predicts degradation of concrete and an emanating high-pH plume that induces alteration to the geologic near-field with resultant modification of the retardation properties for subsequent migration of radionuclides compared to unaltered host rock.

Experimental data on high-pH alteration of argillaceous material are available from batch experiments at elevated temperature (75-200 °C, e.g. Chermak, 1992 and 1993) and from flow-through column experiments at 70 °C (Bateman et al., 1997), all on ground material. Experiments carried out for this study were performed on solid rock samples at low temperature and aim at bridging the gap to evidence from powdered rock samples, and are intended to be used as a test case for alternate hypotheses and techniques underpinning modeling approaches using coupled reactive transport algorithms (e.g., Steefel and Lichtner, 1994, Bateman et al., 1997).

Experimental Methods

Diffusion experiments and flow-through experiments were performed with solid rock Opalinus Clay (middle Jurassic, Mont Terri, Northern Switzerland) and K-Na-Ca-hydroxide solution with an initial pH of 13.2. The mineral composition of Opalinus Clay is approximately 25% kaolinite, 20% illite, 15% calcite, 15% quartz, 10% chlorite, 10% mixed layer illite/smectite and minor K feldspar, albite, siderite, dolomite, pyrite, with a porosity of 14%. Diffusion experiments were arranged to have one fresh rock surface exposed to the high-pH solution with all other surfaces sealed by epoxy, i.e. to confine fluid infiltration to one direction. In the flow-through experiments two parallel faces of the rock sample were unprotected, one exposed to the high-pH solution, the other open to atmosphere in order to enhance fluid transport by evaporation and capillary forces. All experiments were run at a low temperature of 30°C. Diffusion experiments were conducted under controlled N_2 atmospheric conditions and the high-pH solution in the flow-through experiments was isolated from air. Measured specific fluxes in the flow-through experiments range from 4-10 * 10^{-6} kg/s/m^2 (two pore volumes per month).

Analyses on reacted rock samples were carried out after 3, 6, 12 and 18 months for the diffusion experiments and after 7 and 12 months for the flow-through experiments. Reaction products were characterised by scanning electron microscopy (SEM) combined with energy dispersive spectrometry (EDS) and X-ray diffraction (XRD).

Results of Diffusion Experiments

Reaction products after 3 months are Ca-Al-Si gels with minor potassium that formed on the infiltration surface of the samples. After 6 months, prismatic crystals of neoformed zeolite were found on bedding planes adjacent to the infiltration surface. Quantitative EDS analyses indicate high-Si zeolites of mordenite-dachiardite composition. They are partly overgrown by Ca-Si-hydroxide phases (CSH) (Figure 1). Massive calcite precipitation was detected after 12 and 18 months mainly on bedding planes that functioned as major pathways for the high-pH solution. Zeolites and CSH are absent, whereas sheet silicates of unknown composition are presumably present as newly formed phases after 12 and 18 months.

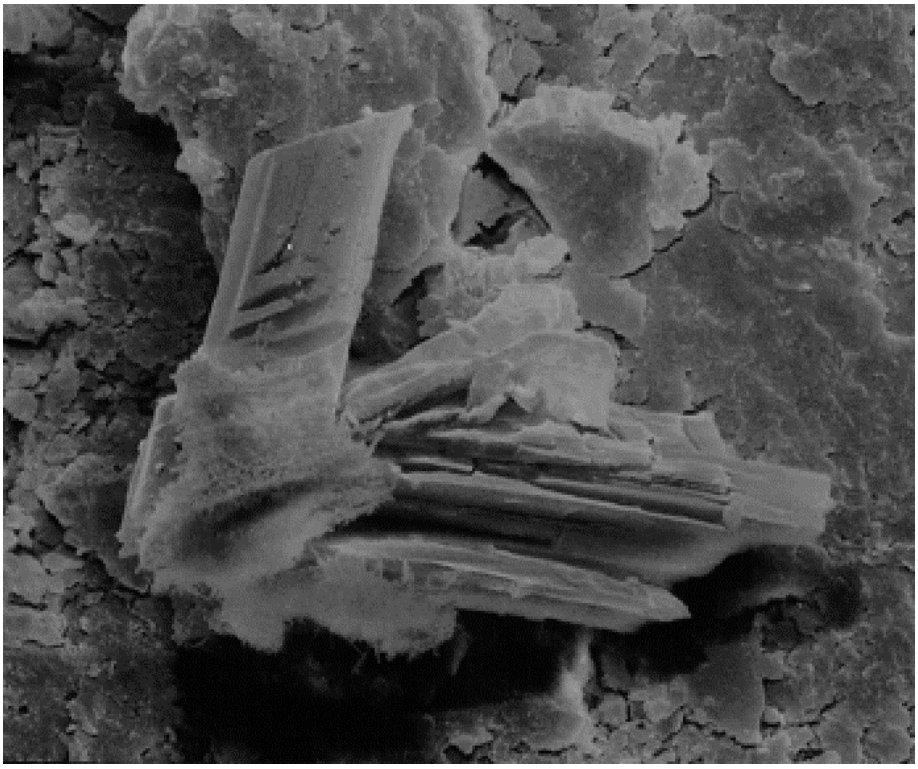

Figure 1: SEM image of a prismatic Ca zeolites and a fibrous CSH phase that formed near the surface exposed to high-pH solution (6 months). Width of image is 30 µm.

Results of Flow-through Experiments

SEM analyses on samples that were reacted with high-pH solution for 7 and 12 months show a chromatographic succession of different secondary mineral phases with increasing distance from the surface where the high-pH solution has infiltrated. A precipitation zone made up of fibrous to honeycomb textured Ca-Al-Si-hydroxide phases (CASH) extends from 0 to 1 cm above the infiltration surface, where also minor amounts of neoformed portlandite occur. At a distance of 3 to 5 cm, a zone characterised by newly formed clay minerals, gypsum and calcite developed. The new clay minerals exhibit flaky morphology with irregular grain shapes, and grain sizes do not exceed 1 µm. XRD analyses show that these clay mineral assemblages consist of illite and Fe-rich chlorite. The zone from 5 to 6 cm adjacent to the evaporation surface is characterised by massive formation of alkali sulphates of syngenite and glauberite composition. Generally, secondary precipitates grow along discrete planar features of enhanced permeability such as bedding planes, interfaces of shell debris and micro-cracks (Figure 2).

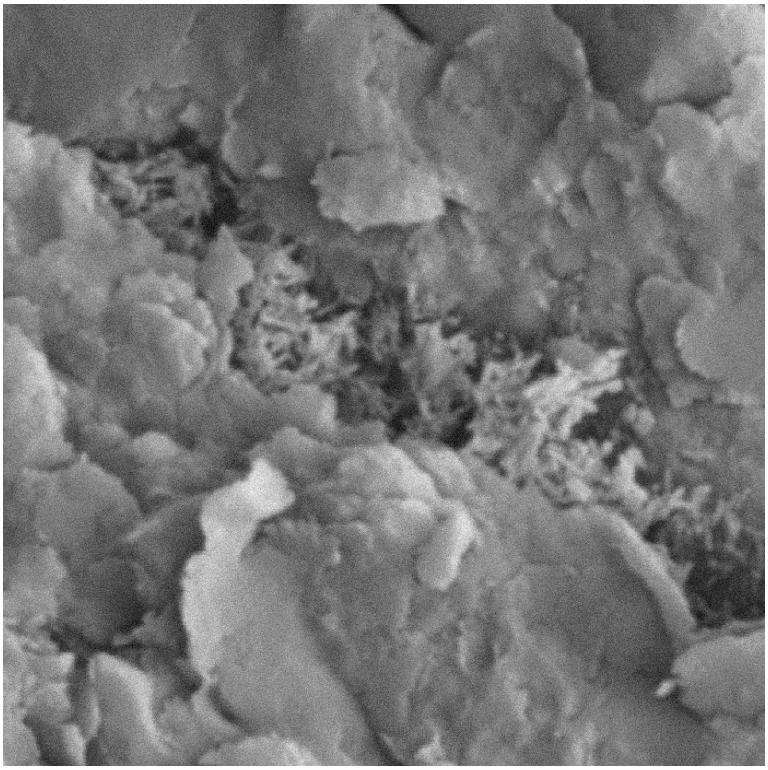

Figure 2: SEM image of a fibrous CASH phase that formed near the infiltration surface. Width of image is 25 µm.

Modeling Approach

The objective of modeling is to build confidence into the numerical description of rock-water interaction, and to evaluate the relative importance of simplifying initial and boundary conditions, as well as the relevance of alternate processes and geometries that can be simulated by different reactive transport models.

Morphological evidence of alteration products suggests that fluid/gas transport occurs preferentially along discrete planar features at the micrometer scale, but that the overall chromatographic sequence is fairly evenly developed at the centimeter-scale. It is thus possible to model portions of the system with a variety of approaches ranging from fully coupled multi-dimensional multi-phase models to relatively simple one-dimensional box models or reaction-path models, or from fracture / dual-porosity models to homogeneous porous medium models.

The diffusion experiments provide for better constrained initial and boundary conditions. The distribution of alteration products also indicates the importance of discrete planar features that form zones of enhanced diffusive transport.

Preliminary modeling results of the saturated zone with a batch model, a reactive transport model, and a 1-D finite difference model require relatively fast reaction rates for silicates at low temperatures and highly alkaline conditions compared to literature values, and suggest a significant sensitivity to the thermodynamic properties of the poorly characterized C(A)SH and zeolite phases. Further modeling work is in progress.

Discussion

The purpose of our controlled experiments under near-natural conditions and those expected to occur in a repository scenario was to demonstrate the feasibility of both laboratory and in-situ experiments. It is demonstrated that mass transfer at low temperatures is traceable after short reaction times under a variety of conditions for the infiltration of a high-pH solution.

The results of diffusion and flow-through experiments show that there are various silicate phases forming in response to the high-pH alteration of argillaceous rocks. Considerations of the experimental conditions under which new mineral phases formed as well as their spatial and temporal mode of occurrence allow to identify possible factors controlling their formation. Zeolites exclusively precipitated in the diffusion experiments. Hence, their formation at low temperatures and highly alkaline conditions is restricted to closed, diffusion dominated systems, whereas open systems produce CASH phases. In both kinds of experiments early formed zeolite and CASH phases are replaced by a clay-carbonate paragenesis. The precipitation of calcite indicates higher pCO_2 than in the zeolite/CASH stage, and the CO_2 is supposed to be progressively produced by carbonate

dissolution (dolomite, ankerite). Increasing pCO_2 during the experiments is thus supposed to control either zeolite/CASH or clay-carbonate precipitation.

The results of the experiments form a valuable test case for alternate modeling approaches as well as to address the issues of thermodynamic properties for poorly characterized phases and highly uncertain reaction rates at low temperature and highly alkaline conditions. Such experiments form a viable avenue for building confidence into predictive modeling of reactive transport.

References

Bateman, K., Coombs, P., Noy, D.J., Pearce, J.M., Wetton, P.D. 1997. 21st International Symposium on the Scientific Basis for Nuclear Waste Mangement, MRS'97, 313.

Chermak, J.A. 1992: Clays and Clay Minerals, **40**, 650.

Chermak, J.A. 1993: Clays and Clay Minerals, **41**, 365.

Steefel, C.I. and Lichtner, P.C. 1994. Geochimica et Cosmochimica Acta, **58**, 3595.

Analyses concerning the estimation of the release behaviour heaps of the former mining activities and uranium ore mining

K. Fischer-Appelt [1], J. Larue [1] , G. Henze [2] and J. Pinka [3]

[1] Gesellschaft für Anlagen und Reaktorsicherheit mbH, Schwertnergasse 1, 50667 Köln
fap@grs.de (Fischer-Appelt) and lar@grs.de (Larue), respectively

[2] Bundesamt für Strahlenschutz, Fachbereich Strahlenschutz, Köpenicker Allee 120-130, 10318 Berlin, ghenze@bfs.de

[3] G.E.O.S Freiberg Ingenieurgesellschaft mbH, Postfach 1162, 09581 Freiberg
geos_freiberg@t-online.de

In the German federal states saxony and thuringia there exist more than 3600 heaps as remains of historical and uranium ore mining which partially show increased specific activities of radionuclides of the uranium-radium decay chain. Within the scope of the project „Radiological Registration, Investigation and Evaluation of Mining Deposits“ (Altlastenkataster: BFS 1992, BFS 1997) a large number of data concerning the radioactive inventory of those heaps and their influence on surface- and groundwater were investigated. These information were compiled and stored in a database (Technical Database for Environmental Radioactivity - FbU). Because of methodical and financial reasons, questions concerning the long term release of contained natural radionuclides as a result of weathering, leaching and groundwater transport were initially left aside. In addition to the radiological assessment of heaps carried out in the frame of the Federal project, it is planned to go ahead with a pre-selection of heap locations with regard to any possible need for remedial actions due to the protection of local inhabitants from increased exposure to radiation caused by radionuclide transport via the aquatic pathway.

In order to obtain decision criteria to enable this pre-selection of heap locations *Gesellschaft für Anlagen- und Reaktorsicherheit (GRS)*- commissioned by the *Federal Office for Radiation Protection (BfS)*- is currently developing a set of instruments with which an estimation of the radionuclide release rate (source term) can be made on a simplified basis.
For this purpose, three selected heaps that are characteristic of the former mining activities and uranium ore mining in Saxony are currently subjected to a thorough investigation of their geochemical, mineralogical and radioactive inventory and their hydrochemical composition of the leachate. At the same time, the elution behaviour of the heap material is simulated in columnar laboratory experiments. This is done on the one hand to generate input data for a definition of the source term on the basis of geochemical model calculations and on the other hand to compile such data for checking the calculated radionuclide release.

At each of the three locations drillings and exploratory excavations holes were performed. The heap materials and the underlying natural soils have been analysed mineralogically and

chemically. Furthermore 50 kg of a mixed sample material has been filled in a column and than sprinkled with water under defined conditions. Conductivity, pH-value and redox potential of the circulating water were analysed permanently to obtain a trend of the ongoing hydrochemical development.

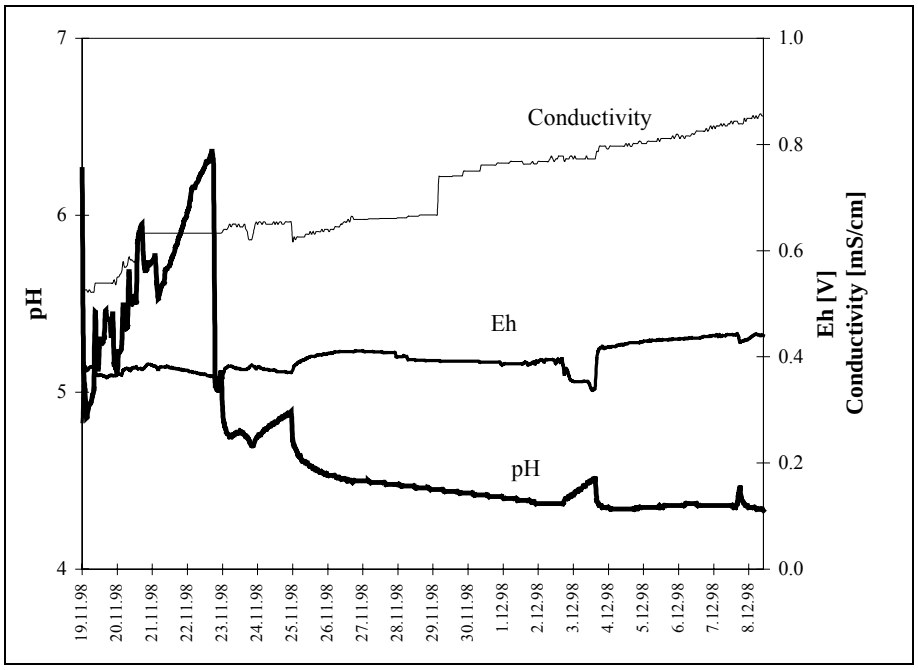

Fig 1. Time-dependent developement of the parameters Eh, pH and conductivity.

Fig. 2: View of the heap at the Haberlandmühle.

Additionally samples were collected at regular intervals and analysed concerning their hydrochemical composition. The results of the analyses program are depicted in the diagram in Fig.1 (material of the heap at the Haberlandmühle near the city Johanngeorgenstadt, Saxon Ore Mountains, Fig. 2).

It is obvious that former carbonate which was originally distributed in the heap material is consumed due to the oxidation of sulphides while reacting with acid water. After completion of this reaction a constant pH-Eh-environment established. This buffer-effect is attributed to the weathering of the mica and feldspar which are the main minerals of the rocks in the heap material, and to their interaction with the sulphate-rich acid water. In other words the adjusted buffer system is characterised by a particular pH-value of the known aluminium buffer range as well as oxidizing redox conditions. Both the seepage water taken from the foot of the heap and the water of the column show that especially the main components aluminium, calcium, potassium, sulphate and free silica are leaving the heap material.

The next step of the work is the creation of a model of the geochemical processes developing within the heaps that is as realistic as possible. The associated model calculations needed for this purpose are performed with the PHREEQC code (PARKHURST 1995).

In this context, special attention needs to be paid to geochemical subprocesses like

- oxidation and reduction processes,
- equilibrium reactions between solution and solid phase (solution/precipitation),
- sorption (ion exchange, surface complexation),
- poss. colloid-borne contaminant transport.

Here, the identification of typical processes that have a substantial influence on the radionuclide release from heaps is particularly important.

As far as it is possible to obtain a sufficiently exact understanding of the geochemical process sequences going on within the investigated heaps, in another step it has to be checked in what way it is possible to apply the geochemical source term to other and in less detail analysed heaps in the sense of a simplified estimation of the release behaviour. If possible a simplified tool will be developed for modelling the geochemical source term of similar heaps. The reliability of such prognoses has to be checked by comparing the analysis results of the three selected heaps, by statistical correlation calculations, and by the comparison of research results on heaps that were obtained by other institutions.

The results of these investigations are to contribute to a guideline of requirements for the site specific investigation of heaps from former mining activities and uranium ore mining, too.

References

BfS (1992):

Radiologische Erfasssung, Untersuchung und Bewertung bergbaulicher Altlasten, Abschlußbericht zum ersten Teilprojekt, BfS- Schriften 8/92.

BfS (1997):

Radiologische Erfassung, Untersuchung und Bewertung bergbaulicher Altlasten, Abschlußbericht zum Teilprojekt 2: Altlasten Bergbau, Verifikation (TP 2), BfS-IB-7; Berlin.

PARKHURST, D. L. (1995):

Users´ Guide to PHREEQC - A Computer Program for Speciation, Reaction-Path, Advective-Transport, and Inverse Geochemical Calculations.- U.S. Geol. Survey Water Resour. Invest. Rept., **95-4227:** 143 S.; Lakewood, Colorado.

The evolution of kaolinite and smectite in high molar KOH solutions

Andreas Bauer

Forschungszentrum Karlsruhe, Institut für Nukleare Entsorgungstechnik,
PO Box 3640, 76021 Karlsruhe, bauer@ine.fzk.de

Introduction

Cement is used in modern waste management as a technical barrier but also as a structural component. The pore fluids in hydraulic cement range in pH from 12.5 to 13.5, have high ionic strengths, and are dominated by Na and K in concentration ranging from 300-4200 ppm and from 100-7500 ppm respectively.

Experimental set up

This study was designed to check the influence of high molar KOH solutions on clays. Experiments measuring kaolinite and smectite transformation rates were carried out using batch reactors at 35° and 80°C. No potential catalysts or inhibitors were present in solution. Each reactor was charged with 1 gram of clay of the ≤ 2 µm fraction and 80, 160, 240 ml of 0.1 - 4 m KOH solution. An untreated but sized kaolinite from St. Austell and two treated industrial smectites were used in the experiments. The change in solution composition and mineralogy was monitored as a function of time.

Results

The reaction of kaolinite with KOH can be analysed in two parts one of dissolution and a second phase where the Si-Al concentration in solution is determined by the growth and redissolution of new phases. During the congruent dissolution period the aqueous concentrations of Si and Al increased linearly with log(t) whatever the temperature and the KOH concentration was. The sudden change of the silica and aluminum concentration (decreasing concentration) in solution with log(t) reflects the beginning of precipitation of a secondary phase. At this point precipitation and crystal growth control the solution concentration and the dissolution of kaolinite. As for other aluminosilicates, preliminary thermodynamic calculations showed that our measured kaolinite dissolution rates cannot be easily related to the chemical affinity of the overall reaction. The speciation calculations showed that the solutions were always largely undersaturated with respect to kaolinite. There was not a unique relation between the rate decrease and the calculated saturation index either. On the other hand, a single relation between r/r_0 and the $Al(OH)_4^-/OH^-$ activity ratio (Fig.1) seems to fit all the data, excepted the rates at lower pH (0.1 m KOH).

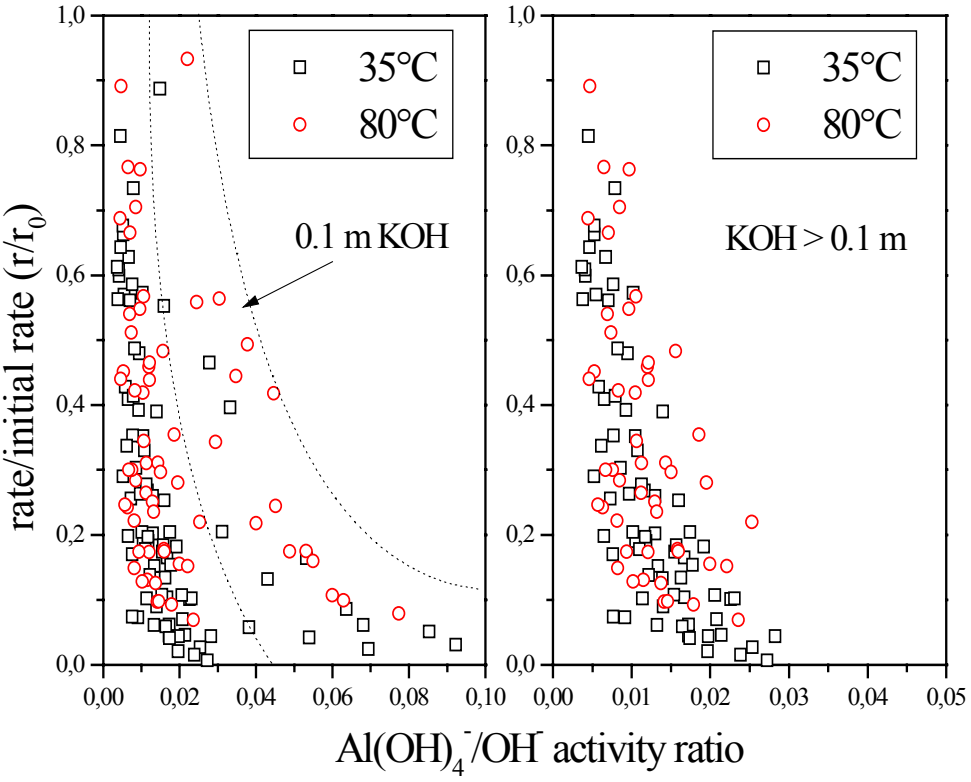

Figure 1: Dependence of the kaolinite dissolution rates and 35 and 80°C on the $Al(OH)_4^-/OH^-$ activity ratio. A single relation seems to fit all the data.

A first dissolution stage reacts smectite with KOH changing the crystal shape and hence coherent diffracting domain for XRD. In contrast to kaolinite, the concentrations of Si and Al in solution increased linearly with time. For a given temperature and KOH concentration, the calculated dissolution rates are constant with time and independent of the solid-solution ratio suggesting no chemical affinity effect. When plotting log(rate) versus log $a_{(OH^-)}$, the same proportionality of the smectite dissolution rate constant to $a_{OH^-}^{0,15\pm0,06}$ is found at 35 and 80°C. The activation energy of smectites dissolution appears independent of pH and is found to be 65 ± 4 kJ/mol at pH 12.5 or 52 ± 4 kJ/mol at a given OH^- activity (Fig. 2).

The differences in behaviour between the two different kinds of minerals is explained by structural differences. The hydrolysis of the tetrahedral and octahedral layers appear as parallel reactions for kaolinite dissolution and serial reactions for the smectite dissolution.

The limiting step is the dissolution of the octahedral layer in the case of kaolinite, and the tetrahedral layer in the case of smectite.
The change in mineralogy is somewhat similar for the tree clays. The general sequence of reaction products observed is:

kaolinite ➢ illite ➢ KI-zeolite ➢ phillipsite ➢ feldspath-K
smectite ➢ I/S ➢ illite ➢ KI-zeolite ➢ phillipsite ➢ feldspath-K + quartz

I/S, Illite**,** KI-zeolite and phillipsite are metastable phases. This evolution can also be compared with the Ostwald's rule of successive transformations (or Law of Stages).

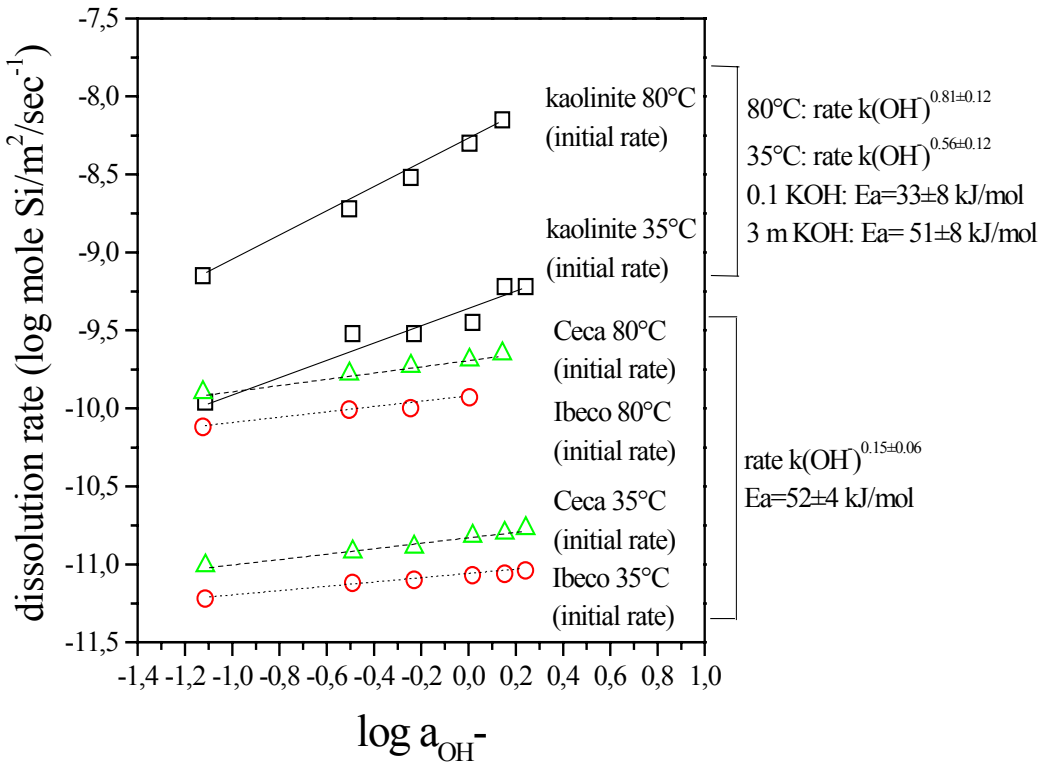

Figure 2: Initial dissolution rate (r_0) of kaolinite and smectites at 35 and 80°C versus the activity of OH^- in solution. The proportionality of r_0 to a_{OH^-} is at 35°C and $a_{OH^-}^{0.81\pm0.12}$ at 80°C The activation energy (Ea) of kaolinite dissolution increases from 33 ± 8 kJ/mol in 0.1m KOH solutions to 51 ± 8 kJ/mol in 3m KOH solutions The same proportionality of the smectite dissolution rate constant to $a_{OH^-}^{0.15\pm0.06}$ is found at 35 and 80°C. The activation energy (Ea) of smectite dissolution appears independent of pH and is found to be 52 ± 4 kJ/mol at a given OH^- activity.

Nature of surfacic reactions versus the dissolution rate of alkali-feldspars

Gilles Berger

UMR CNRS 5563-géochimie, 38 rue des 36 Ponts, F-31400 Toulouse
email: berger@lucid.ups-tlse.fr

Most of the mineral reactions in natural water-rock systems progress at conditions close to chemical equilibrium. However, the kinetics of these reactions still raises a number of fundamental questions which will be illustrated by taking the example of alkali feldspars. This abstract presents dissolution rate measurements of sanidine samples under various conditions. Most of the experiments were caaried out at neutral pH and at equilibrium with quartz.

Theoritical considerations

Recent experimental studies carried out on aluminosilicates have pointed out that more detailed information is necessary to understand the elementary reactions controlling the dissolution process. Far from equilibrium, it has been established that the bulk dissolution rate is related to the surface charge of the mineral (see Walther, 1996, and references herein). This suggests a competitive effect of Si and Al detachment, depending on the specific charge of the relevant surface sites. When the reaction approaches chemical equilibrium, the dependence of dissolution rate on the chemical affinity can be derived in terms of the Transition State Theory (TST; Lasaga, 1981 and references therein) which assumes that the dissolution rate is controlled by the desorption kinetics of an activated complex formed at the suface. However, the extrapolation of this concept from homogeneous to heterogeneous kinetics requires a clear definition of the elementary molecular reactions controlling the overall rate. In case of simple oxides, one can assume that the rupture of the metal-oxygen bond is the only reaction controlling the overall rate and that the activated complex is the same for dissolution and for precipitation. The rate-affinity relation then takes a simple form (first-order law) by balancing the forward and reverse reactions:

$$r = k_+ (1 - (Q/K) \qquad (1)$$

where r denotes the overall dissolution rate (mole/surface/time), k_+ is the rate constant for dissolution at a given temperature and pH, Q/K is the degree of saturation of the solution with respect to the dissolving phase. At a given pH and temperature, Eq.(1) expresses a linear relation between the rate/k_+ ratio and the saturation index of the solid. This simple relation has been established, for example, for quartz dissolution in pure

water. But for more complex silicates, such a simple relation does not describe accurately the dependence of dissolution rate on the chemical affinity of reaction.

For alkali feldspars, several models have been proposed to account for the observed dissolution rate/chemical affinity relationships. Oelkers et al. (1994) and Gautier et al. (1995) observed an inhibitor effect of dissolved aluminum on the dissolution rate of kaolinite and albite at 150°C in acidic or alkaline solutions. These authors assumed that the reaction rate is controlled by silica-rich aluminum-deficient precursor complexes on the mineral surface, and proposed the following rate law for alkaline feldspar dissolution:

$$r = kS\,[1/(K°+(a_{Al(OH)4^-}.a_{H^+})^{1/3})].[1-(Q/K)^{1/3}] \qquad (2)$$

where a_{H^+} and $a_{Al(OH)4^-}$ are activities of H^+ and $Al(OH)4^-$ and k and $K°$ are constants.

For sanidine and albite at 300°C and pH 9, Alekseyev et al. (1997) proposed an empirical rate law derived from Eq.(1), where p and q are constants depending on the mineral:

$$r = k\,S\,[1 - (Q/K)^p]^q \qquad (3)$$

For sanidine at near neutral pH far from equilibrium, Berger (1995) found that the dissolution rate decreases as the aqueous silica concentration increases, without any correlation to the dissolved aluminum concentration. However, when the solution approaches saturation with respect to quartz, the rate becomes dependent on the aqueous aluminum concentration. These results can be interpreted as a competition effect between several controlling reactions.

The equilibrium between a mineral and an aqueous solution ($\Delta G_{reaction}=0$) can be described by the Law of Mass Action which implies the reversibility of the reaction. Although the dissolution and the precipitation of feldspar exist, the continuity between dissolution and precipitation near equilibrium has not been experimentally demonstrated.

Sanidine dissolution far from chemical equilibrium

In a first set of experiments, sanidine samples were reacted at 100 to 300°C with NaCl-NaOH solutions at pH values ranging from 3 to 9 in a titanum mixed-flow reactor. The flow rates ranged from 1 to 9 ml/min. The dissolution rates were measured from the potassium release (Figure 1). The dissolution rate curves display a characteristic U-shape relationship with pH, with no pH dependence in the neutral region. In the acidic and basic region, the measured rates increased with the activity of H^+ and OH^-, respectivelly. The

rate constants of sanidine versus temperature and pH are close to those reported for albite under similar conditions (Hellmann, 1994). At near neutral pH, the calculated activation energy of dissolution was 63 kJ/mol, similar to that found for quartz dissolution. This suggests that a common chemical mechanism controls their dissolution at these conditions.

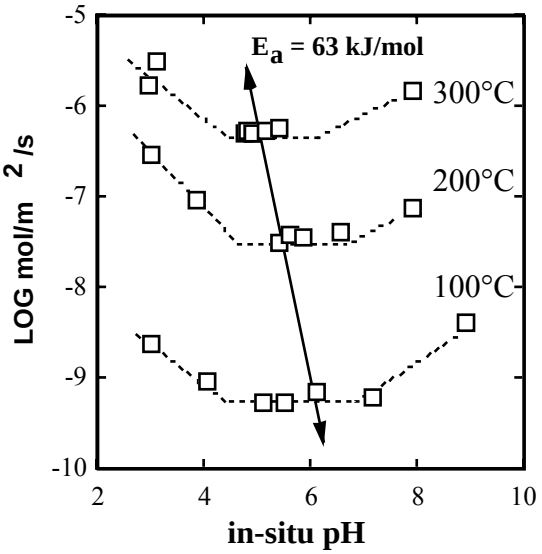

Fig.1 Sanidine dissolution rates far from equilibrium

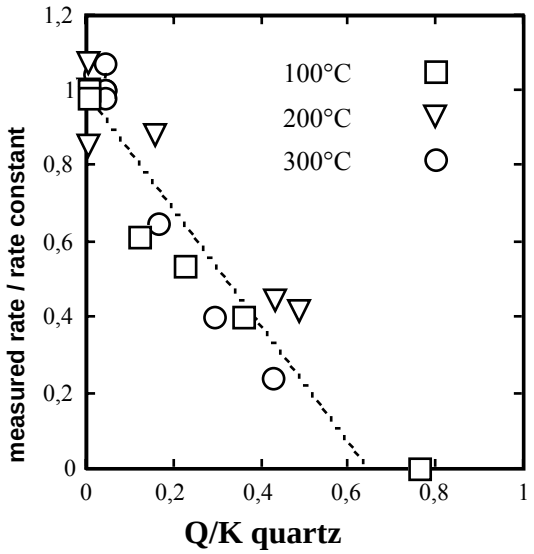

Fig.2 Effect of aqueous silica on sanidine dissolution rates far from équilibrium at near neutral pH

In a second set of experiments, the effect of aqueous silica on the dissolution rate of sanidine was measured in the pH-independent region by using solutions enriched in silica, ranging from few ppm up to the quartz saturation. At the three temperatures, the rates decreased linearly with increasing aqueous silica concentrations (Figure 2). This suggests that the hydrolysis of the Si-O bounds at the mineral surface is the rate limiting step. No correlation was found between the dissolution rates far from equilibrium and the aqueous aluminum concentrations, by contrast with the observations made by Oelkers et al. (1994) and Gautier et al. (1994) in alkaline solutions. However, an inhibition of the dissolution rates by the aqueous aluminum was evidenced when using solutions prevously equilibrated with respect to quartz.

The kinetic effect of aqueous silica or aluminum can be understood within the multi-activated-complex approach developped in Berger et al. (1994) for basaltic glass. This approach considers several independent activated complexes at the surface, each corresponding to the hydrolysis of one former oxide. The most reactive controls the overall rate. Related to sanidine, the hydrolysis of the Si-O bonds controls the bulk rate in silica-poor solutions at neutral pH. In silica-rich solutions, this reaction is inhibited and

the bulk rate is dependent on the Al-O breakdown reaction. In alkaline solutions the Al-dependence of the alkali feldspar dissolution rate far from equilibrium (Oelkers et al.; 1994) reflects an increase of the reactivity of the Al sites with pH. This dependence can also be described using a first order kinetic law, according to the TST when only one elementary reaction controls the rate. Figure 3 shows two typical examples. However, other sources of data (Gautier et al.; 1994) does exhibit such a linear relation.

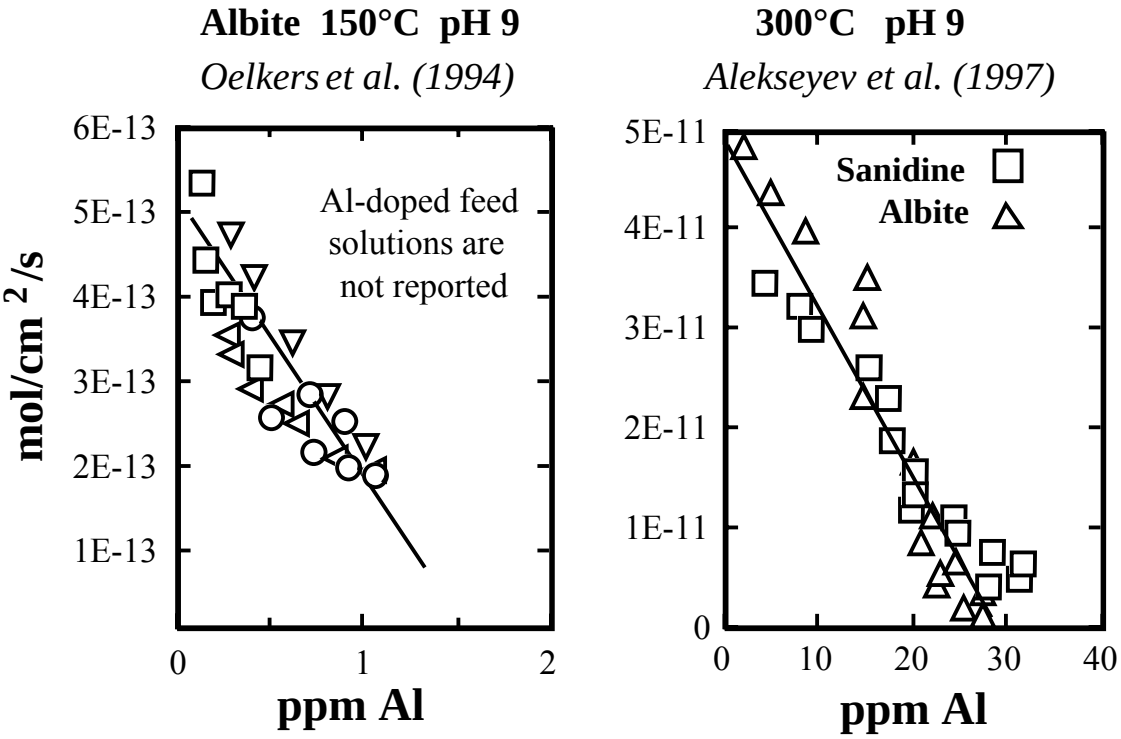

Fig. 3 Examples of feldspar dissolution rate dependence on aqueous aluminum under alkaline conditions far from equilibrium.

Reactions close to chemical equilibrium

The multi-activated complex model raises the question of the equilibrium state. It predicts that dissolution of the network will cease when all the network-former oxides are saturated, whatever the saturation state of the bulk solid (the alkali are not considered here). In order to address this problem, sanidine samples were reacted for several weeks with nearly neutral or slightly acid solutions in a closed system at 100° and 300°C. The starting solutions contained various potassium concentrations (0 to 10^{-2} m KCl) and were previously equilibrated with quartz. These conditions are chosen to prevent or minimize

the precipitation of secondary phases. We assume that, under these conditions, the dissolution of the mineral is controlled by the rupture of the Al-O bonds, because the Si-O bonds were already "saturated". Aliqots of solution were sampled during the course of the runs and analysed for Si, Al, K and pH. At the end of the experiments, the altered samples were cleaned in deionized water and observed by scanning (SEM) and transmission (TEM) electron microscopy. The samples altered at 100°C were analysed by X-ray photoelectron spectroscopy (XPS)

In all runs, the solution chemistry evolves towards a steady-state composition as shownd in Figure 4. In the experiments conducted with K-free solutions, the potassium was preferentially released from the sanidine sample. The calculated thickness of the K-leached layer is 6 nm at 100°C, and 120 to 420 nm at 300°C, depending on the starting pH.

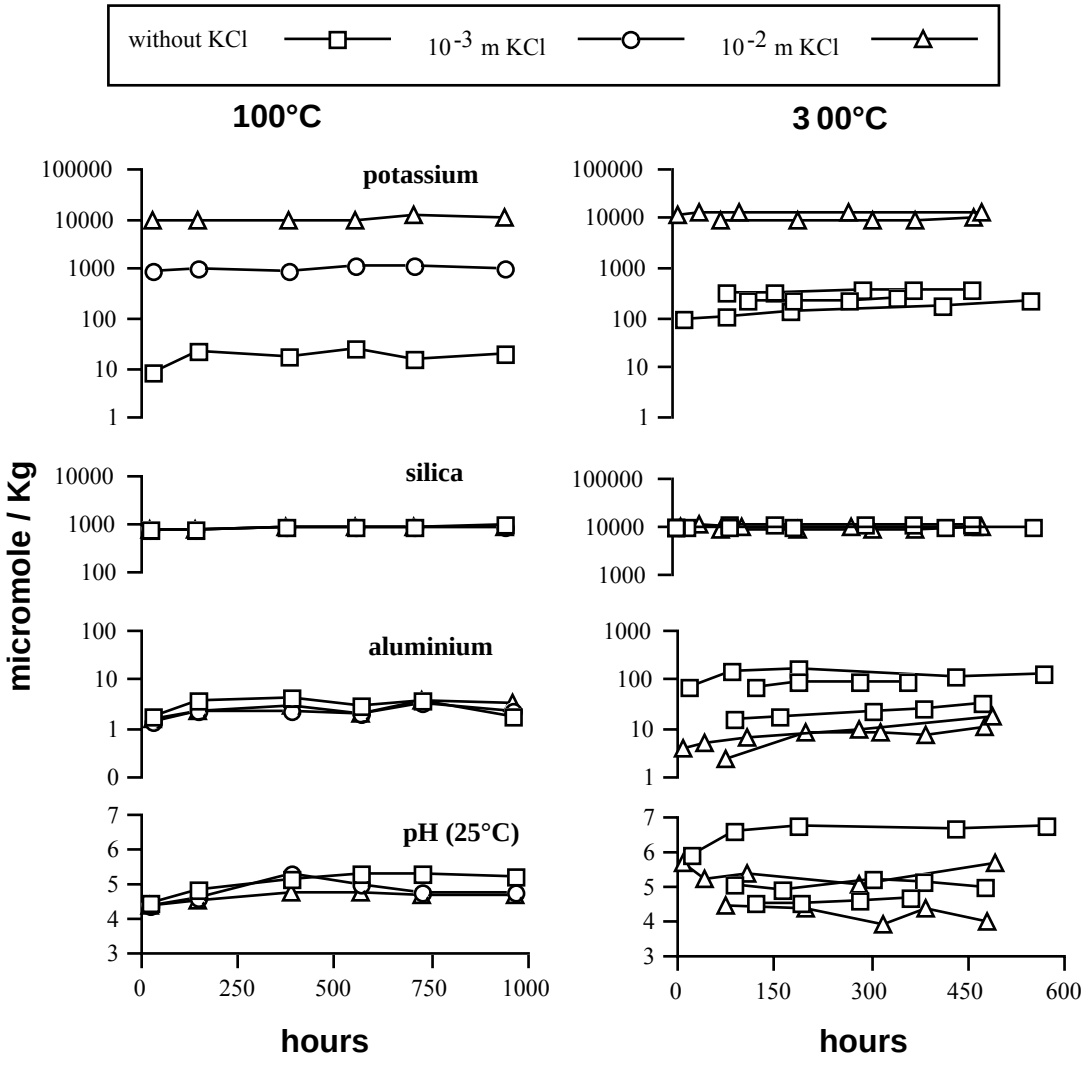

Fig. 4 Chemical composition of the solutions in all the runs conducted at 100° and 300°C.

At 100°C, when potassium is added to the starting solution, Si, Al and H^+ reach the same steady-state concentration. The saturation index for sanidine at the end of the runs, calculated with EQ3/6 and the SUCRT92 database, ranges from 0.02 to 8.89. This suggests that the solution chemistry does not reflect an equilibrium with sanidine. It remains to elucidate the nature of the phase that controls the solution composition. Examination of the altered grains surface by SEM and TEM did not reveal the presence of secondary phases nor any chemical or structural change of the mineral. On the other hand, XPS analyses confirm a K-loss from the grains altered in the K-free solution, and show an assymetry of the Al spectrum (Fig. 5). This assymetry reflects a change in the Al-binding energy which is consistent with a K^+/H^+ exchange at the surface of this sample. However, the solution data indicate that this exchanged layer does not exceed a few nanometers. The absence of a chemical equilibrium between the sanidine sample and the solution supports the assumption that the mineral ceases to dissolve when its former oxides (Si-O and Al-O) are "saturated".

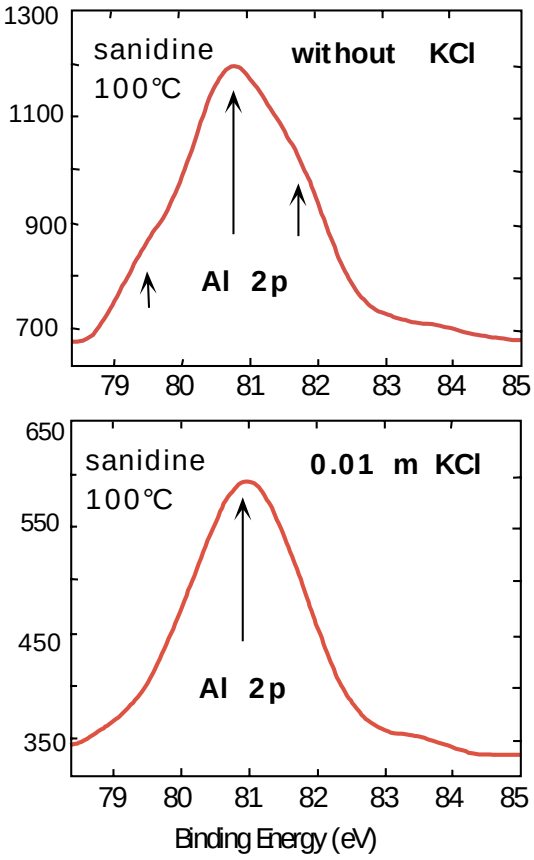

Fig.5 XPS spectra of Al at the surface of samples altered at 100°C

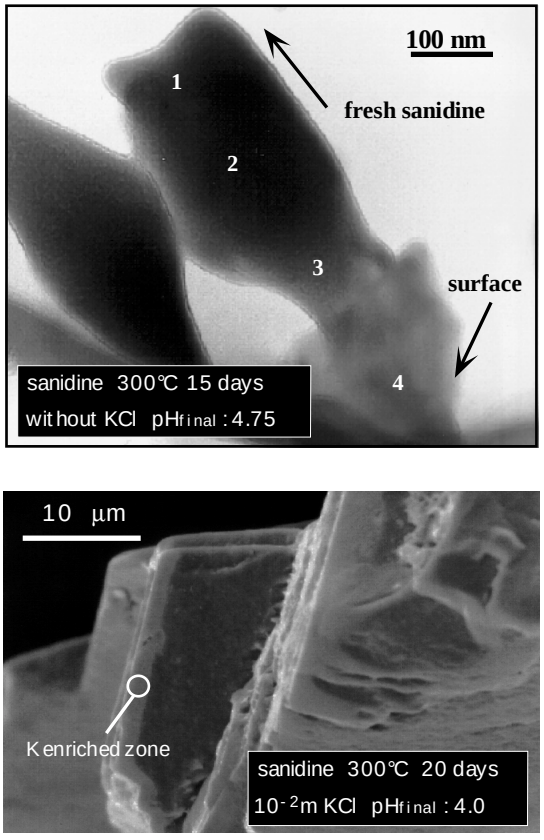

Fig.6 Sanidine reacted at 300°C. Upper = ultrathin section under STEM. Lower = morphology of the altered surface under SEM

At 300°C, the steady-state composition of the solutions are more consistent with a chemical equilibrium with respect to the sanidine than at 100°C. The saturation indexes for this mineral at the end of the 5 runs were 0.99, 3.40, 1.25, 6.32 and 1.26 respectively. On the other hand, although no secondary mineral can be identified by SEM at the surface of the altered samples, chemical analyses and diffraction data collected by TEM on ultrathin sections show the existence of a thick altered surfacic layer. For the runs conducted with K-free solutions this layer is amorphous, while microanalyses show a progressive loss in K and enrichment in Al (Fig.6a, points 1-4). The Si/Al ratio decreases from 3 in the fresh feldspar to 1 at point 4. When potassium was added in the starting solutions, a surfacic K-enrichment was detected under SEM by EDX analyses (Fig.6b).

Although the development of a deep modified surface layer at 300°C the solution data reflect a chemical equilibrium with the fresh mineral. At 100°C where the exchanged zone does not exceed few nm, the solution chemistry does not seem to be controlled by the solubility of the fresh mineral. The lack of detailed investigations on the precipitation of feldspar near equilibrium prevents any definitive conclusion to be drawn. However these results illustrate the difficulty to reach equilibrium at low temperature.

References

Alekseyev V.A., L.S.Medvedeva N.I., Prisyagina S.S., Meshalkin and Balabin I.A. (1997) Change in the dissolution rates of alkali feldspars as a result of secondary mineral precipitation and approach to equilibrium. *Geochim. Cosmochim. Acta* 61: 1125-1142.

Berger G., Claparols C., Guy C. and Daux V. (1994) Dissolution rate of a basalt glass in silica-rich solutions: implications for long-term alteration. *Geochim. Cosmochim. Acta* 58: 4875-4886.

Berger G. (1995) The dissolution rate of sanidine at near neutral pH as a function of silica activity at 100, 200, and 300°C. In Water-Rock-Interaction, Y.K Kharaka and O. Chudaev (ed.), Balkema, Rotterdam: 141-144.

Gautier J.M., Oelkers E.H. and Schott J. (1995) Experimental study of K-feldspar dissolution rates as a function of chemical affinity at 150°C and pH 9. *Geochim. Cosmochim. Acta* 58: 4549-4560.

Hellmann R. (1994) The albite-water system: Part I. The kinetics of dissolution as a function of pH at 100, 200, and 300°C.*Geochim. Cosmochim. Acta* 58: 595-611.

Lasaga A.C. (1981). Transition State Theory. In Kinetics of Geochemical Process, A.C. Lasaga and R.J. Kirkpatrick Ed., Rev. Mineral. 8, Mineral Soc. Am., Washington, D.C, 169-195.

Oelkers E.H., Schott J. and Devidal J.L. (1994) The effect of aluminum, pH, and chemical affinity on the rates of aluminosilicate dissolution reactions. *Geochim. Cosmochim. Acta* 58: 2011-2024.

Walther J. (1996) Relation between rates of alumino-silicate mineral dissolution, pH, temperature, and surface charge. *Amer. J. Sci.* 296: 693-728.

A microscopic view of crystal growth mechanisms, kinetics and inhibition

Dirk Bosbach

Institut für Mineralogie, Universität Münster, Corrensstr. 24, 48149 Münster (Germany)

In many aqueous low temperature environments (e.g. soil, construction material) the dominant crystal growth mechanisms as a function of the supersaturation are not well understood on a molecular level. Depending on the supersaturation **step growth**, **spiral growth** and **surface nucleation** can be the dominant growth mechanisms in pure systems – without impurities/additives (fig. 1) In the case of natural systems these processes become complex due to the presence of foreign ions or molecules which potentially inhibit the further attachment of growth units to the crystal. Consequently, it is often impossible to decipher the actual inhibition mechanism. Simple organic molecules, such as di-carboxylic acids (e.g. maleic acid, aspartic acid) and simple phosphonic acids, such as HEDP (1-hydroxyethylidene-1,1-diphosphonic acid), inhibit the growth of many carbonate and sulfate minerals. Depending on the nature of the functional groups of an inhibitor molecule and the conformational flexibility of these molecules, they can attach specifically to certain sites on a mineral surface and block active growth sites.

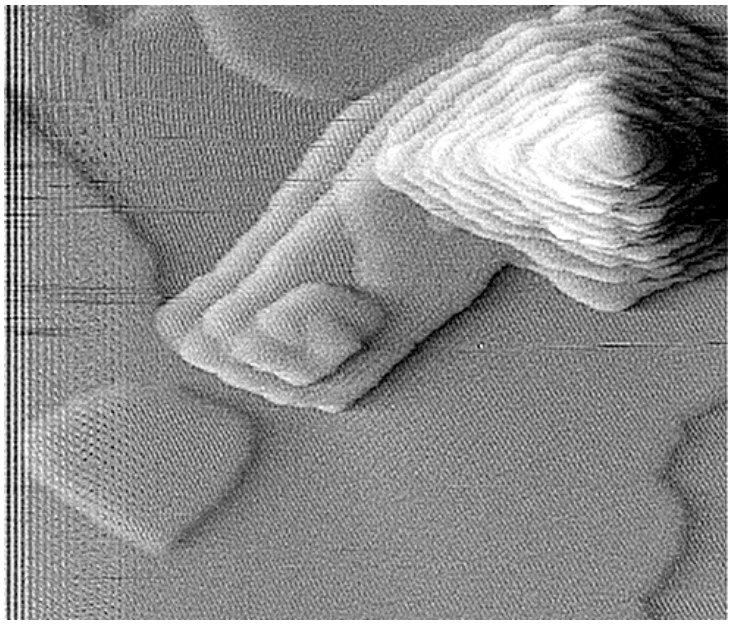

Figure 1. Step growth, spiral growth and the formation of two-dimensional nuclei on a barite (001) surface have been observed in supersaturated solution in-situ. The monolayer steps represent one $BaSO_4$ layer of the barite structure. The morphology of the islands and the growth spirals is controlled by the attachment energy of Ba^{2+} to certain sites along the step edges. (Scan size: 1.7 x 1.3 µm^2; image taken by P. Risthaus, University Münster)

Here, in-situ molecular scale observations of growth and dissolution processes on **barite**, **gypsum** and **calcite** surfaces using Atomic Force Microscopy (AFM) will be presented. Individual growth mechanims have been identified and their contribution to the macroscopic reaction rate could be estimated. Further, in-situ dissolution experiments provide an easy way to gain insight into the interaction between inhibitor molecules and reactive surface sites. Further, molecular modeling (MM) techniques have been used to quantify attachment energies to surface sites on the basis of the AFM observations.

Growth in pure systems

Before the effect of inhibitors on various growth mechanisms can be discussed, these growth mechanisms need to be characterized in a pure system. The growth of monomolecular steps could be observed in-situ on gypsum (010), calcite (104) and barite (001) and (210) surfaces. The growth kinetics of these steps indicate their reactivity and can be characterized for steps with various crystallographic orientations. Also, the step density can be estimated and the reactive surface area can be determined. At low supersaturation the only mechanism which generates new steps on an atomically flat surface is spiral growth, which is related to the occurrence of a screw dislocation on a crystal surface. Again, the number of growth spirals as well as their growth kinetics can be estimated. At higher supersaturations, surface nucleation becomes an important mechanism for the generation of monolayer steps. The formation rate on various crystallographic surfaces can be determined as a function of the supersaturation. Further, interfacial energies can be estimated for individual crystallographic surfaces.

Growth inhibitors

It can be shown from simple macroscopic batch experimens (fig. 2a) that in the presence of trace amounts of HEDP for example the growth kinetics of barite and gypsum is reduced significantly. Adsorption experiments clearly show that HEDP is attached to the mineral surface (fig. 2b) and a significant inhibition effect occurs at quite low surface coverage. This indicates that the inhibitor molecules do not attach to the entire surface but preferentially to active growth sites. However, these sites cannot be identified on the basis of simple macroscopic experiments. AFM provides an easy way to observe changes to monolayer step edge morphology due to the attachment of inhibitor molecules to certain sites (e.g. kink sites) along these steps. Again, the reactive surface area with respect to the inhibitor molecule attachment can be characterized.

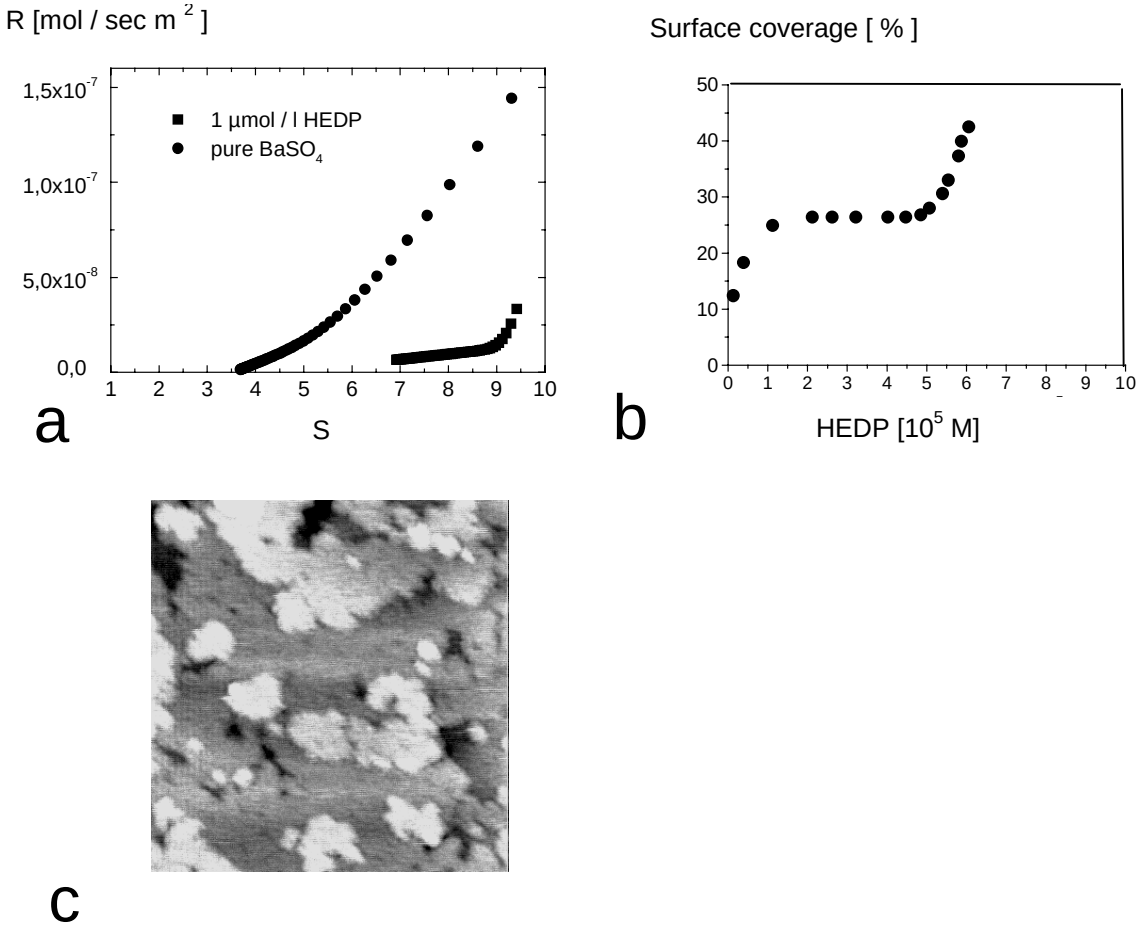

Figure 2. a) Barite growth rate as a function of the supersaturation S = (IAP / K_{sp})$^{0.5}$ in pure $BaSO_4$ solution and in the presence of 1 µM HEDP at pH 5.8. b) Surface coverage as a function of the HEDP concentration at pH 5 (van Rosmalen et al., 1986). c) Surface nucleation on barite (001) in the presence of a phosphonic acid. Island and step edge morphology of molecular steps are different compared to the growth in $BaSO_4$ solution (see. Fig. 1).

Inhibitors and dissolution

The interaction between inhibitor molecules and a mineral surface can be studied in undersaturated solution as well. Distinct changes in step edge morphology have been observed on calcite and barite surfaces in the presence of maleic acid, aspartic acid and HEDP.

For the calcite (104) surface, the replacement energy for a hydrated HEDP molecule replacing one carbonate group along a monomolecular step parallel to [48-1] and [-441] has been calculated on the basis of empirical potentials. Depending on the actual site and the orientation of the HEDP molecule the replacement energy varies between –1.5 and –7.0 eV. One preferential attachment site could be clearly identified. The MM calculations correlate with the AFM observation of the attachment of trace amounts of HEDP onto a calcite surface in pure water. Similar results have been observed for HEDP and barite surfaces – (001) and (210).

The interaction of carboxylic acids with calcite and barite surfaces is much weaker than phosphonic acids. An unambiguous effect on the morphology of monolayer steps occurs only at a concentration in the millimolar range. However, changes in etch pit morphology indicate that steps parallel to certain crystallographic directions dissolve preferentially or become stabilized due to the presence of simple di-carboxylic acids.

Macroscopic batch and adsorption experiments combined with in-situ AFM observations and MM simulation are a powerful tool for identifying reactive sites on a mineral surface and to understand the interaction between ions / molecules in solution and these sites.

Polarization dependent XANES of uranium(VI) sorbed onto smectite

M.A. Denecke [1], A. Bauer [1], J.I. Kim [1] and H. Moll [2]

[1] Forschungszentrum Karlsruhe, Institut für Nukleare Entsorgungstechnik,
PO Box 3640, 76021 Karlsruhe, melissa@ine.fzk.de

[2] Royal Institut of Technology, Department of Chemistry, Inorganic Chemistry,
Teknikringen 30, S-10044 Stockholm

The polarization dependence of the X-ray absorption near edge fine structure (XANES) and extended X-ray absorption fine structure (EXAFS) spectra for an uranium(VI) exchanged smectite clay sample is investigated. These studies are aimed at determining if linear uranyl cations ($O=U=O^{2+}$) sorbed between smectite basal plane layers are oriented in a preferred direction either parallel or perpendicular to the layers.

To this purpose, a disc of Ca^{2+} smectite (IBECO, a montmorillonite with a significant component of beidellitic charge) exchanged with 45 mg U/g clay is prepared in such a way that the basal layers lay parallel to the disc surface. The disc is cut into approximately 15×5 mm rectangular pieces and mounted in layers onto polycarbonate adhesive. In this way, oriented samples with a variable but homogeneous thickness are obtained. The polarization measurements in transition mode are performed at beamline A1 by mounting the samples onto a x,y-sample positioner, equipped with a goniometer, enabling positioning of the smectite basal planes at angles from 0° to 80° relative to the polarization vector (ε) of the incident synchrotron radiation. The Si(311) double-crystal monochromator is detuned 50% of the incident flux.

Determining the orientation of linear $O=U=O^{2+}$ units is possible because the U L3 and L1 edge spectra exhibit remarkable differences, depending on the orientation of $O=U=O^{2+}$ units relative to ε [1]. The coordination polyhedron of uranyl complexes does not vary considerably. It consists of a central, linear $O=U=O^{2+}$ unit and, at right angles to this, 4-6 anions in a near planar arrangement. The $O=U=O^{2+}$ unit is structurally a long rod, generally near 1.8 Å. When these units are oriented in a common direction, changes in white line (WL) and resonant feature intensities as well as shifts in edge energies of U L3 XANES occur, which are characteristic for the angle to ε. The polarization dependency in L1 XANES spectra is more remarkable, due to the lower final state symmetry of p character. A reversal of the most intense peak in Fourier transform L3 edge EXAFS spectra of oriented samples, depending on the angle to ε, is also observed. In the spectrum recorded for a parallel orientation of uranyl units to ε, the most intense peak corresponds to $O=U=O^{2+}$ oxygen atoms (O_{ax}); in the perpendicular spectrum, it is from the 4-6 planar anions (O_{eq}, when oxygen is the anion). By comparing spectra for samples with sorbed uranyl or other actinyl cations onto surfaces or, in this case, sorbed between basal planes

of a layered clay mineral as a function of angle between the sample surface and incident light, it is possible to determine the orientation of cations.

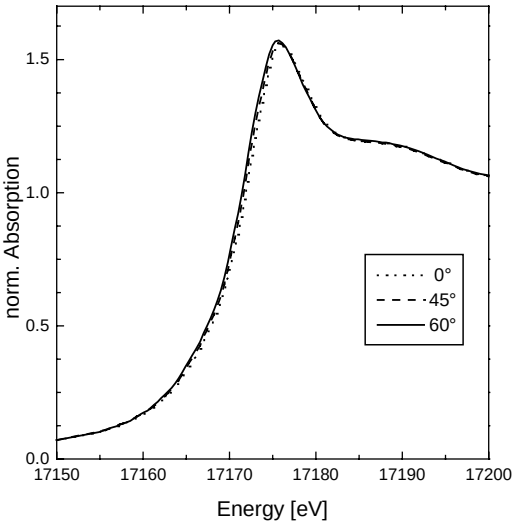

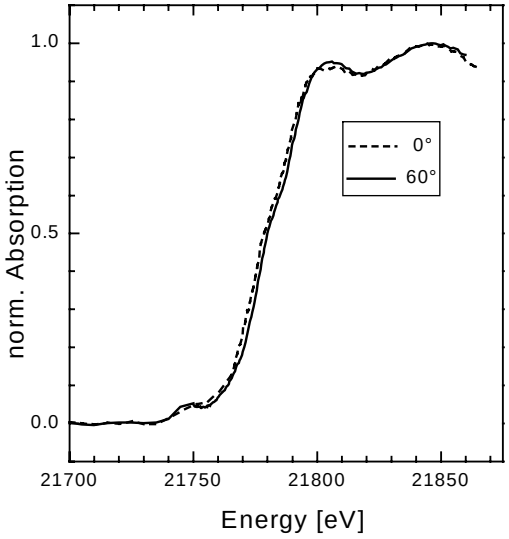

Figure 1: Top left: U L3 XANES spectra for a uranyl exchanged smectite recorded at angles between the clay basal planes and polarization vector indicated. **Top right**: U L1 XANES of the same sample at two different angles. **Bottom:** L3 edge k^3-weighted EXAFS oscillations recorded at 0° and 45°.

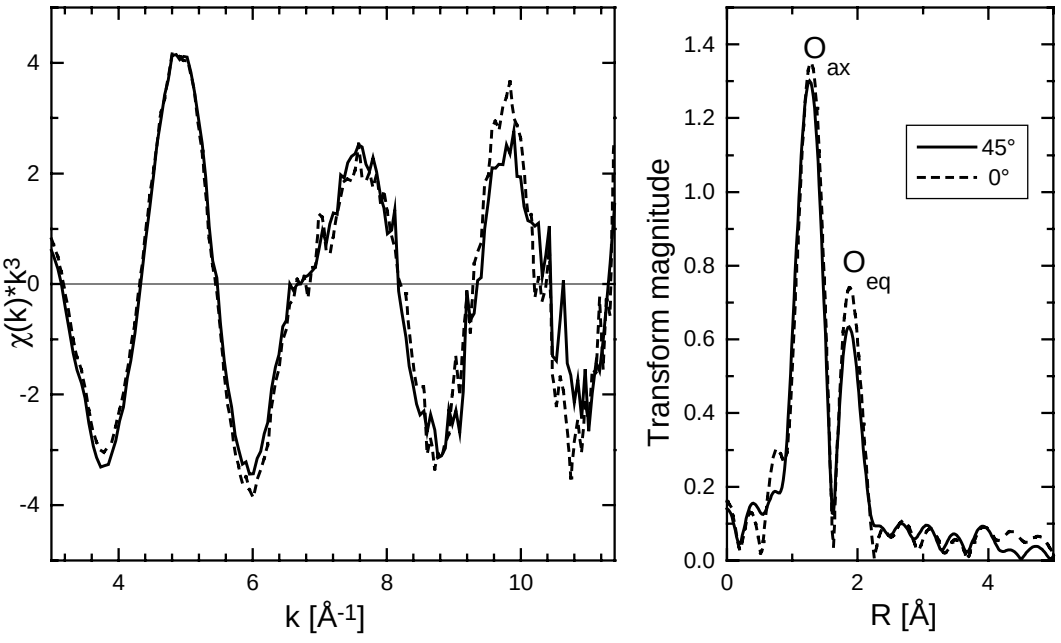

The U L3 edge EXAFS and both L3 and L1 edge XANES spectra measured at the angles indicated are shown in fig. 1. The L3 edge XANES showed no substantial change with the angle of orientation. An extremely small increase in WL intensity and energy shift with increasing angle are observed, which correspond to a general trend of increasing perpendicular orientation of uranyl units to ε with increasing angle. The L1 edge XANES spectra resemble those for polycrystalline (non-oriented) samples: features are intermediate between those observed for oriented spectra. The spectra exhibit a shoulder on the rising edge and a feature about 20 eV above this. The shoulder corresponds to a sharp peak observed for oriented samples with $O=U=O^{2+}$parallel to ε and the second feature is dominant for an orientation perpendicular to ε. This second feature has a slightly greater intensity in the L1 spectrum measured at 60°. The intensity of the FT O_{eq} peak is slightly larger for the spectrum recorded at 45° than that recorded at 0°, indicating that at 45° the 4-5 planar anions are more aligned to ε than they are at 0°. However, there is no corresponding decrease in the O_{ax} peak.

The lack of any significant polarization dependency in the L3 and L1 XANES indicates that sorbed uranyl units are neither perpendicular nor parallel to the basal planes. Rather, their $O=U=O^{2+}$ molecular axis is tilted at an angle relative to the basal plane. The slight changes in the spectra, that generally coincide with changes observed for perpendicular orientation of uranyl units can be also be understood as indicative of this. Over a macroscopic sample volume, uranyl units are oriented at an angle to the plane, but in all directions. The average structure of the uranium coordination polyhedron "seen" by the polarization vector

can be visualized by procession about the axis normal to basal planes with simultaneous rotation about the $O=U=O^{2+}$ molecular axis. The averaged structure of the linear $O=U=O^{2+}$ unit takes on the form of a double cone and the averaged structure of equidistant equatorial atoms takes on the form of a band centered around the node of this double cone. At 0°, 45°, and 60°, the tilted $O=U=O^{2+}$ units are never aligned with ε, and no spectral changes expected for an alignment of the linear units with ε are observed. In contrast, at increasing angles, components of the band representing the averaged O_{eq} structure become aligned with ε, leading to changes in L3 and L1 XANES and to the increasing intensity of the O_{eq} FT peak.

References

[1] E. A. Hudson, P. G. Allen, L. J. Terminello, M. A. Denecke, T. Reich, Phys. Rev. B **54** (1996) 156-65.

The interaction of monosilicic and polysilicic acid with solid surfaces

M. Dietzel

Geochemisches Institut der Universität Göttingen, Goldschmidtstr. 1,
D-37077 Göttingen, mdietze@gwdg.de

The interaction between dissolved silica and solids plays a major role in natural environments. Silicium-bearing compounds are liberated from solids upon dissolution and may be transported to different geochemical environments, where they may be deposited as new solid phases or adsorbed onto mineral surfaces. The adsorption depends on the chemical composition of the solution and the mineral surface and also on the nature of the dissolved silica. In acid and neutral solutions monosilicic acid prevails, whereas in alkaline solutions polysilicic acid is abundant. However polymers may be transferred into acid environment and may be generated also directly upon the dissolution of silicates at acid conditions (Dietzel, 1998). The interaction of polymer and monomer with solid is significantly different. Both cases were studied experimentally taking the adsorption of silica by gibbsite as an example.

Experiments were carried out at a temperature of 20°C and various pH values. The dissolved silica was measured via the ß-silico-molybdato-method (e.g. Iler, 1979; Dietzel and Usdowski, 1995). The results show that the silica concentration of the solution decreases continuously via a pseudo first order reaction, if monomer is adsorbed at the gibbsite surface (Fig.1).

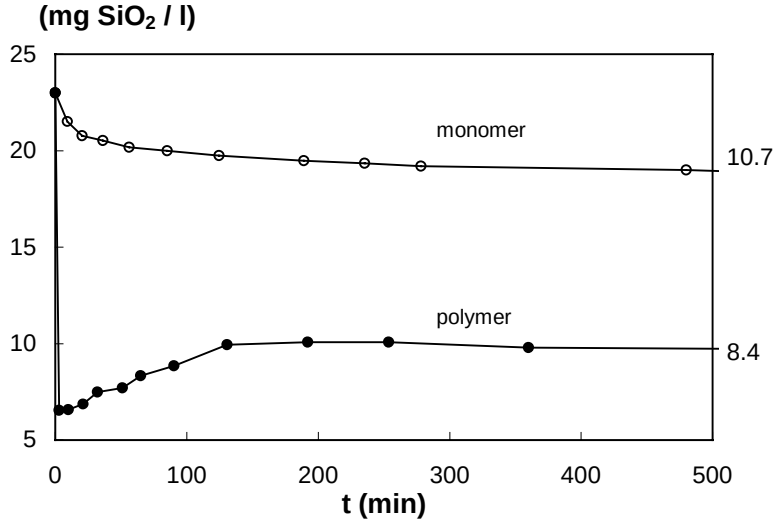

Fig.1 Concentration of total dissolved silica as a function of reaction time. Adsorption experiments with polysilicic and monosilicic acid onto 45 m^2 gibbsite surface / l solution at a pH of 6.2. The values at the right hand side of the diagram denotes the silica concentrations at adsorption equilibrium

At equilibrium the adsorption of monosilicic acid increases up to the pH-value of the first dissociation constant of $Si(OH)_4$ ($pK_S = 9.8$). This behaviour may be described by surface complex formation according the reaction

$$\equiv AlOH° + Si(OH)_4 = \equiv AlOSiO(OH)_2^- + H_2O + H^+ \quad , K_S^{int} \quad (1)$$

where ≡AlOH° denotes the surface hydroxyl group. The value of the intrinsic constant $pK_S^{int} = 3{,}20$ is obtained from the experimental data via the diffuse layer surface complexation model (e.g. Stumm, 1992). Figure 2 shows the resulting concentrations of dissolved silica, of the silica containing surface complex, and of the dissociates of the surface hydroxyl group.

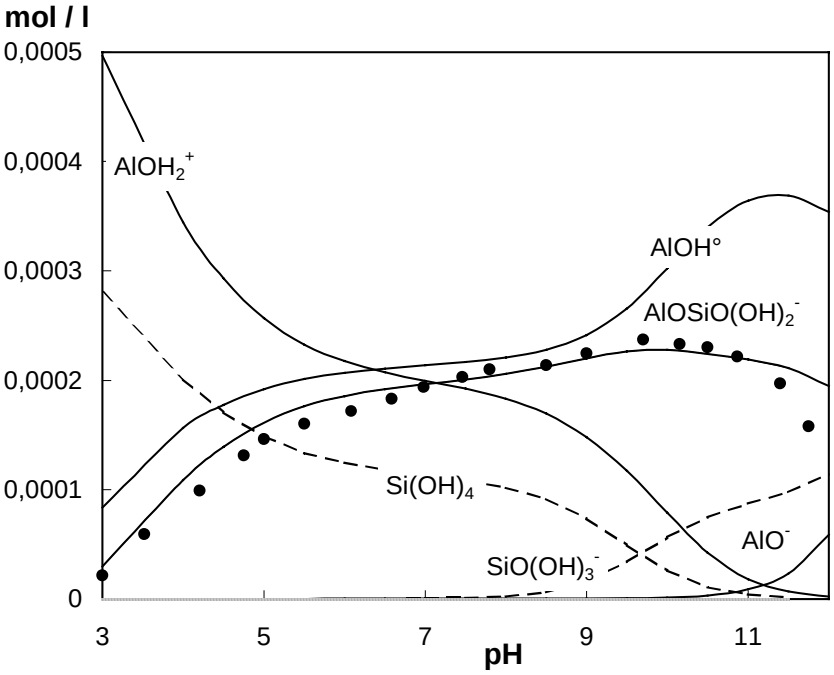

Fig. 2 Concentrations of the dissolved monosilicic acid, of the silica containing surface complex, $AlOSiO(OH)_2^-$, and of the dissociates of the surface hydroxyl group at the gibbsite surface, $AlOH_2^+$, AlOH°, and AlO^- (54 m^2 gibbsite / l; 19 mg SiO_2 total dissolved silica / l)

However, the adsorption behaviour is more complex, if polymeric silica is adsorbed. In this case the interaction between dissolved silica and the solid surface can not described by the above surface reactions. This is caused by the complex structures of the polymeric molecules and the variable number of silicium atoms per molecule (mean value of 50 atoms for the present polymer). Furthermore these polysilicic acids are only stable in

alkaline solutions. In neutral and acid solutions polymer decomposes to monomer according to the second order kinetics (Dietzel and Usdowski, 1995).
To compare the adsorption of monomer and polymer both experimental sets were carried out at identical boundary conditions. In Figure 1 the concentration of total dissolved silica as a function of reaction time for an experiment with polysilicic acid is shown. One portion of the polymer is adsorbed onto the surface of the mineral within a rather short time, whereas the other decomposes to monomer.
The results show that polymer is adsorbed much stronger than monosilicic acid onto the surface of gibbsite (Fig.1). After the initial strong adsorption of polymer the concentration of total dissolved silica increases. This is caused by the decomposition of polymer at the gibbsite surface, which is subsequently liberated as monomer into the solution.

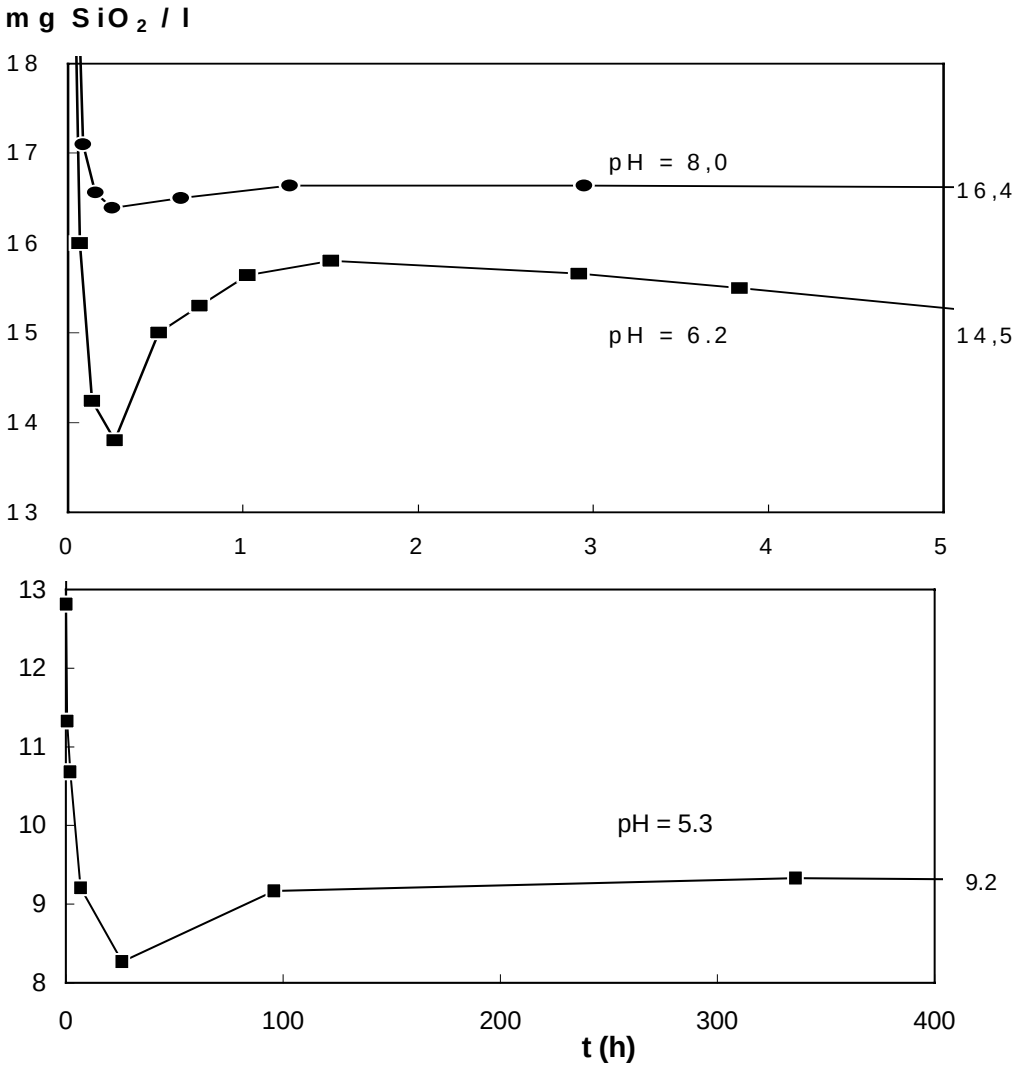

Fig.3 Concentration of total dissolved silica as a function of reaction time. Adsorption experiments with polysilicic acid onto 14 m^2 gibbsite surface / l solution at different pH. The values at the right hand side of the diagram denotes the silica concentrations at adsorption equilibrium (initial concentration: 23 mg SiO_2 / l)

At equilibrium the decomposition of polysilicic acid at the gibbsite surface is not totally complete. A portion of the adsorbed polymer is stabilised at the gibbsite surface. Figure 3 shows that this stabilisation of polymer depends strongly on pH. The amount of the stabilised polysilicic acid increases as pH decreases.

In summary, polymer is adsorbed much stronger onto the mineral surfaces than monomer. Further polymer, adsorbed as a metastable component in acid solutions, is stabilised at the mineral surface. If these results are applied to the polymerisation behaviour of silica at mineral surfaces it appears that polymerisation of silica at gibbsite surfaces may be favoured in solutions with low pH values. This is in agreement with the results obtained from dissolution experiments by Casey et al. (1993), who identified polymeric silica at the surfaces of the minerals in acid solutions.

References

Casey W.H., Westrich H.R., Banfield J.F., Ferruzzi G., Arnold G.W. (1993) *Nature* 366, 253-256

Dietzel M., Usdowski E. (1995) *Colloid Polym. Sci.* 273, 590-597

Dietzel, M. (1998) Min. Mag. 62A, 385-386

Iler, R.K. (1979) The chemistry of silica. 866, Wiley-Interscience, New York

Stumm,W. (1992) Chemistry of the solid-water interface Wiley-Interscience, New York

Effects of catalysts / inhibitors, ionic strength and deviation from equilibrium – separation of variables in practice and in theory

Jiwchar Ganor

Department of Geological and Environmental Sciences,
Ben-Gurion University of the Negev,
P. O. Box 653, Beer-Sheva 84105, Israel. E-mail: ganor@mail.bgu.ac.il

General rate law and separation of variables

In nature, there are many environmental factors that govern the rate of mineral dissolution. The laboratory situation is somewhat simpler. One can conduct a series of experiments in which one factor is manipulated while all other factors are held constant. The outcome of these experiments is usually a simple rate law describing the effect of the manipulated variable on the rate. Many such experiments investigating the effect of temperature, pH, ionic strength, catalysis and inhibition by inorganic and organic compounds and deviation from equilibrium are described in the geochemical literature. Considerable effort has been made to integrate the simple rate laws into a general form (Lasaga, 1981; Aagaard and Helgeson, 1982; Lasaga, 1984; Nagy et al., 1991; Nagy and Lasaga, 1992; Lasaga et al., 1994; Lasaga, 1995).

A general form of rate law for one mechanism of heterogeneous mineral surface reactions can be written as (Lasaga, 1995):

$$Rate = k_0 \cdot S_a \cdot e^{-Ea/RT} \cdot a_{H^+}^{n_{H^+}} \cdot \prod_i a_i^{n_i} \cdot g(I) \cdot f(\Delta G) \qquad (1)$$

where k_0 is a constant that depends on the intrinsic properties of the mineral, S_a is the reactive surface area of the mineral, E_a is the apparent activation energy of the overall reaction, R is the gas constant, T is the temperature (K), a_j is the activity of species j in the solution, n_j the order of the reaction with respect to j, $g(I)$ is a function of the ionic strength and $f(\Delta G)$ is a function of the Gibbs free energy. The much-studied pH dependence of the dissolution/precipitation reactions is represented by the term $a_{H^+}^{n_{H^+}}$ in equation (1). Terms involving activities of species in solution other than H^+, $a_i^{n_i}$, incorporate other possible catalytic effects on the overall rate. The $g(I)$ term indicates a possible dependence of the rate on the ionic strength (I) in addition to the contribution through the activity of a specific ion. The last term, $f(\Delta G)$, accounts for the important variation of the rate with deviation from equilibrium. The role of inhibition is not described in equation (1). Depending on the exact inhibition mechanism, the term a_i may represent an inhibitor. However, often this is not the case (see for example equations (14)

and (43) of Ganor and Lasaga, 1998; and equations 7.78 and 7.79 of Lasaga, 1998; equation (44) of Ganor et al., 1999).

The formulation of equation (1) is very useful because it relates the reaction rate to activities of ions in solution that may be obtained directly from the chemistry of the solution. However, mineral dissolution is a surface process and therefore it is more appropriate to express the dependence of the rate on the concentrations (or activities) of ions adsorbed on the surface rather than on the bulk activities in solution. Therefore, equation 0 can be rewritten in terms of surface concentrations, $X_{i,ads}$ (Lasaga, 1995):

$$Rate = k_0 \cdot S_a \cdot e^{-Ea/RT} \cdot X_{H^+,ads}^{n_{H^+,ads}} \cdot \prod_i X_{i,ads}^{n_{i,ads}} \cdot g(I) \cdot f(\Delta G) \qquad (2)$$

The coefficients $n_{H^+,ads}$ and $n_{,i,ads}$ are the reaction orders in respect to the surface species. Lasaga (1995) emphasized that by writing all the various terms in equations (1) and (2) as products, the kinetics rate laws claim for a "separation of variables", i.e., the effect of one variable is independent of the value of all other variables. Some theoretical kinetic justifications for the "separation of variables" were discussed by Lasaga (1995). It is important to clarify that the "separation of variables" is justified only for the direct effect of a variable on reaction rate, and not for an indirect effect. By direct effect we mean an effect related to the surface processes and therefore, one that can be used to understand the reaction mechanism. For example, the direct effect of pH on dissolution rate is understood as the effect that the proton adsorbed on the mineral surface has on the strength of the bonds. In this example, "separation of variables" implies that this effect of the adsorbed proton is independent of temperature. An example of an indirect effect, is the effect of the pH on the rate as a result of changes in the degree of saturation. This effect depends, among other things, on the temperature.

Direct effects of solution chemistry on reaction rate

The effects of the solution chemistry on the reaction rate are described by the last four variables in equation (1). In the following discussion we will describe from a theoretical point of view, how reaction rate is influenced by the solution chemistry.

Catalysis and inhibition

Adsorption of a catalyst or an inhibitor on a surface site close to the metal may influence the bond strength and thus affect the dissolution rate. For example, an inner-sphere complex with a ligand facilitates the detachment of a central metal ion and enhances the dissolution (Stumm, 1992). Similarly, surface protonation tends to increase the dissolution rate, because it leads to highly polarized inter atomic bonds in the immediate proximity of the surface central ions and thus facilitates the detachment of a cationic surface group into the solution (Stumm, 1992). From a mechanistic point of view, the

catalytic effect of protons is not different from that of other catalysts (Lasaga, 1995). Therefore, the intensely-studied effect of pH on dissolution rate represents a good example of catalysis.

Catalysts permit the system to follow a more favorable alternative reaction path, and serve therefore to enhance the reaction rate. Inhibitors, on the other hand, retard the reaction rate by obstructing the reaction path that dominates the overall rate. In many cases this is the catalyzed reaction path. When a catalyst and an inhibitor are adsorbed on the same mineral surface site, they compete with each other. The inhibitor may block the surface site and thus retard dissolution (Stumm and Wollast, 1990; Stumm, 1992; Biber et al., 1994; Ganor and Lasaga, 1998). Inhibition as a result of competition between an enzyme and an inhibitor is widely discussed in the biochemical literature. Ganor and Lasaga (1998) presented a mechanistic model describing the effects of an inhibitor on mineral dissolution rate in the presence of a catalyst. Ganor and Lasaga (1998) proposed two end member mechanisms. In the first mechanism the catalyst and the inhibitor compete with each other, i.e., they have a full mutual (negative) dependence, while in the second mechanism the adsorption of the catalyst and the inhibitor are absolutely independent of each other.

Deviation from equilibrium

According to transition state theory the dependence of the net rate of an *elementary reaction* on deviation from equilibrium ($f(\Delta G)$, equation (1)) is described by (Lasaga, 1998):

$$f(\Delta G) = (1 - e^{(\Delta G / RT)}) \qquad (3)$$

The form of equation (3) can be applied to overall reactions in a few simple cases that are described by Lasaga (1998). The function $f(\Delta G)$ for other overall reactions is difficult to predict *a-priory* especially if defects such as dislocations are important, and then different functions should be used. In the absence of a sound theory, various forms of experimental $f(\Delta G)$ functions were suggested for overall dissolution reactions of different silicate minerals.

Ionic strength effect

The effect of ionic strength on reaction rate may be explained by primary and secondary kinetic salt effects (Glasstone, 1949). The former refers to the effect of electrolytes on the activity coefficient, and the latter to variation in the concentrations of the reactants in solution. According to transition state theory, reaction rate is proportional to the concentration of the activated complex that is in equilibrium with the reactants. The activity of the reactants depends on their activity coefficients (γ). For an ion in solution,

this effect may be described by the Brønsted-Bjerrum equation, which is based on the Debye-Hückel formula:

$$\log(rate) = \Theta + 2A \cdot Z_1 \cdot Z_2 \cdot \sqrt{I} \qquad (4)$$

where Θ is a coefficient, A is a constant depending on temperature, Z_1 and Z_2 are the charges of the ions that form the activated complex and I is the ionic strength of the solution. Unfortunately, activity coefficients for charged surface species are very poorly known and therefore the Brønsted-Bjerrum equation does not strictly describe the ionic strength effect on mineral dissolution and precipitation.

Indirect effects on reaction rate

To establish a full rate law for a specific mineral, one should study the simple rate laws of all possible variables, by conducting for each variable a series of experiments that are identical in all factors except the investigated variable. This is an impossible mission. For example, one can decrease the pH by adding acid. However, adding acid changes the ionic strength and the concentration of the balancing anion. Moreover, the distribution of many species in solution varies as a function of pH, and both the changes in pH and the changes in the species distribution may affect the deviation from equilibrium. The effect of the pH on the solution chemistry varies as a function of other variables, such as temperature and ionic strength. Being unable to fully separate the experimental variables, many simple rate laws describe an apparent effect of the variable on the rate. These apparent rate laws may adequately describe this effect under the specific experimental conditions, but can not be used to determined the reaction mechanism.

Any chemical species in solution may be a potential catalyst or inhibitor, including the reactants and the products of the reaction. As a result, changing the concentration of such species may influence the rate both as a catalyst / inhibitor and due to its effect on the degree of saturation. Moreover, an ionic species will affect the ionic strength as well. Following are two case studies illustrating the difficulty in separating variables.

Fig. 1a and b (data after Oelkers et al., 1994) plot the dissolution rate of kaolinite at 150°C and pH=2 as a function of ΔG and activity of Al^{3+} in solution, respectively. Dissolution rate exhibits a strong negative dependence of the rate on $a_{Al}3+$ (Fig. 1b), that can be easily explained by strong aluminum inhibition. The effect of deviation from equilibrium on the rate (Fig. 1a) is an artifact of the aluminum inhibition. Using the experimental $f(\Delta G)$ function of Nagy et al. (1991), it can be shown that only the 4 experiments with ΔG>-3 kcal/mol are significantly influenced by the change in the degree of saturation. All the other experiments were conducted under the far from equilibrium conditions of the dissolution plateau regime. Under these far from equilibrium conditions the last term in equation (1) and (2) equals 1, and therefore the observed changes in dissolution rate did not result from changes in the degree of saturation between the experiments.

Fig. 2a and b (data after Ganor et al., 1999) plot log dissolution rate of gibbsite at 25°C as a function of the square root of the ionic strength and of log perchlorate concentration, respectively. In these experiments the ionic strength of the solution is dominated by the concentration of the perchloric acid, because the concentrations of all the other aqueous species are negligible. Therefore, it is impossible to use the data set to differentiate between the effect of the perchlorate and that of the ionic strength. By analogy with ions in solution (equation (4)), it can be expected that for a "primary salt effect", the log of the rate is proportional to the square root of the ionic strength. Fig. 2a plots log dissolution rate vs. the square root of the ionic strength and shows a near linear negative slope of 18±3. As the *A* parameter in the Debye-Hückel equation is very close to 0.5 at 25°C, the absolute value of the predicted slope should be approximately the product of the charges of the ions that form the activated complex (equation (4)). A slope of -18 requires that at least one of the charges is very high, which is improbable. Therefore, a possible alternative explanation is that the decrease in dissolution rate results from perchlorate inhibition (Fig. 2b).

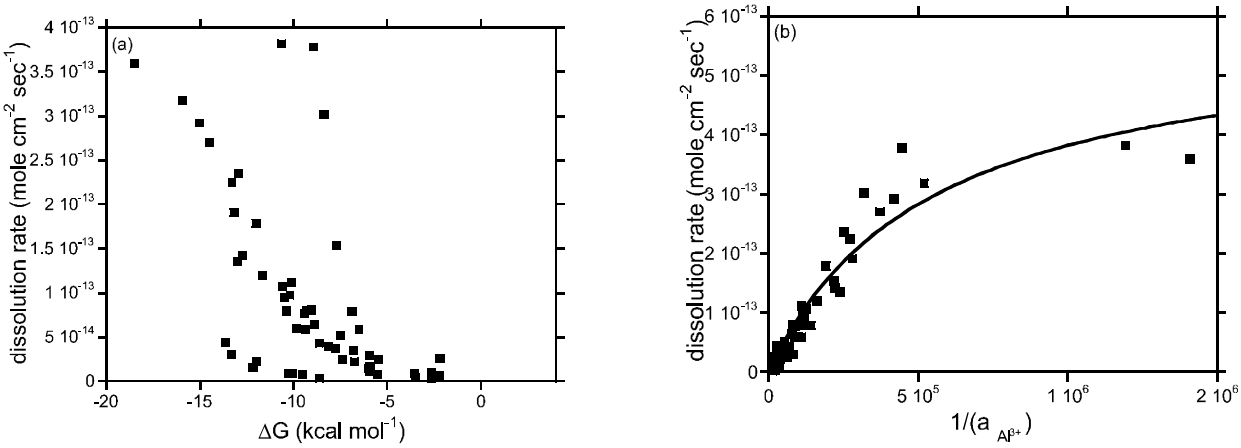

Fig 1: kaolinite dissolution (Data after Oelkers et al., 1994)

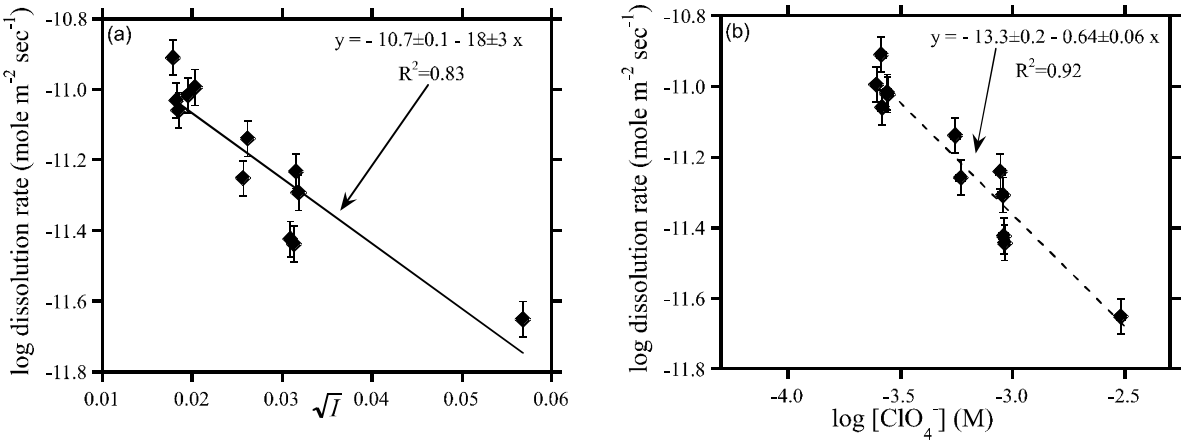

Fig 2: gibbsite dissolution (Data after Ganor and Lasaga, 1999)

References

Aagaard P. and Helgeson H. C. (1982) Thermodynamic and kinetic constraints on reaction rates among minerals and aqueous solutions. I. Theoretical considerations. *American Journal of Science* **282**, 237-285.

Biber M. V., Afonso M. D. S., and Stumm W. (1994) The coordination chemistry of weathering: IV. Inhibition of the dissolution of oxide minerals. *Geochimica et Cosmochimica Acta* **58**(9), 1999-2010.

Ganor J. and Lasaga A. C. (1998) Simple mechanistic models for inhibition of a dissolution reaction. *Geochimica et Cosmochimica Acta* **62**(8), 1295-1306.

Ganor J., Mogollon J. L., and Lasaga A. C. (1999) Kinetics of gibbsite dissolution under low ionic strength conditions. *Geochimica et Cosmochimica Acta* **in press**.

Glasstone S. (1949) *Textbook of physical chemistry*. Van Nostrand Co. Inc.

Lasaga A. C. (1981) Rate laws of chemical reactions. In *Kinetics of Geochemical Processes*, Vol. 8 (ed. A. C. Lasaga and J. R. Kirkpatrick), pp. 1-68. Mineralogical Society of America.

Lasaga A. C. (1984) Chemical kinetics of water-rock interactions. *J. geophys. Res.* **89**(B6), 4009-4025.

Lasaga A. C. (1995) Fundamental approaches in describing mineral dissolution and precipitation rate. In *Chemical Weathering Rates of Silicate Minerals*, Vol. 31 (ed. A. F. White and S. L. Brantley), pp. 23-86. Mineralogical Society of America.

Lasaga A. C. (1998) *Kinetic Theory in the Earth Sciences*. Princeton University Press.

Lasaga A. C., Soler J. M., Ganor J., Burch T. E., and Nagy K. L. (1994) Chemical weathering rate laws and global geochemical cycles. *Geochimica et Cosmochimica Acta* **58**(10), 2361-2386.

Nagy K. L., Blum A. E., and Lasaga A. C. (1991) Dissolution and precipitation kinetics of kaolinite at 80°C and pH 3: The dependence on solution saturation state. *American Journal of Science* **291**, 649-686.

Nagy K. L. and Lasaga A. C. (1992) Dissolution and precipitation kinetics of gibbsite at 80°C and pH 3: The dependence on solution saturation state. *Geochim. Cosmochim. Acta* **56**, 3093-3111.

Oelkers E. H., Schott J., and Devidal J.-L. (1994) The effect of aluminum, pH, and chemical affinity on the rates of aluminosilicate dissolution reactions. *Geochimica et Cosmochimica Acta* **58**(9), 2011-2024.

Stumm W. (1992) *Chemistry of the Solid-Water Interface: Processes at the Mineral-Water and Particle-Water Interface in Natural Systems*. John Wiley and Sons, Inc.

Stumm W. and Wollast R. (1990) Coordination chemistry of weathering : Kinetics of surface-controlled dissolution of oxide minerals. *Reviews of Geophysics* **28**(1), 53-69.

In-situ distribution of trace metals in a natural aquifer overlying the nuclear repository site Morsleben, Germany

H.Geckeis, P.Vejmelka, D.Degering, C. Pohlmann, K. Gompper, D.Hentschel, J.-I. Kim

Institut für Nukleare Entsorgungstechnik, Forschungszentrum Karlsruhe, P.O. Box 3640, D-76021 Karlsruhe, Germany

Abstract

The distribution of the naturally occuring rare earth elements (REE), Th, Zr, and U between sediment and groundwater samples is determined. They are taken as chemical homologues of the artificial tri-, tetra- and hexavalent actinides. The samples originate from an aquifer overlying the German repository for low and intermediate level nuclear waste at Morsleben. The obtained distribution coefficients, the so-called in-situ K_d-values, are higher by orders of magnitude compared with the respective K_d-values obtained for artificial radionuclides in the laboratory. The difference is due to the fact that in the case of the in-situ K_d-values not only surface-sorbed metal species are considered but also the fraction bound into the bulk sediment. A separate determination of the surface-bound metal species is tried by leaching the sediment samples with 1 mol/L acetic acid. For the most investigated sediment-groundwater systems the in-situ K_d-values normalized to the fraction of acetic acid leachable metal species are found to be comparable with the respective laboratory K_d-values for Am, Th, Pu and U. In case of sediments containing calcite, considerable amounts of REE and to a minor extent Th and U are dissolved by acetic acid together with the calcite. It is concluded that calcite acts as a host mineral phase especially for the trivalent REE. In general, the normalized in-situ K_d-values are consistent with sorption data obtained in the laboratory and reflect co-precipitation processes occuring during long time scales in the natural system.

Introduction

The retardation of radionuclides at mineral surfaces during their migration along the groundwater flow path still today is mainly described using K_d-values [1]. The radionuclide sorption reaction is assumed to be reversible and independent of the radionuclide concentration. Uncertainties inherent to the K_d-concept are:

- The validity of the laboratory K_d-value for the long time scales relevant for a natural system is not proven.
- The sorption process might not be reversible in case of coprecipitation, surface precipitation reactions or diffusion into the solid matrix.
- The sorption reaction is very often found to depend on the metal ion concentration even at trace concentration level.

- K_d-values are only valid for the investigated system. They are incompatible to systems characterized by different geochemical parameters (ionic strength, radionuclide concentration, pH, redox potential etc.).

In the present work the naturally abundant rare earth elements (REE), Th, Zr, and U are taken as natural homologues of the tri-, tetra- and hexavalent artificial actinides. Their so-called in-situ K_d-values are determined by analysis of their concentration in the sediment and groundwater phase, respectively. They are used to validate laboratory K_d-values determined for the same sediment/groundwater system. Sediment and groundwater samples are taken from the aquifer system overlying the German site for the disposal of low and intermediate nuclear waste at Morsleben.

A simple procedure is applied to differentiate the surface sorbed trace elements from the fraction bound into the interior of the sediment grains. The sediment is leached by 1 mol/L acetic acid and the trace element fraction in the leachate is attributed to the surface sorbed metal species.

Experimental

All samples have been taken and stored under anaerobic conditions, i.e. under Ar and Ar/1% CO_2 atmosphere in order to avoid oxidation of sediment and groundwater components. Sediment/groundwater systems are preequilibrated under Ar/1% CO_2 for at least 12 months. The groundwater composition is analyzed by ICP-AES and HPIC; pH and redox potential are determined by using a Ross type glass electrode and a platinum electrode, respectively. REE, Th, Zr and U in the groundwater samples and the individual leachates are determined by ICP-mass spectrometry (ICP-MS). Sediment samples are dried, ground and characterized by XRF, XRD and after a microwave assisted HNO_3/HF acid digestion procedure by ICP-MS. Zr in the sediments is determined by instrumental neutron activation analysis (INAA).

Laboratory K_d-values for U, Th and Pu are determined after addition of radionuclide spiked groundwater aliquots to the sediment preequilibrated with the respective groundwater. Steady state radionuclide concentrations are established after 9 months and are analyzed by liquid scintillation counting and alpha spectrometry, respectively. Batch sorption experiments are carried out in triplicate.

Results and discussion

The in-situ K_d-values for the individual trace elements calculated from the bulk composition of the sediment and the groundwater concentration according to Eq.(1) are plotted in Fig.1.

$$\text{In-situ}\quad K_d = \frac{c_s}{c_w}\left[\text{ml}\cdot\text{g}^{-1}\right] \qquad \text{Eq. (1)}$$

c_s: element concentration in the solid phase $\left[\text{mol}\cdot\text{g}^{-1}\right]$

c_w: element concentration in the groundwater $\left[\text{mol}\cdot\text{ml}^{-1}\right]$

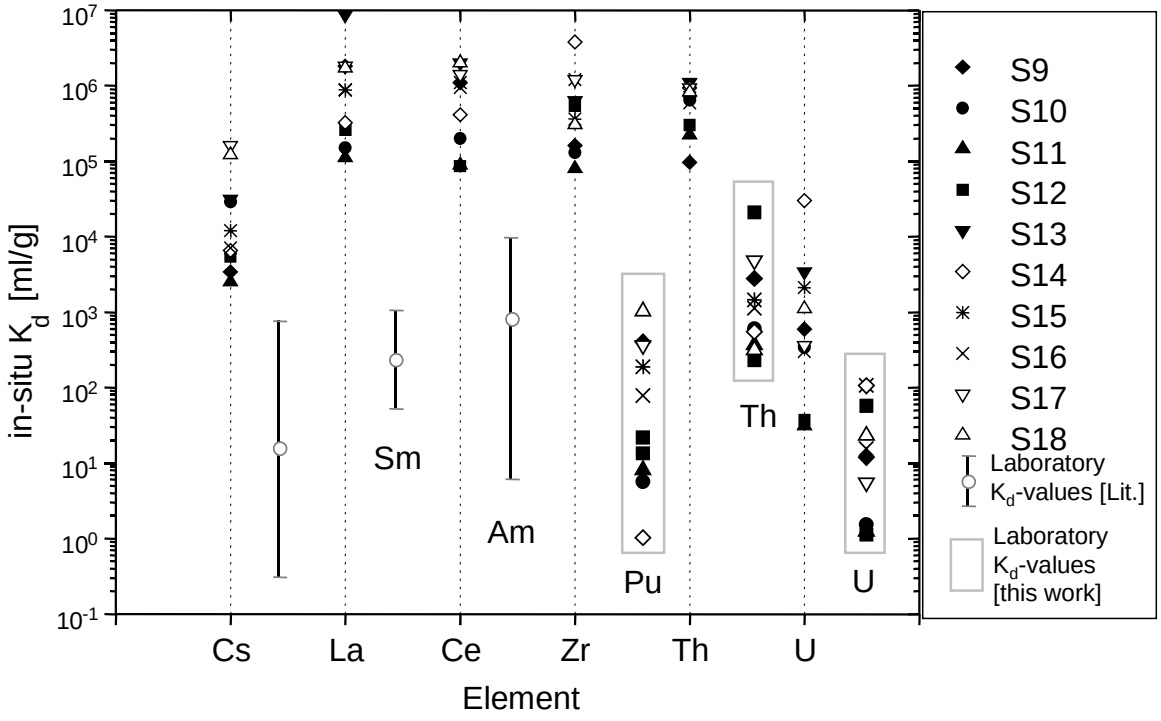

Fig. 1 in-situ K_d-values for Cs, REE, Zr, Th and U compared with laboratory K_d-values

Laboratory K_d-values are included for comparison in Fig.1. It should be noted that due to the low solubility of Pu and Th in the respective groundwater samples the radionuclide concentrations drop below the detection limit during the batch sorption experiments. Therefore, all laboratory K_d-values for both nuclides are lower limits. Sorption data for Cs, Am and Sm have not been determined in this work and are taken from the literature [2]. They have been measured in systems with comparable sediment and groundwater composition. In-situ K_d-values related to the trace metal content of the bulk sediment are higher by several orders of magnitude and similar to those found by Tullborg and Landström [3] for a granitic fracture system. This behaviour is not only observed for the polyvalent metal ion species but also for Cs. It is clear that such type of in-situ K_d-values are not comparable with sorption data obtained in batch experiments. The analysis of the total sediment sample gives the content of the entire bulk phase while in case of batch sorption experiments the partitioning of radionuclides between the solution and the solid surface is observed. A prerequisite for the comparability of both K_d-values is, therefore,

the differentiation between the trace elements bound in the sediment bulk and the surface-bound fraction. Under certain conditions this fraction can be obtained by an acetic acid leaching step. In-situ K_d-values normalized to the trace metal fraction leached by acetic acid from the sediment surface are calculated and plotted in Fig. 2.

The normalized in-situ K_d-values for those systems containing calcite free sediments are in agreement with the order of magnitude of corresponding laboratory K_d-values. In case of carbonate phases (e.g. calcite) being detected in the sediment, they are dissolved during the leaching step by acetic acid.

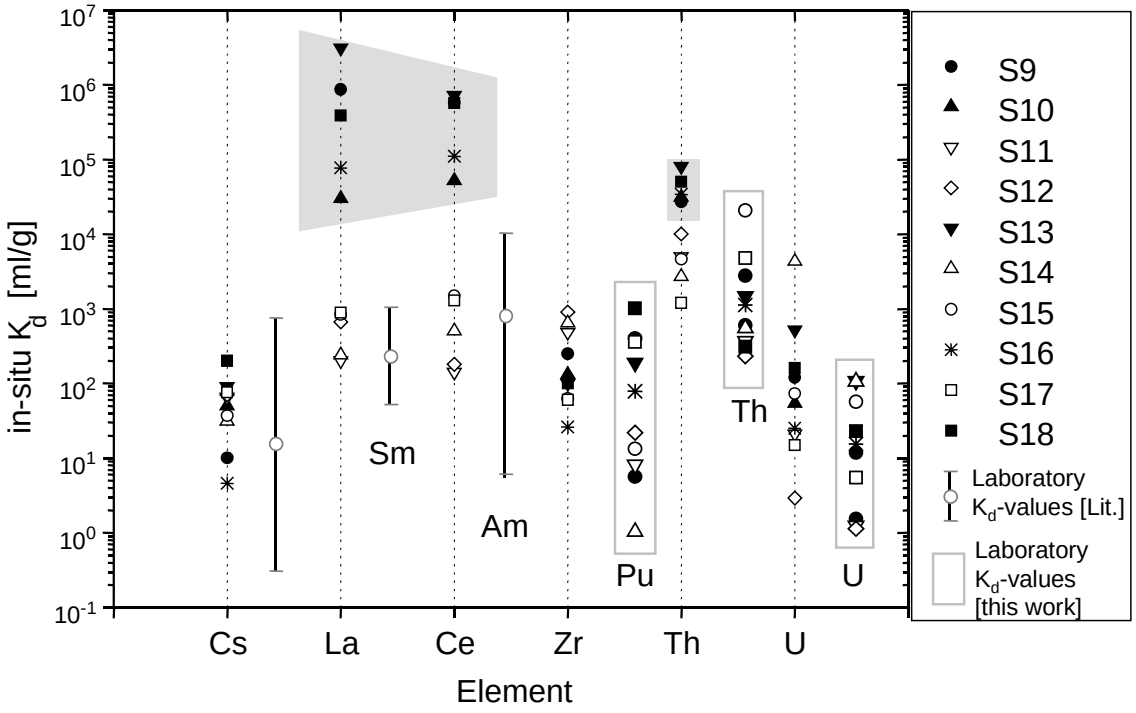

Fig. 2 normalized in-situ K_d-values for Cs, REE, Zr, Th and U compared with laboratory K_d-values; in-situ K_d-values are normalized to the acetic acid leachable fraction of the trace elements; filled symbols correspond to systems containing a calcite containing sediment.

For those sediments not only the surface sorbed but also the calcite bound trace element fraction is dissolved. As a consequence, considerably higher normalized in-situ K_d-values are observed in the case of the REE. This indicates that REE and to a lesser extent also Th and U are incorporated into calcite phases.

The results indicate that in-situ K_d-values of the chemical homologues of the actinides might be applicable to increase the confidence into laboratory K_d-values or to validate at least the order of magnitude of such type of sorption data. The correlation of the trace element content to individual mineral phases by e.g. chemical leaching steps provides hints to potential major host phases relevant for the retention of individual trace elements

over long time scales. These host phases are assumed to be relevant as well for the artificial radionuclides, which show a similar geochemical behaviour. Provided that such phases are generated during relevant time scales their formation might represent a considerable barrier function of the geosphere due to the immobilization of radionuclides by mineralization.

References:

[1] B. Boese, D.Buhmann, R. P.Hirsekorn, R.Storck, C.Tix, Advanced approaches for modelling chemical and physical effects in the underground structure of a radwaste repository in salt rock, Gesellschaft fuer Anlagen- und Reaktorsicherheit mbH (GRS), Koeln, GRS-123 (Mar 1996)

[2] Gesellschaft für Anlagen- und Reaktorsicherheit (GRS), Köln, personal communications

[3] O. Landström, E.-L. Tullborg, Interactions of trace elements with fracture filling minerals from Äspö Hard Rock Laboratoy, SKB Technical Report 95-13, June, 1995

Long-term thermodynamic and kinetic study of mineral-soil solutions interactions in an acid brown soil

F. Gérard, J. G. Genon and J. Ranger

INRA, Centre de Nancy, Equipe Cycles Biogéochimiques, Forêt d'Amance, 54280 Champenoux, France. gerard@nancy.inra.fr

Introduction

Quantification of weathering reactions in soils is required in order to study middle and long-term soil fertility and water quality. Knowledge of soil solution chemistry is a requisite because both dissolution and precipitation reactions depend on aqueous chemistry. The precipitation of secondary phases likely controls the chemistry of soil solutions and in turn the weathering flux, depending on the interplay between reaction kinetics and solution/mineral residence times, as is the case for dissolution reactions. The use of computer codes is required to calculate aqueous speciation in natural solutions. In forest soils, most of the modeling studies of soil solutions chemistry have shown undersaturated solutions with respect to primary and secondary minerals (e.g. Boudot et al., 1996). It is well known that natural surface waters are in general slightly undersaturated and that weathering reactions mainly occur close to equilibrium. Thus mineral dissolution rates, and the associated flux of chemical elements released from this process, may be affected by the chemical affinity of the reactions (*Ar*) and therefore slowed down. The saturation and supersaturation of secondary mineral phases, in general low temperature aluminosilicates (e.g. kaolinite) and aluminium hydroxides, have been indicated in a few studies (e.g. Simonsson and Berggren, 1998). According to the Transition-State Theory (TST), the rate-limiting step of the overall reaction is the formation of an activated complex at high-energy surface sites. It is commonly assumed that the concentration of activated complex is proportional to a precursor complex at the mineral surface and both complexes are in a state of local equilibrium. Until recently, precursor complexes for multi-oxide minerals were believed to consist of either hydrogenated, hydroxylated, or hydrated surface sites. Far more mineral dissolution experiments have been performed than mineral growth experiments. Taking these assumptions into account, the TST dictates that dissolution rates only depend on pH if the affinity of the reaction (*Ar*) is less than -10 kJ/mol approximately. Recently, a new mechanistic kinetic rate law consistent with the TST and surface chemistry has been proposed in the literature (e.g. Schott and Oelkers, 1995). This new mechanistic rate law takes account of the inhibitor effect of dissolved aluminium on alkali-feldspars, kaolinite and muscovite dissolution. In addition, these silicates apparently have a greater dissolution rate dependence on chemical affinity than was previously assumed. A theoretical study (Gérard et al., 1998) has shown that the new rate law may significantly affect the calculated mineral dissolution rates in most natural systems. The changes in dissolution rates may reach certain orders of magnitude, depending on the mineral, pH, temperature and aluminium concentration.

The aims of this paper are to (1) study in a field system the effect of the aluminium-dependent rate law on mineral dissolution rates (acid brown soil, 40 years Douglas stand, Vauxrenard, Rhônes, France); (2) study the role of hydrology on chemical imbalances and reaction rates; (3) document the long-term effects (4-5 years).

Materials and methods

Compositions of gravitational and capillary solutions have been measured monthly during a period of 5 and 4 years respectively at different depths (15-30-60-120 cm). The geochemical software EQ3NR is used for speciation calculations. From EQ3NR outputs, dissolution rates of minerals leached by the soil solutions are calculated with a spreadsheet program. Several aqueous species and minerals typically used in low temperature geochemical modeling have been added to the thermodynamic database. The thermodynamic equilibrium constants of the aluminium-bearing species have been updated according new published values for Al^{3+} stability (Shock et al., 1997). Aluminium-organic speciation is modeled by means of an analogue model (Driscoll et al., 1994). Calculations are performed at the average *in situ* soil temperature: 8°C.

Results and discussion

Most soil solutions are close to saturation or supersaturation with respect to aluminium hydroxides, kaolinite and low temperature Al-Si minerals (e.g. imogolite). From suitable activity diagrams one can conclude that kaolinite and other Al-Si mineral are not controlling dissolved aluminium concentration in soil solutions. Activity values are largely dispersed and do not line up with any of the stability lines plotted. Dissolved aluminium seems to be controlled by the fast precipitation of a gibbsitic or aluminium hydroxide phase, as illustrated for gravitational waters in figure 1. Data is lined up transversally, moving from the stability line of the well-crystallized gibbsite at acid pH to amorphous $Al(OH)_3$ stability line from around pH = 5.5. Between these two end-members, the aluminium hydroxide phase turns to natural gibbsite, poorly crystallized and microcrystallized gibbsite stability lines respectively with increasing pH. This trend is consistent with the TST and surface chemistry kinetic theories. These results thus suggest that aluminium hydroxide precipitation is surface-controlled up to equilibrium.

Capillary solutions show a similar behavior for aluminium hydroxides. However, the most soluble $Al(OH)_3$ phase found is microcrystalline gibbsite. This is due to the smaller pH range measured in these soil solutions.

Kinetic parameters published in Gérard et al. (1998) are used to calculate alkali-feldspars and muscovite dissolution rates in contact with gravitational and capillary solutions. For capillary solutions, the aluminium-dependent dissolution rates show seasonal variations (figure 2.). The maximum is reached in autumn and the minimum in spring. The dissolution rate variations may reach 0.7 log units. No seasonal variation occurs in macropores solutions (i.e. gravitational solutions), where aluminium-dependent rates are

deeply influenced by rain events. When using the standard pH-dependent rate law, there is no seasonal variation of dissolution rate whatever the nature of the soil solutions.

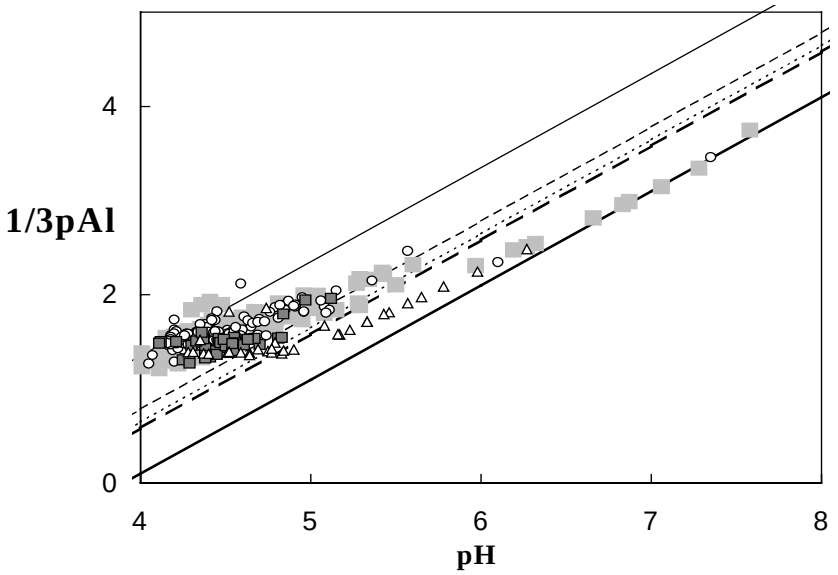

Figure 1. Activity diagram for aluminium hydroxides in gravitational waters at four depths. Shaded squares: 15 cm, open circles: 30 cm, dark squares: 60 cm, open triangles: 120 cm. Thin line: stability of the well-crystallized gibbsite, thick line: amorphous $Al(OH)_3$. The thin and thick dashed lines stand for natural and poorly crystallized gibbsite respectively. The dot-dashed line denotes microcrystalline gibbsite stability.

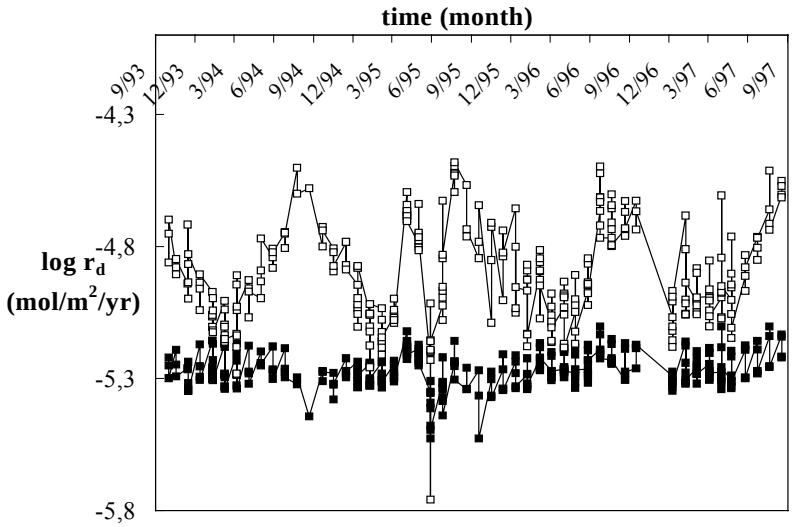

Figure 2. Time variation of the K-feldspar dissolution rate leached by capillary solutions (60 cm deep). Open symbol: aluminium-dependent rates, filled symbol: standard dissolution rates.

Compared to the aluminium-dependent dissolution rates, the saturation index of $Al(OH)_3$ phases behave in a totally different way (figures 2 and 3.). This result demonstrates that, in spite of the higher dependence of the dissolution rates with respect to the chemical affinity, and of the proximity to equilibrium (*Ar* ≅ -3.5 kcal/mol for K-feldspar), alkali-feldspar and muscovite dissolution rates are mostly controlled by the inhibitor term of the aluminium-dependent rate law: $(a_{H+})/(a_{Al}^{3+})^{1/3}$. One can also infer from figure 3. the higher solubility of the aluminium hydroxide controlling aluminium concentration through Al^{3+}activity in spring and summer. This result is consistent with the higher soil temperature during this period.

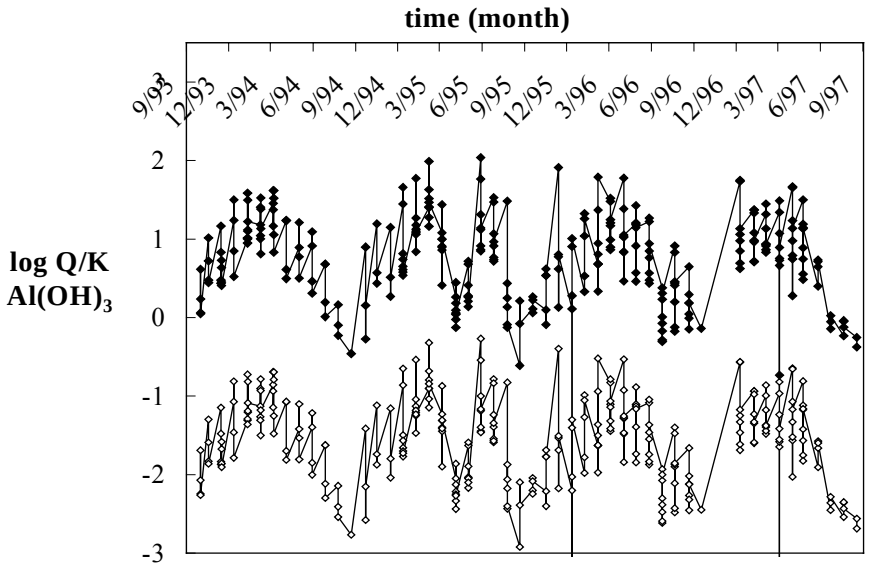

Figure 3. Time variation of the $Al(OH)_3$ saturation index in capillary solutions (30 cm deep). Open symbol: amorphous $Al(OH)_3$, filled symbol: well-crystallized gibbsite.

For capillary solutions, dissolution rates are nearly independent of depth whatever the kinetic law used. For gravitational waters, regardless the kinetic law used, dissolution rates decrease (maximum of 1.5 order of magnitude) when the depth is between 30 and 120 cm. Dissolution rates at 15 and 30 cm are broadly similar. Gravitational waters are closer to equilibrium when the depth increases. The differences between dissolution rate behavior in gravitational and capillary waters according to the depth are largely due to silica activity. The mineral dissolution rate calculated with the Al-dependent law expression is 1 to 1.5 log units larger than with the standard law. Hence, taking account of the inhibitor effect of dissolved aluminium and the greater dependence on chemical affinity does not slow down dissolution rates. This is due to the apparent nature of the experimental kinetic constants used in the standard kinetic expression, which integrates the dissolved aluminium effect.

Summary and conclusion

A thermodynamic and kinetic analysis of water-minerals interactions has been carried out on an acid brown soil for a period of 4-5 years. Low and high residence time soil solutions (i.e. gravitational and capillary waters respectively) measured at different depths have been studied. The main results obtained are as follows: (1) there are no significant difference between capillary and gravitational solutions in terms of saturation indexes for secondary products, namely Al-hydroxides and kaolinite. The solutions are supersaturated with respect to kaolinite, which does not control aluminium concentrations. There are some evidences for the presence of kaolinite (Ezzaïm, 1997). Dissolved aluminium appears to be controlled by the fast precipitation of some Al-hydroxide phases. Those phases progressively become more soluble (i.e. less crystallized) as the pH increases. This trend is consistent with a surface-controlled precipitation reaction. Crystallized $Al(OH)_3$ has not been observed in this soil. However, the quantity may be to weak to ensure detection; (2) the aluminium-dependent dissolution rates, as calculated for alkali-feldspars and muscovite, are subjected to seasonal variations and are primarily controlled by the inhibitor term. The fast precipitation of some high solubility Al-hydroxides occurs in summer and spring. This is consistent with the higher soil temperature; (3) seasonal variations are not observed using a standard pH-dependent kinetic expression; (4) mineral dissolution rates in macropores (gravitational solutions) increase with depth but are relatively constant in micropores (capillary solutions), whatever the kinetic equation used; (5) taking account of the aluminium-dependent kinetic law does not slow down the mineral dissolution rate but increases it by 1 to 1.5 order.

This study demonstrates that the weathering fluxes in this forest ecosystem are subjected to seasonal variations and can only be modeled by considering the aluminium-dependent rate law. In addition, such a rate law may fasten the release rate of nutrients like K and Ca. Finally, reactive transport is relatively homogeneous in this soil for aluminium, which is primarily controlled by fast $Al(OH)_3$ precipitation. Reactive transport shows greater heterogeneity for silica, implying differences in dissolution rates between capillary and gravitational porous subsystems due to chemical affinity effects.

References

Boudot, J.-P., Maitat, O., Merlet, D., and Rouiller, J., 1996. J. Hydrol., 177, 47-63.

Driscoll, C. T., Lehtinen, M. D., and Sullivan, T.J., 1994. Water Resour. Res., 30, 297-306.

Ezzaïm, A., 1997. Thesis, Université Nancy I, 181 p.

Gérard, F., Fritz, B., Clément, C. and Crovisier, J.-L. , 1998. Chem. Geol., 151, 247-258.

Schott, J. and Oelkers, E. H., 1995. Pure and Appl. Chem., 67, 903-910.

Shock, E.L., Sassani, D.C., Willis, M., and Sverjensky, D.A., 1997. Geochim. Cosmochim. Acta, 61, 907-950.

Simonsson, M. and Berggren, D., 1998. Eur. J. Soil Sci., 49, 317-326.

Mechanisms limiting the alteration kinetics of R7T7 nuclear glass

Stéphane Gin, Christophe Jégou and Étienne Vernaz

Commissariat à l'Énergie Atomique (CEA), Rhône Valley Research Center
DRRV/SCD, BP 171, 30207 Bagnols-sur-Cèze Cedex, France

A key step in developing long-term behavior models for nuclear waste glasses is to determine the mechanisms that limit the alteration kinetics. In view of the geological disposal conditions proposed for these materials, investigating the evolution of the nuclear glass alteration rate under saturated conditions is an essential point—even if it does not elicit unanimous agreement within the scientific community.

The authors describe experiments with the French R7T7 nuclear waste glass and with other simplified glass formulations showing that the alteration kinetics are controlled exclusively by the gel that forms on the surface during alteration. This observation challenges kinetic laws based on the notion of chemical affinity for this type of matrix, and encourages consideration of laws incorporating the gel formation and material transport mechanisms within this barrier. The possibility of kinetic control by a gel/solution equilibrium (Bourcier's model) is also called into question by these experiments.

Affinity of glass corrosion close to saturation

B. Grambow

Ecole des Mines de Nantes, grambow@subatech.in2p3.fr

Often, a decrease of glass corrosion rates with time is observed. Initially this was interpreted as an effect of protective layers, later it was shown for silicate glasses to be a saturation effect of the solution [1,2,3]. Saturation effects were also reported for some phosphate glasses. With approach of saturation the affinity [4] of glass dissolution and thus the reaction rate decreases [5,6,7]. The saturation effect results in an effect of solution volume on glass corrosion rates: the larger the volume, the longer it takes for saturation to occur and the higher are the reaction rates. The effect of surface area to volume ratio (S/V) on glass corrosion rates is known since more than 20 years [8,9].

The use of affinity terms requires knowledge of the chemical nature of the reference equilibrium state. For certain minerals, thermodynamic equilibrium with an aqueous solution appears to be clearly defined: the mineral precipitates along well defined crystal planes from oversaturated solutions and these crystal planes dissolve in undersaturated solutions. Solution concentrations of dissolved mineral constituents in static dissolution and precipitation test approach each other asymptotically with time. Not so with glasses. Forward reaction (dissolution) and backward reaction (precipitation of secondary phases, not of glass) do not have the same stoichiometry. Secondary phases can be in equilibrium with the solution, but this may have no bearing on glass dissolution affinity.

What then is the meaning of equilibrium in glass corrosion tests? Glass is metastable solid with respect to a hypothetical suite of more stable crystalline alteration products. This precludes achievement of a true overall thermodynamic equilibrium, but it does not preclude equilibria between the surface of this metastable solid and an aqueous phase. However, due to leaching of alkali ions and other mobile species, the composition of the surface may be different than the bulk glass.

What is the surface of glass? Glasses have a rather open structure, not only the outer surface of the glass can react with water, water penetrates also deep into the glass structure (depending on glass structure and time up to mm) and attacks network bonds. This water penetration cannot be accounted for by a simple surface roughness factor or by the definition of an “effective surface area”, as frequently used for minerals. The dynamics of the reaction of a glass in an aquatic medium is controlled both by energetic and topological constraints. Important is not only the hydrolytic affinity of a bond of the glass structure, but also the accessibility of a bonds to the aqueous reactant in the volume of the surface region.

Thus, for understanding the role of affinity terms in glass corrosion certain fundamental knowledge of glass structure is necessary. The amorphous structure (glass network) is

very complex. Neutron scattering analyses and EXAFS allow to distinguish three ranges of order for silicate glasses (I) ordered cation coordination spheres with similar bond length as in crystals [10] with a tendency to smaller coordination number [11,12] (II) Cation polyhedra connected by oxygen and (III) larger units such as rings, chains (e.g. in phosphate glasses) or infinite three dimensional frameworks etc.. Glass network connectivity is maintained by mixed ionic/covalent bonds [13] of network former elements (Si, P, B, Al...), a typical example are ≡Si-O-Si≡ siloxane bridges. In contrast, connectivity is loosened by strongly ionic non-bridging oxygen bonds (NBO), such as ≡Si-O^-Na^+. The loosely bound alkali ions are in principal rather mobile, prone to be leached, but they can be immobilized by needs for charge compensation in case of presence of anionic aluminate or borate tetrahedra bound to Si-Q^3-Sites [14] in the glass. At a molar ratio (Al +B)/Na in the glass of 1 the anionic charge is compensated entirely and Na-ions are very immobile [15].

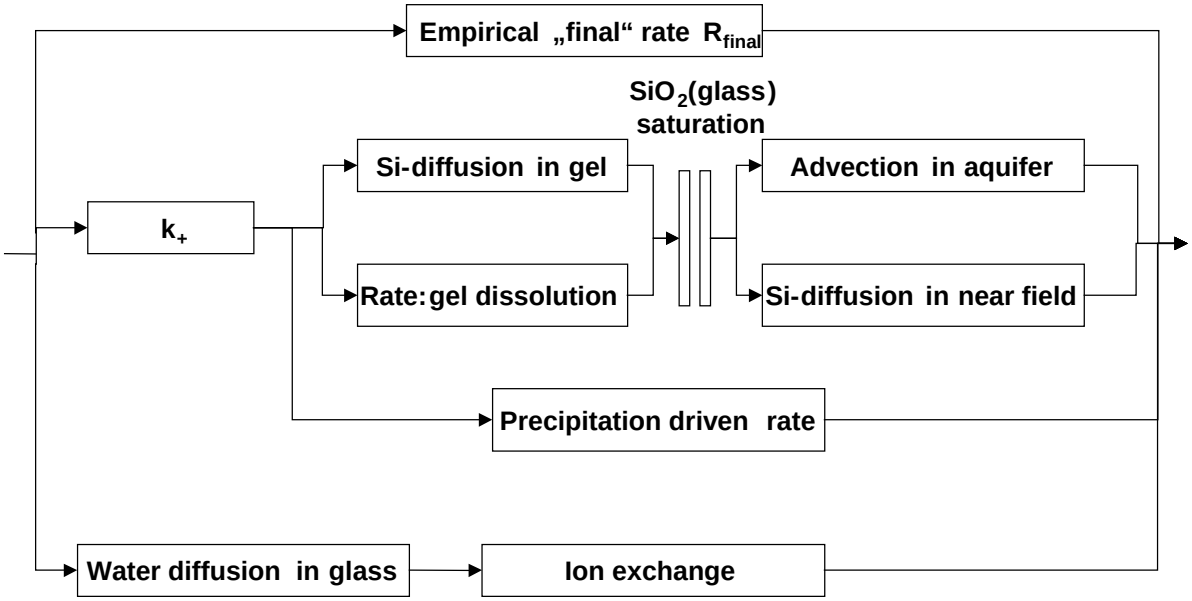

Figure 1: Interrelationship of rate controls in the dissolution process of glass, expressed in terms of resistors (for rates) and capacitors (for saturation).

The principal glass/water reactions are directly related to the glass structure: glass network hydration, ion exchange at NBO sites and dissolution of the glass network (hydrolysis of mixed covalent/ionic bonds). Additionally, transport processes such as access of reactants (e.g. water molecules) and removal of products (e.g. dissolved glass network formers) become rate limiting under certain conditions. Different reaction rates and empirical rate laws (time exponents) are interpreted as resulting from the different relative importance of the various reaction steps in the overall reaction scheme, as shown in Figure 1 in terms of resistors representing rates and capacitors representing solubilities. In parallel reactions the fastest rate (lowest resistance) determines the overall rate whereas in sequential reactions the slowest rate (highest resistance) is rate determining. Glass hydration and Alkali/H^+ ion exchange on the one hand and glass network dissolution on the other are parallel reactions [16,17,18,19].

For each reaction step j (glass hydration, ion exchange, network dissolution, transport of reactants, transport of products, growth of secondary phases, etc.) and each chemical component i of the glass and of the leachant, an equilibrium state and an affinity term ($A_{i,j}=\Sigma\mu_{i,j}$) may be formulated. Certain reaction steps apply only to a small suite of glass constituents, others to the entire glass. Individual element dissolution affinity values are not directly accessible by measurement but may be estimated from a solid solution end member representation of the glass phase. Release of individual elements is not controlled by these affinity terms, but is a collective property of the whole glass phase. Various affinity terms may be distinguished: The network dissolution affinity $A_i^{\text{Network dissolution}} = -\Sigma\mu_i^{\text{product}}-\mu_i^{\text{reactant}}$ (implies saturation effects of dissolved silica and other network formers with the glass surface. The transport affinity $A_i^{\text{transport}} =\Sigma\mu_i^{\text{surface}}-\mu_i^{\text{near field}}$ is associated to chemical gradients (for mass transfer resistance of surface layers etc.). Another affinity term is imposed by sink-terms $A_i^{\text{products}} =\Sigma\mu_i^{\text{product 1}} -\mu_i^{\text{product 2}}$ describing pump effects such as those imposed by zeolite formation during glass dissolution. Finally the affinity for ion exchange must be considered, which mainly but not exclusively apply to alkali elements. In the following the reference equilibrium states for these affinities are discussed.

The initial surface modification is glass hydration. The equilibrium state for glass network hydration is the solubility limit of water in the glass structure, representing a certain distribution of siloxane and silanol groups as well as molecular water. The only specie involved is water.

If sufficient network bonds are hydrolyzed, a transformed layer [20] (gel) is formed, with a clear phase boundary to the glassy phase. The transformed surface layers are porous [21], containing molecular water [22,23] and allowing for high ionic mobility [24] as well as high water mobility, thus ion exchange is easy. For the ion exchange reaction, a typical ion exchange equilibrium with an ion exchange constant can be formulated. In general ion exchange reactions are fast and equilibrium is attained immediately ($A^{\text{ion exchange}} = 0$). Experimental observed kinetics of ion exchange reactions are due to transport affinity control of reactants (water, hydronium ion) or of products (Na). The alkali/H^+ ion exchange process is often (not always [25]) diffusion controlled, implying that the rate of selective alkali release from glasses is initially highest and decreases with the square root of time until it becomes equal to the rate of matrix dissolution. Based on findings that the pH-response of glass electrodes is essentially determined by exchange equilibria of outermost surface species with solution species, it was suggested that ion-exchange is driven by (electro)chemical potential differences between charged and uncharged surfaces species and the bulk glass [26]. However, the electrical coupling of H^+ and Na^+ migration in the surface layer leads to electrical fields much stronger than those between the surface and the glass [27]. The process may be governed either by the electroneutrality coupled (inter)diffusion coefficients of alkali ions and H^+ ions in opposite direction, with the lower mobility of H^+ or H_3O^+ ions [28,29] normally being rate controlling. Alternatively, rate limiting may be the diffusion of water molecules in glass network [30,31].

Network dissolution may be described with a general law of irreversible thermodynamics and transition state theory, as applied to mineral surfaces according to Aargaard and Helgeson [32].

$$r = \frac{d\xi}{s \cdot dt} = r \cdot \left(1 - \exp\left(\frac{-A_j}{RT}\right)\right)$$

where ξ refers to reaction progress, r (k_+ in Fig 1) is a forward rate and s the effective surface area, $A_j = 2.3RT \cdot \log(K_{so}/Q)$ the chemical reaction affinity, K_{so} is the equilibrium constant and Q the ion activity product of the rate limiting reaction, R the gas constant and T the absolute temperature. In this equation the overall rate r of the dissolution reaction is implicitly related to a series of sequential elementary hydrolysis reactions by the affinity term (parallell elementary reactions require a different mathematical treatment) ("contextual affinity" [33]). The global glass dissolution affinity $A_{tot}=\Sigma_i \nu_i A_i$ can be measured calometrically, and may be estimated by solid solution hypotheses, but empirical saturation affinity terms A_{emp} seem not to be related to this value. Instead saturation of a silica end member plays a decisive role in slowing down glass corrosion rates ($A_{emp} \approx A_{SiO2}$) and the rate law often takes the simple from:

$$r = k_+ \cdot \left(1 - \frac{C_{Si,actuel\_solution\_conc.}}{C_{Si,saturation\_conc.}}\right)$$

Before silica saturation is reached (the capacitor in Fig. 1 is not loaded), the release of soluble elements, such as boron, follows the general trend of silica but, the composition normalized rate of Na and boron release is higher than of silica, because a certain quantity of silica is sorbed within the surface layer or is incorporated into secondary phases (smectites etc.). Nevertheless, a collective response of soluble elements such as Na and to saturation effects exists (tendence towards "congruent dissolution") indicating that also the release of these elements is controlled by A_{emp}. At Si-saturation, the release rate of the soluble elements slows down by some orders of magnitude (the capacitor in Fig. 1 is fully loaded). In long-term corrosion tests, releases of soluble elements, normalized to glass composition, were observed to become more than a factor of 10000 higher than those of silica [34].

Saturation of silica has another role in glass corrosion kinetics than for example saturation of Al or Fe. Often, due to release control by secondary phases, Al or Fe reaches saturation concentration without influencing glass corrosion kinetics. In contrast, for slowing glass dissolution saturation must affect the primary and not secondary phases. There are some indications that, besides Si, other glass network former elements such as Al or Zr contribute to $A_{emp,}$ but it is clear that alkali elements and B do not contribute. Consequently, the equilibrium state for the network dissolution reaction does not represent an equilibrium with the glass phase, but with an altered silica rich and alkali and for borosilicate glasses as well as boron depleted surface region. This surface region is more stable than the glass and may be considered as protecting the pristine glass beneath

from dissolution. Since A_{tot} is still large when A_{emp} =0, a driving force for long term corrosion continues to exist. The protective effect of this surface region is of a quite different nature than the protective effect of surface layers of secondary alteration products, which are deposited on the glass surface. With secondary alteration products, the approach of silica saturation in solution is sometimes retarded by hindering diffusion of dissolved silica (diffusion resistance higher than corrosion resistance k_+ in Fig. 1). In contrast, with $A_{emp} \approx A_{SiO2}$, at saturation also $A_{SiO2} \approx 0$, and the long term corrosion affinity A_{tot}-A_{emp} is independent of silica concentration and is governed mainly by A_{alkali} and A_B. As the alkali depleted and silica rich surface region remains stable at saturation, penetration of reactants as well as release of alkali and boron from the glass beneath can occur only by diffusion. Experimental data indicate that water diffusion may be rate limiting [35].

It may be concluded that there is no unique affinity term and equilibrium state for glass corrosion. Instead, affinity terms and equilibrium state apply to certain steps and certain glass constituents in the overall irreversible dissolution reaction.

References

[1.] Grambow, B., Glastechn Ber. 56K (1983) 566-571.

[2.] Barkatt, A., P.B. Macedo, B.C. Gibson, C.J. Montrose, Mat. Res. Soc. Symp. Proc. 44 (1985) 3-14

[3.] Harvey, K. B.; Litke, C. D.; Larocque, A. B.", The dissolution of a simple glass. Part 4. Behavior in saturating and saturated systems", Phys. Chem. Glasses (1992), 33(2), 43-50 (1992)

[4.] Massard, Pierre, "Thermodynamic approach for dissolution phenomena. Kinetic aspects in an open system", Bull. Soc. Fr. Mineral. Cristallogr. (1977), 100(3-4), 177-84

[5.] Advocat, T.; Crovisier, J. L.; Fritz, B.; Vernaz, E., "Thermokinetic model of borosilicate glass dissolution: contextual affinity", Mater. Res. Soc. Symp. Proc. (1990), 176 (Sci. Basis Nucl. Waste Manage. 13), 241-8

[6.] Grambow, B. A general rate equation for nuclear waste glass corrosion Mater. Res. Soc. Symp. Proc. (1985), 44(Sci. Basis Nucl. Waste Manage.), 15-27

[7.] William L. Bourcier, Dennis W. Peiffer, Kevin G. Knauss, Kevin D. McKeegan, David K. Smith, "A Kinetic Model for Borosilicate Glass Dissolution based on the Dissolution Affinity of a Surface Alteration Layer", Lawrence Livermore National Laboratory, Report No.: UCRL-101107 (1989)

[8.] L.L. Hench, J. Non-Cryst. Solids 25, (1977) 343-369

[9.] E.C. Ethridge, D.E. Clark und L.L. Hench, Phys. Chem. Glasses 20 (1979) 35-40

[10.] G.N. Greaves, A. Fontaine, P. Lagarde, D. Raoux and S.J. Gurman, Nature 293, 611 (1981)

[11.] D.A. McKeown, G.A. Waychunas, und G.E. Brown, J. non-cryst. Solids, 74, 345 (1985)

[12.] N. Binsted, G.N. Greaves, C.M.B. Henderson, J. Phys. (Paris) C8, 18 (1986)

[13.] A.Smekal, Glastechn. Ber. 22, 278 (1949)

[14.] G. N. Greaves, K.L. Ngai, J. non-cryst. Solids 192-193, 405 (1995)

[15.] J. A. Topping und J.O. Isard, Phys. Chem. Glasses, 12, 145 (1971)

[16.] Schröder, H. Glastechn. Ber. 26 (1953) 91-97

[17.] Zagar, K., Schillmöller, A. Glastechn. Ber. 33 (1960) 109-116

[18.] Douglas, R.W., T.M. ElShamy, J. Amer. Cer. Soc. 50 (1967) 1

[19.] Dormemus, R.H., J. Non-Cryst. Solids 19 (1975) 137-144

[20.] H. Schnatter, H. Doremus, W.A. Lanford, J. Non-Cryst. Solids **102**, (1988) 11-18

[21.] Bunker, B.C., T.J. Headly and D.C. Douglas, Mat. Res. Soc. Symp. Proc. 32 (1984)

[22.] R.D. Aines, H.C. Weed, J.K. Bates, Mat. Res. Soc. Symp. Proc. (1986)

[23.] Ernsberger, F.M., Glastechn. Ber. 56K (1983) 963-968

[24.] Doremus, R.H., Y. Mehrotra, W.A. Lanford, C. Burman, J. Mater. Science 18 (1983) 612-622

[25.] Schäfer, J. und H.A. Schaeffer, U.S.C.V Conference, Brüssel, Juni 1984

[26.] Baucke, F. G. K., "Phosphate and fluoride error of pH glass electrodes. Erroneous potentials caused by a component of some membrane glasses", J. Electroanal. Chem. (1994), 367(1-2), 131-9

[27.] Sullivan, Terrence M.; Machiels, Albert J., "Influence of the electric double layer on glass leaching", J. Non-Cryst. Solids (1983), 55(2), 269-82

[28.] Landford W.A., K. Davis, P. Lamarche T. Laursen, R. Groleau, J. Non-Cryst. Solids 33 (1979) 249-266

[29.] Scholze, H., J. Am. Ceram. Soc. 60 (1977) 186

[30.] Smets, R.M.J., T.P.A. Lommen, Phys. Chem. Glasses, 23 (1982) 83-87

[31.] Bunker, B.C., G.W. Arnold und E.K. Beauchamp, J. Non-Cryst. Solids 58 (1983) 295-322

[32.] H. C. Helgeson, W. M. Murphy and P. Aagaard,Geochim. Cosm. Acta 48, 2405-2432 (1984)

[33.] T. Advocat, Thèse du doctorat, Université Louis Pasteur, Strasbourg , 1991

[34.] B. Grambow, W. Lutze, L. Kahl, H.Geckeis, E.Bohnert, A.Loida, P. Dressler, R.Pejsa, Commission of the European Union : EU 17114 EN (1997)

[35.] Grambow, B., W. Lutze, R. Müller; „Empirical Dissolution Rate Law for the Glass R7T7 Contacting Halite and Silica Saturated Solutions" Mater. Res. Soc. Symp. Proc. **257**, 143 (1992)

Experimental quantification of permeability change of the Fontainebleau sandstone during mineral dissolution

Jové, C.F., Oelkers, E.H., and Schott, J.

Laboratoire de Géochimie, CNRS-OMP-Université Paul Sabatier, 38 Rue des Trente-Six Ponts, 31400 Toulouse, France. E-mail: jove@lucid.ups-tlse.fr

Introduction

Knowledge of the chemical effects of fluids during flow through porous media is essential for the elucidation of mechanistic models aimed to predict the modification of porous rock physical properties during water-rock interaction. It is well known that in sedimentary basins rocks experience a succession of burial processes which include mineral/cement dissolution and precipitation, mineral recrystallization, and mechanical compaction. A large wealth of evidence from many studies characterizing diagenetic processes in sedimentary rocks suggest that all these are strongly influenced by fluid flow (Bjørlykke et al., 1989; Lasaga and Rye, 1993). Therefore, a comprehensive description of the evolution of permeability, porosity, and reactive surface area during reactive fluid flow deserves significant attention for the development and validation of predictive models aiming at characterizing the evolving physical properties of rock. Despite all the recent theoretical developments describing reactive flow through porous media (Lichtner, 1988; Lasaga and Rye, 1993; Steefel and Lasaga, 1994), only a very few number of studies concerning the experimental quantification of the temporal evolution of permeability, porosity, and reactive surface area during fluid-rock interaction have been carried out on natural porous rocks.

The present study reports flow-through experiments performed on natural Fontainebleau sandstone cores at 80°C using an aqueous NaOH solution as the percolating fluid. Our results show that *in situ* permeability increases with time consistent with a cubic law dependence on porosity aside from changes in reactive surface area.

Experimental Methodology

The percolation experiments were conducted on Fontainebleau sandstone cores from the Ile de France region near Paris, France. This sandstone is composed ~100% quartz grains of ~250 μm in diameter. The core dimensions are 2.2 cm in diameter, and 4 and 4.5 cm long depending on the runs. The percolation cell is composed of an externally-heated single-pass flow-through reactor equipped with a pressure transducer to measure differential pressures between the inlet and outlet end of the core and thus obtain *in situ* permeabilities according to Darcy's law at a constant fluid flow rate. The flow rates used in this study are 0.1 mL/min in the cores with porosities of 5.1 and 8.9%, and 1 mL/min for the sample with a porosity of 16.6%. The percolator cell also allows for the

application of confining pressures on the sample by enclosing the sandstone core within a rubber jacket at a constant confining nitrogen gas pressure of ~5-6 bars to avoid fluid flowing through the periphery of the sample. The input solution consisted of 0.1 Molar NaOH and pH 13 at 25°C (pH 11.4 at 80°C) prepared from a concentrated 1 Molar reagent-grade NaOH solution. Quartz dissolution rates increases in alkaline solutions allowing for measurable concentrations of Si in the outlet solutions and inducing significant changes in the rock's porosity and permeability in relatively short periods of time. Fluids were sampled daily for $SiO_2(aq)$ concentration and pH analyses. Solution viscosity was corrected at 80°C for determination of permeability using the formulations of Zaytsev and Aseyev (1992).

Results and Discussion

The temporal variation of permeability of the sandstone cores with porosities of 5.1% and 8.9% are depicted in figure 1a and 1b, respectively. The permeability data in both experiments was fitted using a simplified version of the equation after Walder and Nur (1984) based on the relationship between porosity and permeability,

$$\kappa = \kappa \left(\frac{\phi}{\phi} \right)^{n} \qquad (1)$$

where κ designates permeability, κ stands for the initial core permeability at the onset of the experiments, ϕ represents the initial core porosity, and ϕ refers to the core porosity incremented during the course of the experiment. The increments in ϕ are calculated from the outlet dissolved mass of Si per unit volume of rock. The exponent $\mathbf{n}$ is a constant which usually varies from 2 to larger values. In this study, the exponent $\mathbf{n}$ is taken as 3.8 after Doyen (1988) based on his image analysis of digitized petrographic thin sections for characterizing the porosity and permeability dependencies of the Fontainebleau sandstone. As shown in figures 1a and 1b, the exponent $\mathbf{n} = 3.8$ describes the experimental data very well showing a strong correspondence with a traditional cubic law dependence $\left(\kappa \propto \phi^{3}\right)$ for the permeability dependence on porosity. Notice that the relative increase in permeability (~2.2 times) with elapsed time is more accentuated in the sandstone core with 5.1% porosity. This is probably due to the tighter grain packing and a larger fraction of blocked throats in the connective pore-channel structure of the sandstone at this low porosity value (Bryant et al., 1993). In general, this implies that rocks with low porosities become more susceptible to permeability changes under continuous fluid flow. This is also evidenced in the samples with higher porosity. For example, the core with a porosity of 8.9% did not experienced any significant increment in permeability in the first ~1342 hours (52 days). Subsequently, the *in situ* core permeability increased approximate 1.3 times from its original value in the remaining of the experiment. This observation indicates that an initial stage of mineral dissolution involving mineral surface roughening and possible fine particle dissolution is restricted within the pore structure prior to a subsequent enlargement of connecting pore-throats and channels that can cause an increase in permeability. Moreover, this observation is

evidenced by the linear increase in reactive surface area with time in this core (Jové et al., 1998). The increase in core porosity due to quartz dissolution in the samples with 5.1% and 8.9% porosity is about 1 and 1.3%, respectively.

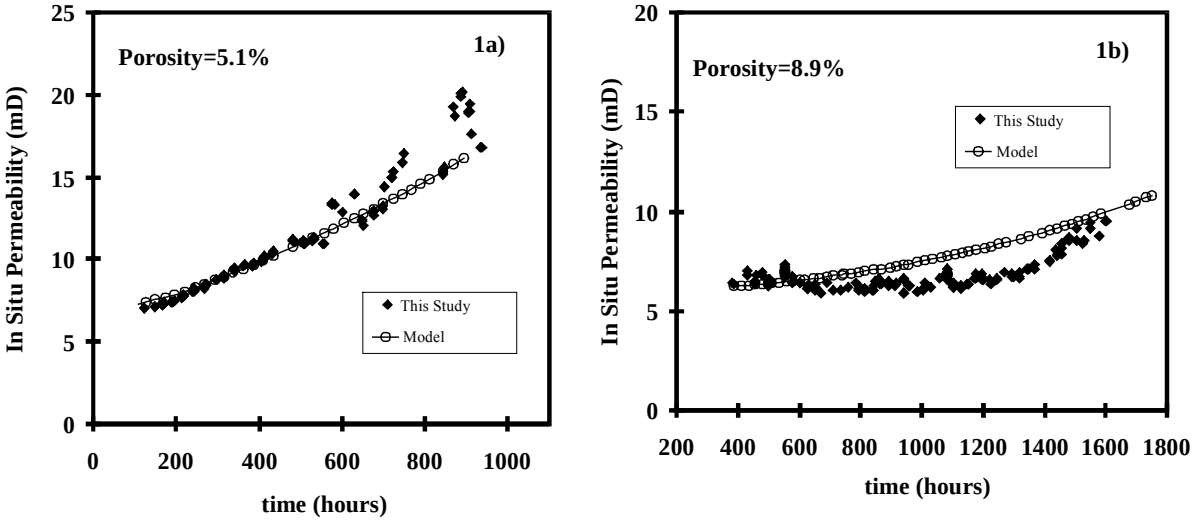

Figure 1: *In situ* permeability (solid diamonds) vs elapsed time. The solid line with open circles corresponds to the exponential law model of permeability dependence on porosity given by equation (1) with n = 3.8 as suggested by Doyen (1988) for the Fontainebleau sandstone (see text): a) core porosity = 5.1% and b) core porosity = 8.9%.

The results of this experimental study show that the effect of mineral dissolution on increasing rock permeability follow a porosity dependence that is more intensified on samples with low porosity. This observation has major implications on the prediction of porous rock physical properties during reactive transport. For example, in natural open systems where large mass transfer fluxes are common, the enhancement of porosity and permeability can greatly increase the rates of alteration processes affecting porous rocks. It is foreseen that these observations will be incorporated along with formulations used in reaction-transport models to predict more accurately the temporal evolution of rock flow properties during water-rock interaction.

References

Bjørlykke, K., Mogens, R., and Girish, S.C. (1989). *Geol. Runds.*, vol. **78**, 243-268.

Bryant, S., Cade, C., and Mellor (1993) *AAPG Bull.* **77**, 1338-1350.

Doyen, P.M. (1988). *J.G.R.*, **93**, 7729-7740.

Jové, C.F., Oelkers, E.H., and Schott, J. (1998) *Min. Mag.*, **62a**, 727-728.

Lasaga, A.C. and Rye, D.M. (1993). *Am. J. Sci*. **293**, 361-404.

Walder, J. and Nur, A. (1984) *J.G.R.*, **89**, 11539-11548.

Zaytsev, I.D. and Aseyev, G.G. (1992). *CRC Press Inc.* Boca Raton, Florida, 1773 pp.

Evaluation of the solid solution-aqueous solution equilibrium state for trace metals partitioned in the carbonate – porewater system of a natural sediment

Dimitrii A. Kulik and Michael Kersten

Geoscience Institute, Gutenberg-University, D-55099 Mainz, Germany
E-mail: michael.kersten@uni-mainz.de

Ion activity products calculated from measured total concentrations of dissolved trace metals in sediment-water systems often deviate from the solubility products (K_{SP}) of the respective pure solid phases. Trace metals, however, usually do not form pure minerals in nature, but rather are sorbed to other host minerals by substitution, forming solid solution – aqueous solution (SSAS) equilibria (Kersten and Böttcher, 1997). Such solid solution systems often display non-ideal mixing behavior of the end-members, which, together with differences in aqueous speciation and activity coefficients of the participating trace metals, produces complex non-linear relationships between measurable bulk compositions of the co-existing aqueous solution and solid phases, usually expressed in terms of "distribution coefficients", K_d. Further complications result from the influence of precipitation kinetics on trace metal incorporation into natural mineral phases, which is especially pronounced for carbonates (e.g., Morse and Bender, 1990; Rimstidt et al., 1998; Pokrovsky, this issue). The complex system behaviour makes it non-trivial to retrieve thermodynamic properties of solid solutions from experimental SSAS data and neccessitates consideration of non-equilibrium states, which imply that the metal partitioning behaviour may be also strongly affected by kinetic factors.

Unlike the many laboratory studies which all suffer from inherently short equilibration times in the range of weeks to months, we have studied an example of natural anoxic sediment-porewater system of the Gotland deep (central Baltic Sea), where pure authigenic Ca/Mn-bearing carbonates are encountered in distinct albeit thin sediment layers precipitated up to thousands of years B.P. (e.g., Neumann et al., 1997). This natural porewater - Ca-rhodochrosite system is viewed as a kind of a unique natural SSAS precipitation experiment alternative to the many short-term laboratory studies (e.g., Sternbeck, 1997; Böttcher, 1998; Rimstidt et al., 1998, McBeath et al., 1998).

Partitioning of a trace element (Tr) between a mineral of a major element (M) and aqueous solution is usually described by the distribution coefficient, D:

$$D = \frac{X_{Tr}}{X_M} \times \frac{m_M}{m_{Tr}} \qquad (1)$$

where X denotes the mole fraction in solid phase and m stands for the molality (moles in 1 kg H_2O) in aqueous phase. Theoretical equilibrium distribution constant, K_d, can be expressed in logarithmic form by the McIntire (1963) equation for divalent metal carbonates as

$$\log K_d = \log\frac{K_{MCO_3}}{K_{TrCO_3}} + \log\frac{\gamma_{Tr}}{\gamma_M} + \frac{-\Delta\mu}{2.303RT} \qquad (2)$$

where the first term on the right side is the ratio of thermodynamic solubility products, the second term is the ratio of activity coefficients in aqueous solution, and $\Delta\mu$ stands for the difference between the chemical potential $g^0_{TrCO_3}$ of $TrCO_3$ in a pure crystal of $TrCO_3$ and its chemical potential μ_{TrCO_3} as a solid solution component in MCO_3 (Rimstidt et al., 1998). From this definition and thermodynamic theory it follows that

$$\Delta\mu = \mu_{TrCO_3} - g^0_{TrCO_3} = RT\left(\ln X_{TrCO_3} + \ln\lambda_{TrCO_3}\right) \qquad (3)$$

where λ_{TrCO_3} is the rational activity coefficient of trace end-member in solid solution. Equation (3) is strictly true only if $X_{TrCO_3} << 1$ and $X_{MCO_3} \approx 1$. The more general equation, substituting the rightmost term in Eqn.(2), would be

$$\frac{-\Delta\mu}{2.303RT} = \log\frac{X_{MCO_3}}{X_{TrCO_3}} + \log\frac{\lambda_{MCO_3}}{\lambda_{TrCO_3}} \qquad (4)$$

Comparison of Eqns. (3) and (4) shows that in cases when $X_{MCO_3} < 1$, or $\lambda_{MCO_3} > 1$, Eqn. (2) may bias the theoretical values of K_d.

It is a well established experimental fact that the partition of trace elements in carbonate minerals is affected by kinetic factors such as super-saturation and precipitation rate and is therefore stronger or weaker than predicted by theoretical K_d, or $D_{Tr} \neq K_{d,Tr}$ (Böttcher, 1998; Rimstidt et al., 1998 and refs. therein). Rimstidt et al. (1998) plotted a number of empirical distribution coefficients ($\log D_{Tr}$) for divalent trace elements in calcite and siderite versus $\log(K_{MCO_3}/ K_{TrCO_3})$ and obtained linear regressions of the form

$$\log D = \alpha\log\frac{K_{MCO_3}}{K_{TrCO_3}} + \beta \qquad (5)$$

with $\alpha \approx 0.6 \pm 0.1$ and $\beta = 0.2 \pm 0.11$ for Mn, Zn, Cu, Co, Cd, Fe, and Mg in $CaCO_3$; $\beta \approx -1.66$ for Sr, Ba and Ra in $CaCO_3$; and $\beta = 0.61 \pm 0.36$ for Mn, Co, Ca, Ni and Mg in siderite ($FeCO_3$). Comparison of Eqn. (5) with Eqns. (1) and (2) suggests that the values of β (which have a large scatter of about ± 50%) can be

related to different solid solution behavior of trace carbonate end-members. An equilibrium distribution should result in a slope $\alpha = 1$, hence the value of $\alpha = 0.6$ retrieved for calcite can be attributed to the impact of precipitation kinetics onto incorporation of trace elements in a "solution-boundary-related process". Rimstidt and coworkers infer a general trend where for elements with $K_d > 1$, the experimental D values are smaller, and for elements with $K_d < 1$, the D values are larger than the equilibrium distribution constants. The D values would approach closer to theoretical K_d values with decreasing precipitation rates, which could be expected when shifting from laboratory to natural conditions. No such diagrams are yet available for trace metals in rhodochrosite ($MnCO_3$). However, it is known that at the same super-saturation ($5 < \Omega < 50$), precipitation rates of rhodochrosite are 4000 to 5000 times slower than that of calcite (Sternbeck, 1997), probably due to different rate-controlling mechanisms. Hence, we can expect that the regressed α coefficient in Eqn. (5) for rhodochrosite will be closer to unity than that for calcite.

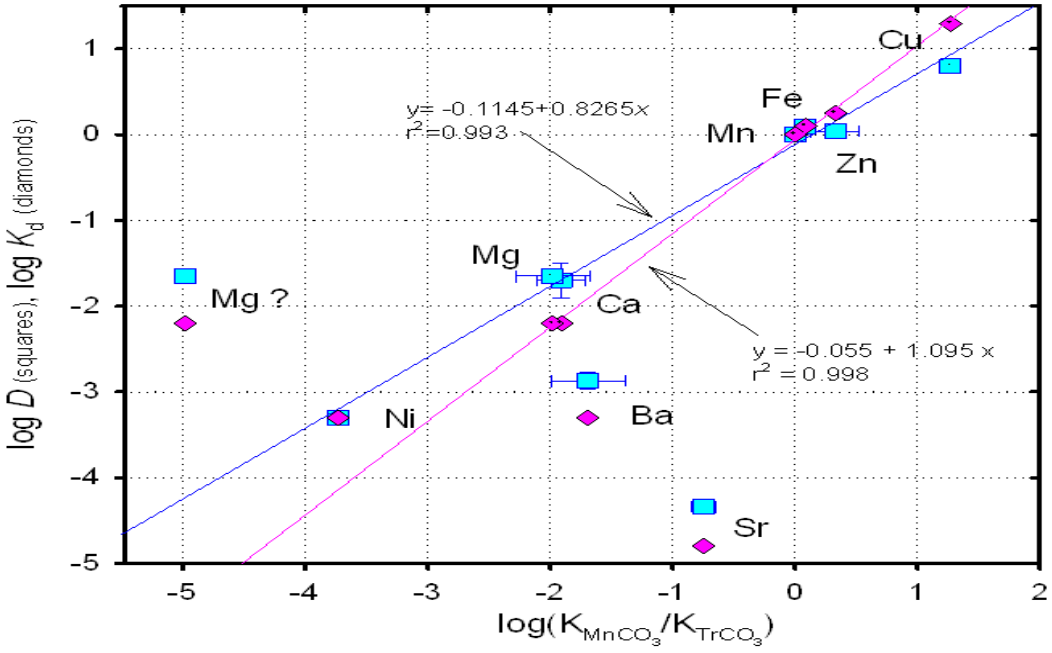

Fig. 1. Rimstidt plots of K_d and D fitted or predicted for authigenic rhodochrosite in Gotland deep sediment.

Fig. 1 shows such a "Rimstidt plot" using our dataset for natural authigenic rhodochrosites and porewater in the Gotland Deep sediment. D values obtained from the porewater-sediment data accounting for the aqueous speciation and non-ideal solid solution behaviour by the Gibbs energy minimization approach allowed us to construct this $\log D - \log(K_{MnCO_3}/K_{TrCO_3})$ diagram (details to be published by Kulik et al., 1999). The data points for the various elements show a very good correlation

(r = 0.996) with a positive linear regression slope of 0.83 and an intercept of –0.11, except for the Mg data point based on a frequently reported lower pK_{SP} = 5.1 instead of the more relevant pK_{SP} = 8.1, but also excluding for the Ba and Sr data points. Both the latter elements do not fit to this regression due probably to the crystallochemical incompatibility of those larger cations with the rhombohedral carbonate lattice. This slope is greater than that of 0.6 found by Rimstidt et al. (1998) for calcite and siderite from laboratory experiments which can be readily explained by a closer approach to equilibrium in the natural rhodochrosite-porewater system. Note that *D* values for Zn, Ni and Cu are quite compatible to that regression. Another set of points on Fig. 1 (diamonds) correspond to (non-ideal) thermodynamic values of K_d obtained from Lippmann plots at respective mole fractions of trace end-members in Mn-Tr binaries. Regression of K_d points for Mn, Ca, Fe, Mg, Zn and Cu results again in a very good correlation with an intercept of as low as –0.055 and a slope of 1.095, close to the theoretical unity slope expected for equilibrium distribution constants, i.e. evidencing SSAS near-equilibrium conditions for this complex carbonate system. We recommend therefore to use Rimstidt plots in any such experimental study of metastable solid solutions before claiming that the parameters retrieved (such as Gibbs energies of mixing, e.g. McBeath et al., 1998) are representing real thermodynamic equilibrium values. Our consistent results encouraged us to apply this approach also to other even more complex SSAS systems particularly relevant to environmental engineering such as those describing S/S of trace metals and radionuclides in cementitious systems (e.g., the Tr-CSH system).

References

Böttcher,ME (1998): Manganese(II) partitioning during experimental precipitation of rhodochrosite-calcite solid solutions from aqueous solutions. Mar. Chem. 62, 287-297.

Kersten,M; Böttcher,ME (1997): Geochemische Modellierung von Partikel/Wasser-Wechselwirkungen. Geowissenschaften 15, 34-39.

Kulik, DA; Kersten, M; Heiser, U; Neumann, T (1999): Metastable SSAS equilibriainvolving authigenic rhodochrosites in Baltic Sea sediments: Application ofGibbs energy minimization and Lippmann diagrams. Aquat. Geochem. (submitted).

McBeath,MK; Rock,PA; Casey,WH; Mandell,GK (1998): Gibbs energies of metal-carbonate solid solutions: Part 3. The $Ca_xMn_{1-x}CO_3$ system at 298 K and 1 bar. Geochim. Cosmochim. Acta 62, 2799-2808.

McIntire,W (1963): Trace element partition coefficients - a review of theory and applications to geology. Geochim. Cosmochim. Acta 27, 1209-1264.

Morse,JW; Bender,ML (1990): Partition coefficients in calcite: Examination of factors influencing the validity of experimental results and their application to natural systems. Chem. Geol. 82, 265-277.

Neumann,T; Christiansen,C; Clasen,S; Emeis,KC; Kunzendorf,H (1997): Geochemical records of salt-water inflows into the deep basins of the Baltic Sea. Cont. Shelf Res. 17, 95-115.

Rimstidt,JD; Balog,A; Webb,J (1998): Distribution of trace elements between carbonate minerals and aqueous solutions. Geochim. Cosmochim. Acta 62, 1851-1863.

Sternbeck,J (1997): Kinetics of rhodochrosite crystal growth at 25 ^{o}C: The role of surface speciation. Geochim. Cosmochim. Acta 61, 785-793.

Distribution of Uranium(VI) on biotite surfaces

G. Mainka, T. Zorn, T. Arnold, G. Bernhard

Forschungszentrum Rossendorf, Institute of Radiochemistry
P.O.-Box 510119, D-01314 Dresden, Germany; mainka@fz-rossendorf.de

Experimental

Biotite specimen (mica, 2*3*0,5 cm pieces) [K $(Mg, Fe, Ti, Al)_3$ $(AlSi_3O_{10})$ $(OH, F)_2$] were immersed for 48 hours in 0.1M sodium perchlorate solution containing 25 ppm uranyl perchlorate at pH 6.5. To distinguish the difference between uranyl sorption and the perchlorate-altered surface, reference pieces were treated only with 0.1 M perchlorate solution. The samples were rinsed with deionized water and dried at 80° C for 1 hour.

SEM (Scanning-Electron-Microscopy) pictures were taken from the surface and the edge of the biotite of non-treated, the reference and the uranyl treated samples. EDX (Energy-Dispersive-X-ray-fluorescence-analysis) measurements were carried out at different points of the surface and at the edge of the samples.

Results

Fig. 1 shows an SEM image of a biotite surface. The surface shows edges, damages and particles that are distributed over the whole surface. With the detection of recoil electrons a distinction is possible between different elements and their distribution on surfaces. The lighter elements are depicted in lighter grey colors than the heavier ones. Fig. 2 shows a SEM picture of a biotite edge. The different layers are visible and the surface of the edge is very rough.

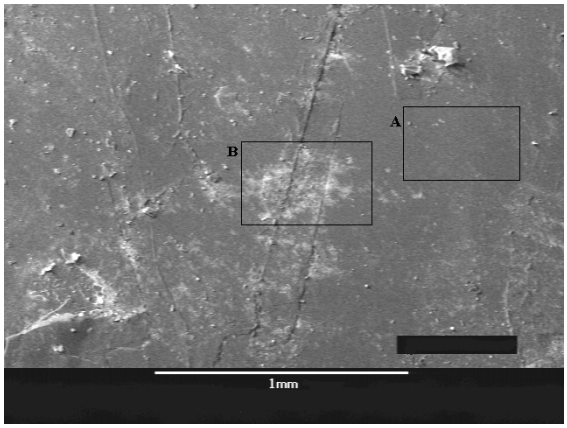

Fig. 1: SEM picture of a biotite surface 100xD

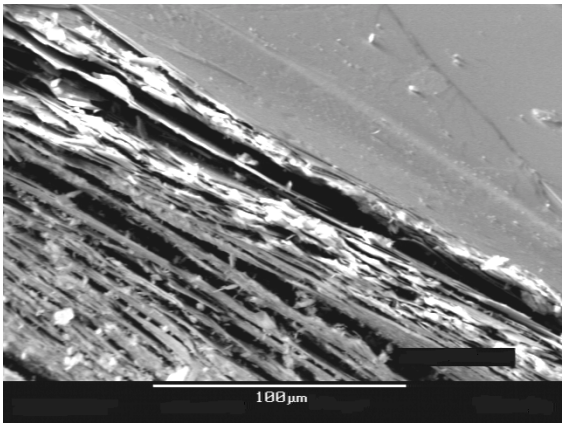

Fig. 2: SEM picture of a biotite edge 1000xD

The EDX detection on the surface in fig. 3 shows different elemental distribution for two selected surface areas (Fig. 1 box A and B). The EDX measurements of the uranyl treated sample shows a slightly lower potassium and magnesium and much higher sodium and chloride concentrat-ions on the surface than the non-treated sample. Uranium sorption could only be found with EDX measurements in the area of box B where the biotite surface is damaged.

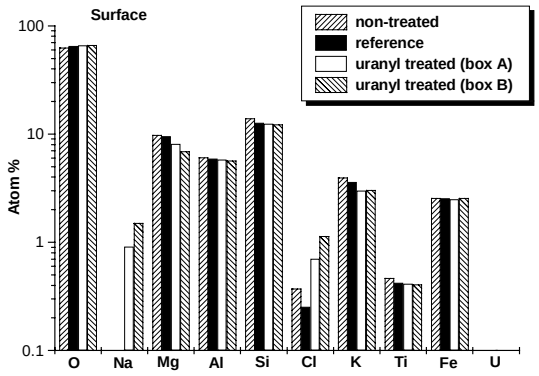

Fig. 3: EDX measurement of the biotite surface

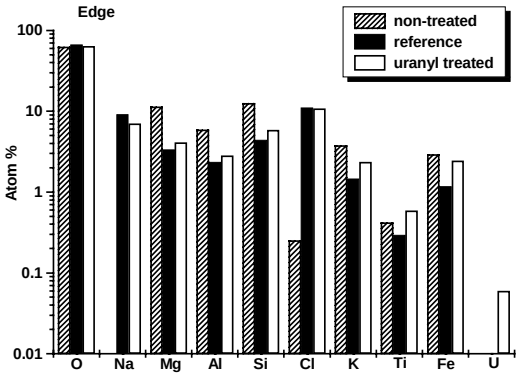

Fig. 4: EDX measurement of the biotite edge

Fig. 4 shows the elemental composition of the edge and their change by immersion into sodium perchlorate or uranyl solution. The sodium and the chloride concentrat-ions of the edge samples are much higher for the reference and the con-taminated sample than for the non-treated sample. The concentration of the other elements seems to be lower for the uranyl treated and the reference sample than for the non-treated sample.

Discussion

The comparison between EDX measurements at different points of the surface shows that uranium is preferably adsorbed either at the edge or at points where the surface is damaged. At this points the surface is more reactive.

The immersion of biotite in solution leads to a loss of interlayer potassium at the edge which is replaced by hydrated cations. This immediately leads to a modification of the octa-hedral sheet with loss of iron. This iron not necessarily remains in solution. It also can precipitate as amorphous or crystallized oxyhydroxide at the surface /1/. Iron-oxyhydroxide compounds are preferred adsorption sites for uranium(VI) /2/.

The adsorption of a sodium perchlorate layer may be the reason for the lower detection of the other elements on the edge.

References

/1/ Nahon, D.B. : Introduction to the petrology of soils and chemical weathering; Wiley and Sons 1991 p. 52

/2/ T. Zorn, T. Arnold, G. Bernhard, H. Nitsche: Sorption of uranium(VI) onto phyllite and its mineralogical constituents; FZR Annual Report 1997 p. 3

Acknowledgment

The authors are grateful to Prof. Dr. B.O. Kolbesen / J.W. Goethe-University Frankfurt/Main and his working group for the SEM pictures and EDX measurements.

Congruent dissolution of smectite in a flow-through system

V. Metz and J. Ganor

Department of Geological and Environmental Sciences
Ben-Gurion University of the Negev, P.O. Box 653, 84105 Beer Sheva, Israel.
E-mail volker@bgumail.bgu.ac.il

Introduction

Currently, there is much interest in understanding dissolution processes of smectite, because of its use as a backfill material in radioactive waste repositories and its manifold industrial and environmental usage. Still, little is known about the kinetics of smectite dissolution under acidic conditions. Batch experiments carried out at ultra-acidic conditions (lower than pH 1) resulted in incongruent digestion of smectite (Novak and Cicel, 1978; Luca and MacLachlan, 1992; Gates et al., 1996). Furrer et al. (1993) studied the dissolution kinetics of smectite at pH 1 to 4, using both batch and flow-through reactors. The Al/Si ratios in their experiments were different than that of the whole-rock smectite sample (0.37) and varied as a function of pH between 0.6 at pH 1 to 0.29 around pH 4. The main goal of the present study is to measure the congruent dissolution of smectite under acidic conditions (pH 2 to 3), 50°C and various degrees of saturation state.

Materials and Methods

Experiments were carried out with two natural samples of montmorillonitic smectite (SAz-1 and SWy-1; from the Source Clay Minerals Repository, University of Missouri). Montmorillonite mineral formulas derived from the whole rock analyses indicate unreasonably high Si contents: 8.0 or above 8.0 Si per $O_{20}(OH)_4$ unit. X-ray diffraction showed that sample SWy-1 contained traces of quartz and K-feldspar. Another silica phase was observed using IR spectroscopy (Van Olphen and Fripiat, 1979). Only amorphous silica was detected in sample SAz-1 (Breen et al., 1996).

The clay particle fraction of the samples was obtained using sedimentation technique. The fractionated smectite samples were pretreated for several months in a 0.001 M $HClO_4$ solution at 80°C. The samples were analyzed by XRF and XRD before and after pretreatment, and no significant change due to the $HClO_4$ treatment was observed. Dissolution experiments were performed using a flow-through reactor that was fully immersed in a water bath held at 50.0 ±0.02°C. Each experiment was composed of one to five stages. Experimental conditions were varied by changes in flow rate, initial mass, pH or adding various amounts of metasilicate to the input solution.

Results and Discussion

We performed 19 experiments (35 steady states) with smectite SAz-1, and two single-stage runs with smectite SWy-1. Two experiments were conducted with a non-fractionated and untreated SAz-1 sample. The results of these experiments were not significantly different than results of experiments done under the same conditions with pretreated SAz-1. Figure 1 shows the variation of the output pH and the output concentrations of aluminum and silicon as a function of time in a typical single stage experiment. In the beginning of each experiment the silicon concentration increased, reached a maximum after relatively short time and thereafter declined over a period of several hundreds hours until it approached a steady state. As long as the concentration of Si was high, Al concentration was close to zero. When Si concentration began to decrease, Al concentration increased until reaching a steady state. Al/Si ratio at steady state was within error the same for all 35 experiments of SAz-1 (Fig. 2). This Al/Si ratio (0.40±0.02) is significantly higher than the Al/Si ratio of the whole rock sample (0.35) (Table 1). Similarly, the Al/Si ratios at the two steady-state of sample SWy-1 are higher than the whole rock ratio (Table 1).

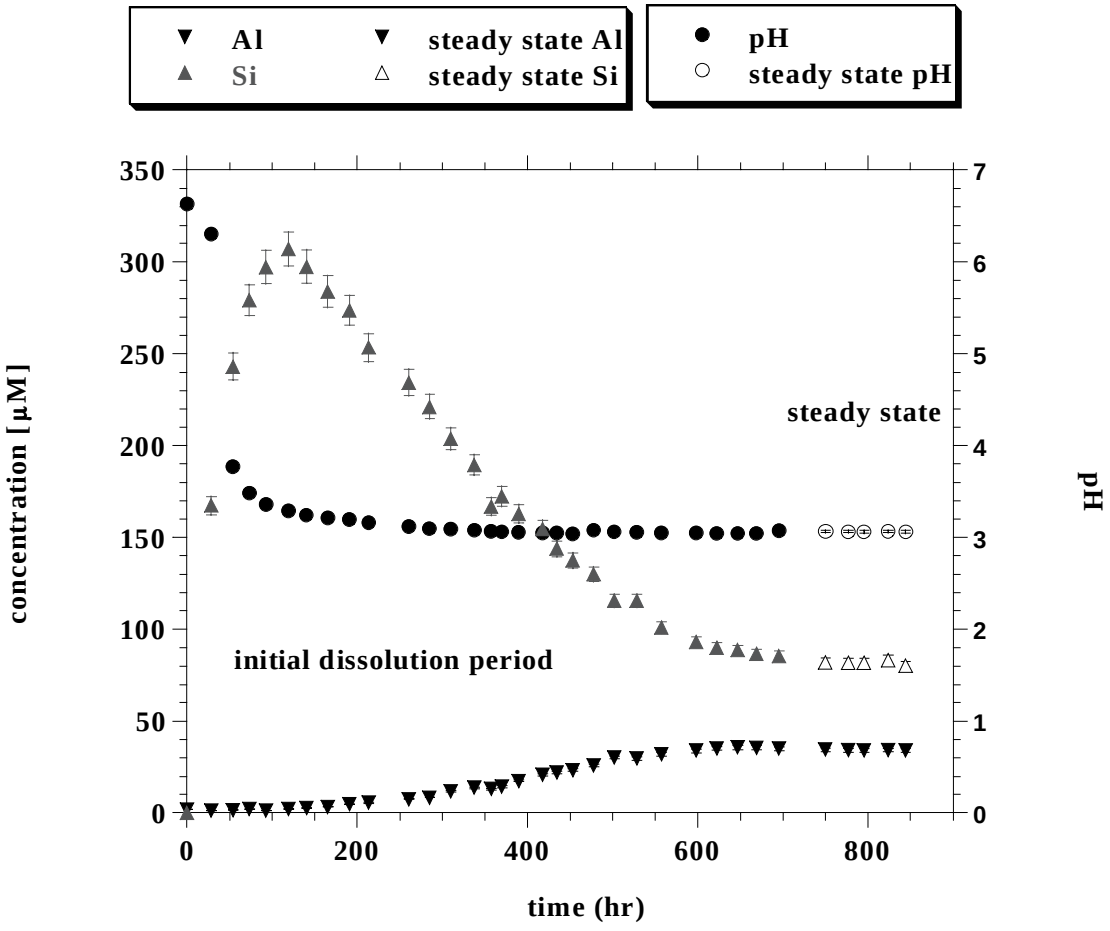

Figure 1: Variation of pH, Al and Si concentration as a function of time during a smectite dissolution experiment.

We suggest that the constant Al/Si release ratio in steady state in all experiments conducted with SAz-1 reflects a stoichiometric dissolution of a single mineral phase, i.e., smectite. The enhanced release of Si in the beginning of the experiment is explained by hydrolysis of a silica rich phase that dissolves faster than smectite, probably amorphous silica. Due to the high Si concentration in the initial stage of the experiment, the solution is close to equilibrium with respect to smectite dissolution reaction. As a result, smectite dissolution rate is very slow and hardly any Al is released into the solution. When the amount of amorphous silica is almost exhausted, the concentration of silicon decreases, and the solution becomes more undersaturated with respect to smectite. Consequently, dissolution of smectite is enhanced, and Al concentration increases. As the amorphous silica is completely consumed Al and Si concentrations approach a steady state. Assuming that the steady-state Al/Si ratio reflects the Al/Si ratio in the smectite and that the ratios of the other elements to Al in the whole-rock analysis are good proxies to these ratios in the smectite, the chemical composition of the smectite can be calculated:

SAz-1: $K_{0.02}Na_{0.01}Ca_{0.44}(Al_{2.71}Fe_{0.17}Mg_{1.38})(Si_{7.67}Al_{0.33}O_{20}(OH)_4)$

SWy-1: $K_{0.07}Na_{0.29}Ca_{0.18}(Al_{3.02}Fe_{0.40}Mg_{0.56})(Si_{7.88}Al_{0.12}O_{20}(OH)_4)$

Based on the above recalculated smectite formulas, two independent calculations of the total amount of excess SiO_2 and the amount of the fast dissolving silica phase may be conducted. By subtracting the amount of silica in the calculated smectite formula from that of the whole-rock analysis we calculated that sample SAz-1 contains 8 wt.% and SWy-1 9 wt.% of total excess SiO_2 that is not part of the smectite formula (Table 1). The amount of the fast dissolving (amorphous) silica phase in the whole rock sample is calculated as follow. We integrated the amount of aluminum and silicon that was released to solution before steady-state. The amount of silicon released as a result of smectite dissolution during this period is calculated from the amount of Al released, based on the stoichiometry of the above recalculated smectite formula. This amount of Si is subtracted from the total integrated amount of released silicon. The resulting molar amount of silicon is the amount of silica that dissolves faster than smectite (Table 1).

	SAz-1	**SWy-1**
Al/Si whole rock - raw sample	0.34	0.37
Al/Si whole rock - pretreated sample	0.35	0.35
Al/Si at steady state	0.40 ± 0.02	0.40
total amount of excess SiO_2	8 ± 3 wt.%	9 wt.%
amount of fast dissolving silica phase	8 ± 1 wt.%	5 wt.%

Table 1: Al/Si ratios of smectite samples and estimation of excess silica content in whole rock sample.

In case of SAz-1 the estimate of the total percentage of excess SiO_2 (8±3) is the same as that of the fast dissolving silica phase (8±1). This is in agreement with XRD and IR observations that SAz-1 contains only amorphous silica as an accessory phase. For SWy-1 on the other hand, the amount of total excess SiO_2 (9%) is almost twice than that of the fast dissolving silica phase (5%). Sample SWy-1 contains two different silica phases: quartz that is observed using XRD and IR, and another silica phase that is observed only using IR spectroscopy. The dissolution rate of quartz is much slower than that of smectite and therefore it is not dissolving significantly during the dissolution experiments. We explain the fast release of silicon during the beginning of the dissolution experiments of sample SWy-1 by dissolution of the other silica phase.

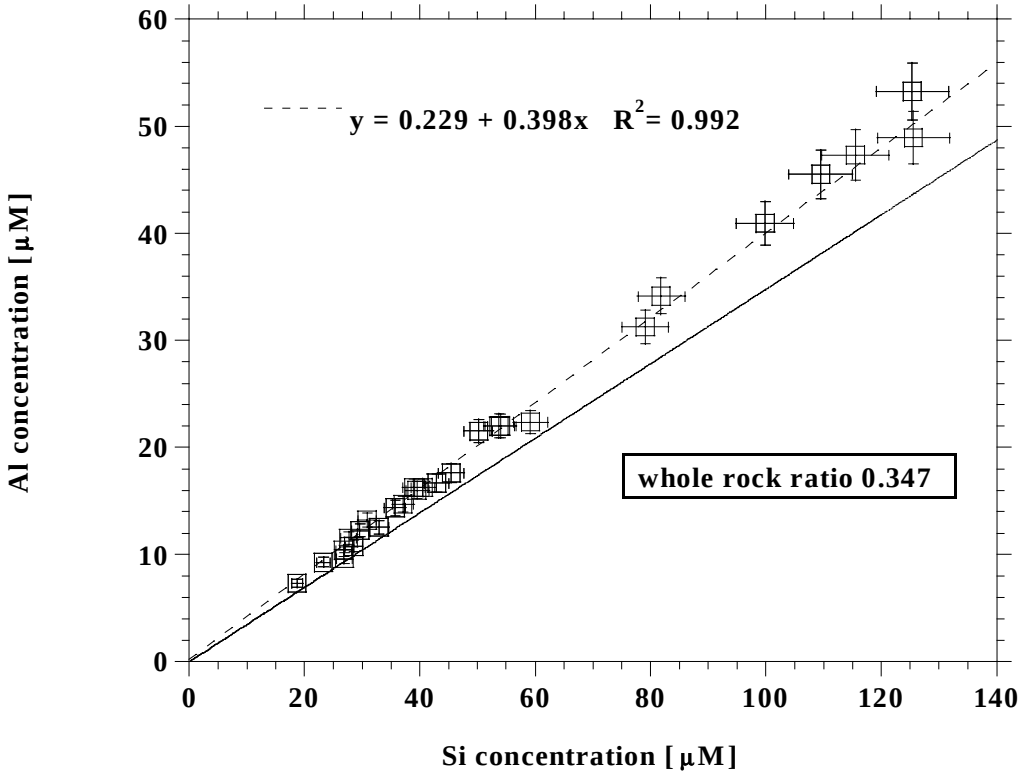

Figure 2: Al/Si ratio of SAz-1 dissolution at steady state. The dashed line is deducted from a regression of the steady states, whereas the solid line shows the Al/Si ratio of the whole rock analysis.

Conclusions

We conducted flow-through dissolution experiments of smectite at 50°C and acidic conditions. Congruent dissolution of smectite is obtained at steady state, after an initial dissolution period in which a silica phase is dissolved. The release of silicon from this silica phase change the degree of saturation with respect to smectite dissolution and consequently, the smectite is dissolving slowly in the beginning of the experiments.

Using the Al/Si ratio at steady-state, the whole-rock composition of the sample and the excess amount of silicon released during the beginning of the experiments, we calculated both the total amount of excess SiO_2 and the amount of the fast dissolving silica phase. This study shows that purification of bentonite samples from phases dissolving faster than smectite can be monitored by means of the flow-through technique.

References

Breen, C., Zahoor, F.D., Madejova, J., and Komadel, P. (1997): Characterization and catalytic activity of acid-treated, size-fractionated smectites. J. Phys. Chem. B 101, 5324-5331

Furrer, G., Zysset, M. and Schindler, P.W. (1993): Weathering kinetics of montmorillonite: Investigations in batch and mixed-flow reactors. In: D.A.C. Manning, P.L. Hall and C.R. Hughes (eds.): Geochemistry of Clay-Pore Fluid Interactions. Min. Soc. Series 4, 243-262

Gates, W.P., Madejova, J., Janek, M. and Komadel, P. (1996): Spectroscopic study of hectorite dissolution in HCl. Acta Universitatis Carolinae Geologica 38, 183-191

Luca, V. and MacLachlan, D.J. (1992): Site occupancy in nontronite studied by acid dissolution and Moessbauer spectroscopy. Clays Clay Min. 40, 1-7

Novak, I. and Cicel, B. (1978): Dissolution of smectites in hydrochloric acid: II Dissolution rates as a function of crystallochemical composition. Clays Clay Min. 26, 341-344

van Olphen, H. and Fripiat, J.J. (1979): Data handbook for clay minerals and other non-metallic minerals. Pergamon Press

The chemical long-term behaviour of cement based materials in highly salinar solutions

Th. Meyer and H.-J. Herbert

Gesellschaft für Anlagen- und Reaktorsicherheit (GRS) mbH,
Theodor-Heuss-Str. 4, 38122 Braunschweig, Germany

The German concept for the final disposal of radioactive and hazardous wastes in salt formations includes the use of technical barriers like sealing and backfilling materials, which are partially based on cement. For that reason the safety assessment of the repository system implies detailed knowledge of the geochemical behaviour of cement and concrete in the salt-solution environment. In the case of brine intrusion in the repository, the cemented wastes show a significant change in their structure. The changes result in dissolution and precipitation reactions, effecting a change in the solution composition and the brines pH.

The long-term stability of a cemented coal fly ash in highly salinar solutions was investigated by means of a cascade experiment, a time accelerating leaching experiment, and by the geochemical modelling of the observed reactions. The employed leaching experiment was developed in the GRS specifically for the boundary conditions of underground repositories in salt formations.

The investigated material was a mixture of pit coal fly ash, Portland cement and NaCl-solution. It was leached with an IP21 solution, a highly salinar salt-solution in equilibrium with the salt minerals halite, carnallite, sylvite, kainite and polyhalite. Such solutions are very likely to occur in flooded old potash mines which are used in Germany as repositories. During the experiment that goes on for several month the temperature was kept constant and evaporation was excluded. The grinding of the cemented material led to an increased material surface and thus a time accelerating effect was obtained. The experiment was conducted in several steps towards the thermodynamical equilibrium between the leaching fluid and all involved phases. In each step the resulting chemical composition of the leaching solution was determined as well as the dissolved and precipitated phases.

The experimentally observed reaction path was modelled using the computer code EQ3/6 and the thermodynamical database of Harvie, Möller, Weare (1984) for the seawater system. The solubility data used for the concrete phases were those published by Reardon (1990) and Revertegat et al. (1997).

In a first step to simulate the corrosion of cemented materials the dissolution of $Ca(OH)_2$, a main component in Portland Cement, was modelled, Kienzler (1998). In the second step the chemical composition of the cemented fly ash was defined as a special reactant and its reaction with IP21 solution modelled.

A good agreement between experimental data and the modelling results was obtained. Thus the mineral and volume changes during each step of the reaction could be quantified. By adopting a diffusion model for the reaction kinetics it was possible to attach a time scale to the reaction path. Whereas the chemical part of the reaction path is well known the time frame involved is dependant on the model assumptions which still must be confirmed. The employed experimental and modelling tools have proved to be suitable for the demanding task. We conclude that the long-term behaviour of cement based materials in salt formations can be predicted.

References

Harvie, C. E., Møller, N. and Weare, J. H. (1984): The prediction of mineral solubilities in natural waters: the Na-K-Mg-Ca-H-Cl-SO_4-OH-HCO_3-CO_3-CO_2-H_2O system to high ionic strengths at 25°C. - Geochimica et Cosmochimica Acta, v. 48, 723 - 751.

Reardon, E.J. (1990): An ion interaction model for the determination of chemical equilibria in cement/water systems, Cement and Conrete Research, 20, 175-192.

Revertegat, E.; Adenot, F.; Richet, C.; Wu, L.; Glasser, F.P.; Damidot, D.; Stronach, S.A. (1997): Theoretical and experimental study of degradation mechanisms of cement in the repository environment, Report EUR 17642 EN.

Kienzler B. (1998): Geochemische Modellierung der Korrosion von zementierten Abfallprodukten in Salzlösungen, FZKA 6046.

Heterogeneous nucleation and growth kinetics of clays on mineral substrates

Kathryn L. Nagy

co-authors in alphabetical order:
Donald J. Beno, Laurent Charlet, Randall T. Cygan, Paul Fenter, Robert J. Finch, John M. Hanchar, Alain Manceau, Michel Schlegel, and Neil C. Sturchio

kathryn.nagy@colorado.edu, Department of Geological Sciences, Campus Box 399, University of Colorado, Boulder, CO 80309-0399, U. S. A.

Introduction:

Observations of mineral textures in soils, sediments, and sedimentary rocks show that clay minerals with sheet structures frequently nucleate and grow on other mineral surfaces (e.g., Banfield and Barker, 1994). The relationship between substrate and overgrowth may be topotactic, epitaxial, or random and is related to the source of constituents for the clays. Both a dissolving mineral substrate and the solution it is in contact with can provide the components necessary for clay growth. If this is the case, then nucleation and growth kinetics will depend on a combination of reactions that occur at different saturation states with respect to the reacting solids. In this abstract, I summarize some recent work performed with a number of collaborators (Nagy et al., 1999; Manceau et al., 1999; Hanchar et al., 1999) on identifying and quantifying aspects of the nucleation and growth kinetics of clays on mineral substrates. I will discuss comparison of growth rates of gibbsite on gibbsite, kaolinite, and muscovite substrates, and the nucleation of trioctahedral Co-bearing clays on quartz. The data provoke a more detailed examination of the meaning of reactive surface area and demonstrate how kinetic rate measurements must be incorporated with microscopic surface analyses, especially for situations close to equilibrium.

Gibbsite Nucleation and Growth on Gibbsite, Kaolinite, and Muscovite

Gibbsite was selected as the initial phase for study in a broader investigation of growth kinetics of sheet-silicate clays on other sheet-silicate mineral substrates. Experiments were conducted at 80°C, pH 3 using single-pass stirred-flow reactors. Solutions were supersaturated with respect to gibbsite using reagent grade $AlCl_3$-HCl solutions. Saturation states were determined using the thermodynamic model described in Nagy and Lasaga (1992) which is based on the Al thermodynamic data of Palmer and Wesolowski (1992) and Wesolowski (1992), and is also fully consistent with the more recent critical synthesis of thermodynamic data for aqueous aluminum by Pokrovskii and Helgeson (1995). Substrates for growth were either mineral powders (gibbsite (Nagy and Lasaga, 1992) and kaolinite) or single 1 cm^2 sheets of muscovite (Nagy et al., 1999). Growth rates on the mineral powders were determined by the steady-state change in Al concentration

between the inlet and outlet solutions of the reactor (Nagy and Lasaga, 1992). Growth rates on muscovite were determined by measuring the volume of crystals that formed on the muscovite surface using three-dimensional images of surface topography obtained by Tapping Mode Atomic Force Microscopy (TMAFM). X-ray diffraction (XRD) patterns of solid products from the kaolinite powder substrate experiments were obtained using a rotating anode X-ray diffractometer and confirmed that the precipitate was gibbsite. The XRD patterns also were used to quantify the precipitate based on the method of Klug and Alexander (1974).

Results show that growth rates for gibbsite obey one function of saturation state on all three mineral substrates provided "reactive" surface area is evaluated separately for each substrate (Fig. 1). Rates (in units of mol m^{-2} sec^{-1}) obey a linear function of saturation state given by $Al^{3+} + 3H_2O = Al(OH)_3 + 3H^+$, and R, T, Q, and K have their usual meanings.

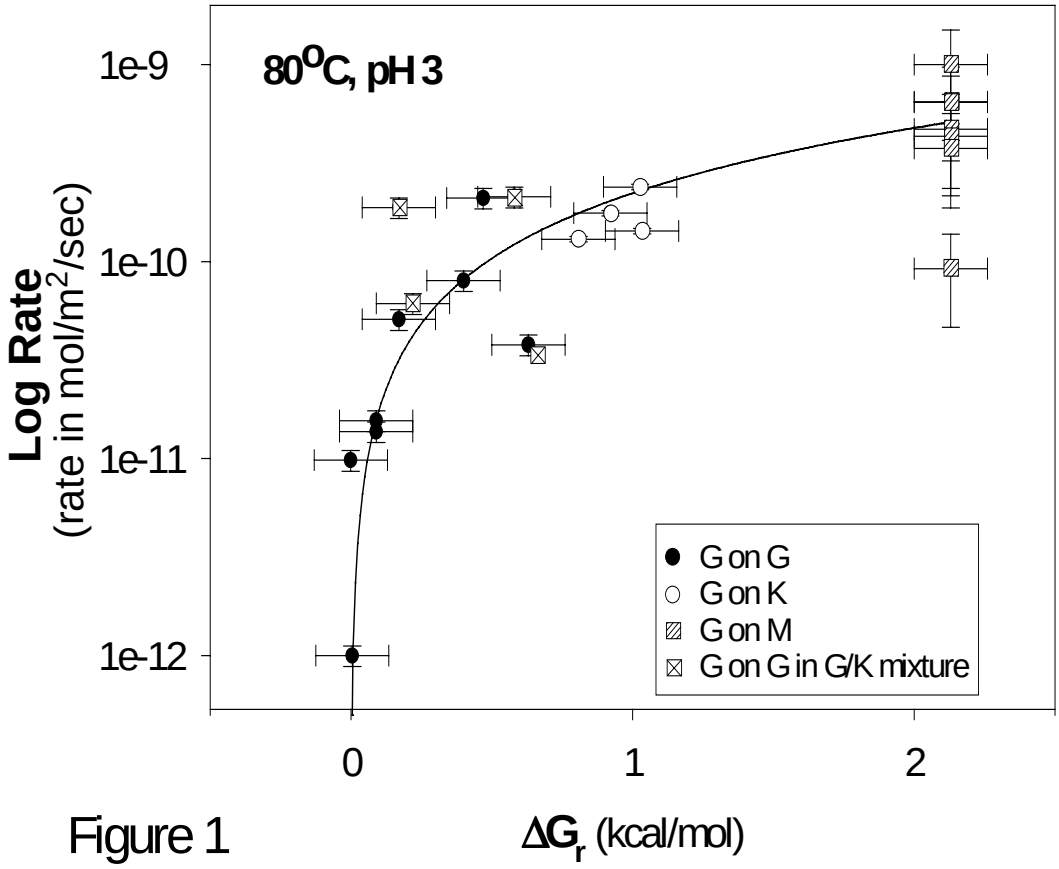

Figure 1

Rates shown in Figure 1 were calculated using the full BET surface area (3 point N_2) for gibbsite (G), 8% of the BET surface area for kaolinite (K), and the geometric basal surface area from TMAFM images for muscovite (M). Included are data for gibbsite growth on gibbsite powders (Nagy and Lasaga, 1992; solid circles) and on mixed gibbsite and kaolinite powders (Nagy and Lasaga, 1993; "crossed" squares).

Figure 2 shows the intensity ratio of the gibbsite XRD signal vs. mass fraction of gibbsite for gibbsite-kaolinite mixed-powder standards (solid circles) and experimental run products (KG designations) (Hanchar et al., 1999). In all experiments, the amount of gibbsite determined by XRD was less than or equal to that determined from the solution compositional changes (indicated by x-axis coordinates).

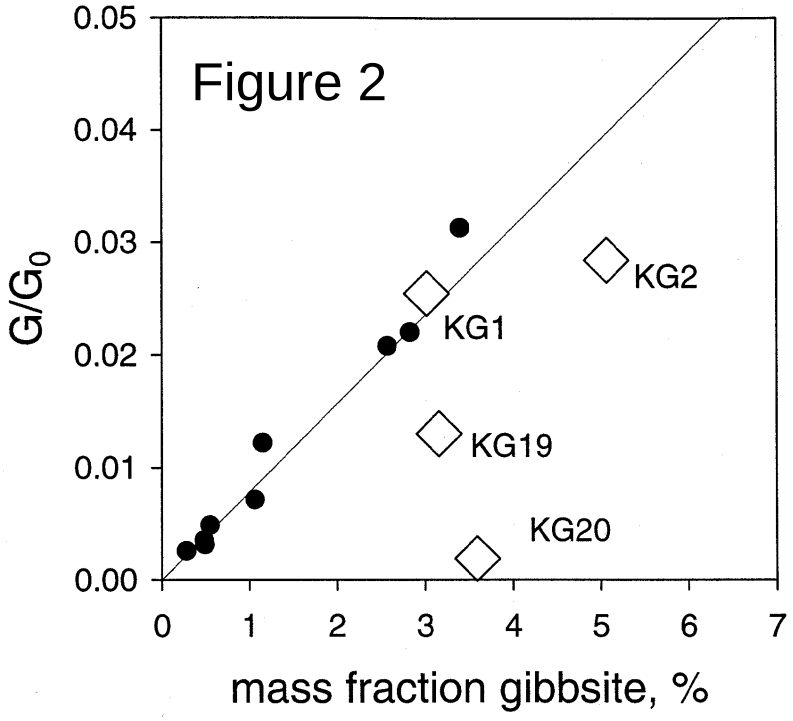

The morphology of gibbsite crystals that formed on the muscovite included clusters of intergrown crystallites (Fig. 3a), small elongated crystallites oriented in a hexagonal pattern reflecting the basal plane molecular structure of the phyllosilicate, and areas of "thin films" with hexagonally-shaped edges (Fig. 3b). The rate results indicate that the density of nucleation sites on the three substrate surfaces is different. The nucleation site densities of gibbsite on gibbsite and muscovite appear to be similar and in direct proportion to the BET and geometric surface areas, respectively. In contrast, the nucleation site density on kaolinite is much less, and is approximately 10% of the BET surface area. The latter interpretation is based on (1) AFM measurements showing that about 20% of the surface area of kaolinite is edges (Brady et al., 1996; Sutheimer et al., in press) and (2) molecular modeling indicating that sorption of cations occurs preferentially at the Al-octahedral edge sites in low pH solutions (Cygan et al., 1998). The concentration of Al-octahedral edge sites would be 50% of the edge surface area, or ~10% of the total BET surface area. Nucleation and growth on the entire gibbsite BET surface area is consistent with protonation of all surfaces at approximately the same density in solution. The Si-tetrahedral basal surfaces of muscovite should not be protonated, but they contain instead a high surface charge arising from the isomorphous substitution of Al for Si in the tetrahedral sheet. This high permanent surface charge

and/or edge charge in shallow dissolution pits that may form on the basal surface may be controlling nucleation. Once nucleated, additional growth of gibbsite may occur both on the heterogeneous substrate as well as the neoformed gibbsite.

Figure 3

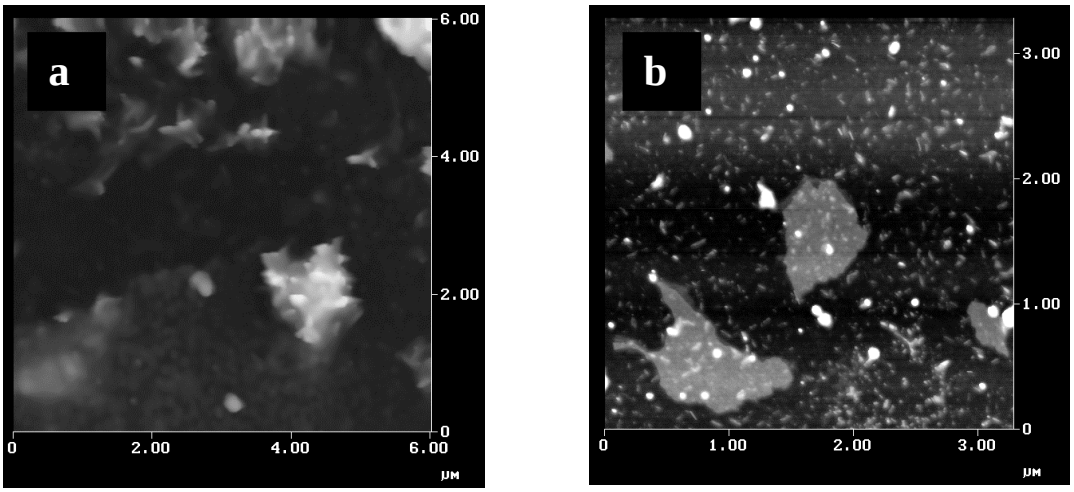

The discrepancy in quantity of gibbsite formed in some of the experiments on the kaolinite powder substrates obtained by solution composition and by XRD can be accounted for by considering the precipitate crystal size and shape. For example, a monolayer of gibbsite precipitating uniformly over the kaolinite surface would not be detectable using our XRD analytical conditions. The morphology of gibbsite precipitates on the muscovite surfaces, although obtained at a higher saturation state, indicate that uniform monolayer growth does not occur. The minimum measured thickness of the elongated crystallites and areas of "thin films" was 30-40 Å, or 3-4 unit cells. Thinner crystals approaching monolayer thickness may occur under solution conditions closer to equilibrium, which were not examined here.

Nucleation of Co-trioctahedral clays on quartz

Re-examination of published experimental and EXAFS data on Co-sorption onto quartz surfaces at room temperature (O'Day et al., 1996) coupled with theoretical determination of Co-clay solubilities and Si dissolution rates in similar Co-sorption experiments show that Co-sorption onto quartz surfaces in mildly alkaline solutions results in the formation of trioctahedral clay nuclei (Manceau et al., 1999). These conclusions were reached, in part, by detailed analysis and comparison of EXAFS spectra for Co sorbed on quartz, Co-hydroxide, and Co-kerolite ($Co_3Si_4O_{10}(OH)_2$). In addition, batch Co-sorption experiments were conducted and evolution of the full solution composition was monitored. Final solution compositions after up to 6 days of "sorption" time, indicated near-equilibrium conditions with respect to theoretically calculated solubilities (Tardy and Duplay, 1992) for Co-kerolite, Co-chrysotile ($Co_3Si_2O_5(OH)_4$), and Co-stevensite ($NaCo_{2.5}Si_4O_{10}(OH)_2$)

phases and approximately one order of magnitude undersaturation with respect to Co-hydroxide. The Co-clays are analogues of Mg-clays (kerolite, chrysotile, and stevensite) which can form naturally in alkaline lake environments (Jones and Galan, 1988).

The source of aqueous silica was the dissolving quartz surface. Rates of quartz dissolution were about 7 times higher than published rates at similar pHs. Various experimental factors can explain the higher rates. One possible interpretation is that Co may accelerate the dissolution rate at the same time clay nuclei are forming. The results indicate that nucleation on the quartz surface is not uniform and does not, at least at for these particular experimental compositions, prevent the quartz from continuing to dissolve. On the quartz surface both a dissolution and nucleation/growth reaction are occurring at variable and changing saturation states with respect to both the substrate and secondary phases.

Summary

New data on heterogeneous nucleation and growth of clays on mineral substrates demonstrate the importance of obtaining a better understanding of reactive surface area as well as simultaneous dissolution and growth reactions as a function of deviation from equilibrium. The role of the substrate in nucleating clays cannot be overlooked in interpreting the reaction kinetics.

Acknowledgments

Research support to KLN has been through the U. S. Department of Defense, Strategic Environmental Research and Development Program and to KLN, RTC, and NCS through the U. S. Department of Energy, Office of Basic Energy Sciences Geoscience Program.

References

Banfield J. F. and Barker W. W. (1994) Direct observation of reactant-product interfaces formed in natural weathering of exsolved, defective amphibole to smectite: Evidence for episodic, isovolumetric reactions involving structural inheritance. Geochimica et Cosmochimica Acta 58, 1419-1429.

Brady P. V., Cygan R. T., and Nagy K. L. (1996) Molecular controls on kaolinite surface charge. Journal of Colloid and Interface Science 183, 356-364.

Cygan R. T., Nagy K. L., and Brady P. V. (1998) Molecular models of cesium sorption on kaolinite. Chapter 18 in Adsorption of Metals by Geomedia (E. A. Jenne, ed.), Academic Press, 383-399.

Hanchar J. M., Nagy K. L., Fenter P., Finch R. J., Beno D. J., and Sturchio N. C. (1999) Quantification of minor phases in growth kinetics experiments with powder X-ray diffraction. American Mineralogist, in review.

Jones B. F. and Galan E. (1988) Sepiolite and palygorskite. In "Hydrous Phyllosilicates", Reviews in Mineralogy 19, 631-674. Mineralogical Society of America.
Klug H. P. and Alexander L. E. (1974) X-ray diffraction procedures (2nd edition), 966 p. John Wiley and Sons, New York.

Manceau A., Schlegel M., Nagy K. L., and Charlet L. (1999) Evidence for the formation of trioctahedral clay upon sorption of Co^{2+} on quartz. American Mineralogist, in review.
Nagy K. L. and Lasaga A. C. (1992) Dissolution and precipitation kinetics of gibbsite at 80ºC and pH 3: The dependence on solution saturation state. Geochimica et Cosmochimica Acta 56, 3093-3111.

Nagy K. L. and Lasaga A. C. (1993) Simultaneous precipitation kinetics of kaolinite and gibbsite at 80ºC and pH 3. Geochimica et Cosmochimica Acta 57, 4329-4335.

Nagy K. L., Cygan R. T., Hanchar J. M., and Sturchio N. C. (1999) Gibbsite growth kinetics on gibbsite, kaolinite, and muscovite substrates: AFM evidence for epitaxy and an assessment of reactive surface area. Geochimica et Cosmochimica Acta, in press.

O'Day P. A., Chisholm-Brause C. J., Towle S. N., Parks G. A. and Brown G. E. (1996) X-ray absorption spectroscopy of Co(II) sorption complexes on quartz (alpha SiO_2) and rutile (TiO_2). Geochimica et Cosmochimica Acta 60, 2515-2532.

Palmer D. A. and Wesolowski D. J. (1992) Aluminum speciation and equilibria in aqueous solution: Part 2. The solubility of gibbsite in acidic sodium chloride solutions from 30 to 70ºC. Geochimica et Cosmochimica Acta 56, 1093-1111.

Pokrovskii V. A. and Helgeson H. C. (1995) Thermodynamic properties of aqueous species and the solubilities of minerals at high pressures and temperatures: they system Al_2O_3-H_2O-NaCl. American Journal of Science 295, 1255-1342.

Sutheimer S. H., Maurice P. A., and Zhou Q. (1999) Dissolution of well and poorly crystallized kaolinites: Al speciation and effects of surface characteristics. American Mineralogist, in press.

Tardy Y. and Duplay J. (1992) A method of estimating the Gibbs free energy of formation of hydrated and dehydrated clay minerals. Geochimica et Cosmochimica Acta 56, 3007-3029.

Wesolowski D. J. (1992) Aluminum speciation and equilibria in aqueous solution: I. the solubility of gibbsite in the system Na-K-$AlOH_4$-OH-Cl from 0 to 100ºC. Geochimica et Cosmochimica Acta 56, 1065-1091.

A general mechanism for the dissolution of multi-oxide solids. Application to basaltic glass

Eric H. Oelkers [1] and Sigurdur R. Gislason [2]

[1] Laboratoire de Géochimie, Université Paul Sabatier, 38 rue des Trente Six Ponts, 31400 Toulouse, FRANCE. oelkers@cict.fr

[2] Science Institute, University of Iceland, Dunhagi 3, 107 Reykjavik, ICELAND. sigrg@raunvis.hi.is

The bulk of minerals and glasses found in nature are comprised of more than one type of metal-oxygen bond. The dissolution of these solids may proceed via the breaking of either one or more than one type of metal-oxygen bond depending on the structure of the solid, and the relative rates at which each of these bonds break. The relative rates at which the metal-oxygen bonds break can be deduced from two basic assumptions: 1) the relative rates of breaking any metal-oxygen bond is similar regardless of the identity of the mineral and 2) bonds of metals that are partially detached from the structure reacts faster than those that are fully attached. Consideration of the dissolution rates of single oxides and hydroxides minerals suggests that the relative rate at which metal-oxygen bond breaks follows the order

Na≈K>Ca>Mg> tetrehedrally coordinated Al>Si≈Fe(III)>octahedrally coordinated Al.

The breaking of each metal-oxygen bond of a multi-oxide solid apparently occurs via hydrogen exchange reactions that liberate the metal (M_i) according to

$$M_i< + \nu_i H^+ \longleftrightarrow M_i^{\nu_i+} + H_{\nu_i}< \quad (1)$$

where the symbol < indicates the species is attached to the surface and ν_i represents the charge of the i*th* aqueous metal ion. Dissolution proceeds via the sequential equilibration of the metal-hydrogen exchange reactions in the order of their relative reaction rates until no further viable structure remains. As the last of these sequential exchange reactions destroys the structure it cannot equilibrate, and is thus irreversible. By analogy with the dissolution of single oxides seems likely that each exchange reaction itself consists of several steps (the sorption of one or more hydrogen ions or other aqueous species at the surface followed by the breaking of the metal-oxygen bonds), however, with the exception of the final exchange reaction that destroys the structure such sorption reactions are transparent.

Note that in many cases not all of the metal-oxygen bonds present in the structure need be broken to completely destroy a mineral. For example, the forsterite structure, which contains both Mg-O and Si-O bonds can be destroyed by breaking only Mg-O bonds (see

Oelkers 1999), and the anorthite structure, which contains Ca-O, tetrahedral Al-O, and Si-O bonds is completely destroyed by breaking only the Ca-O and Al-O bonds (see Oelkers and Schott, 1995). In both cases Si-O bonds do not need to be broken to dissolve the mineral. A summary of various mineral dissolution mechanisms are summarized in Table 1.

Table 1: Summary of dissolution mechanisms of some minerals and basaltic glass.

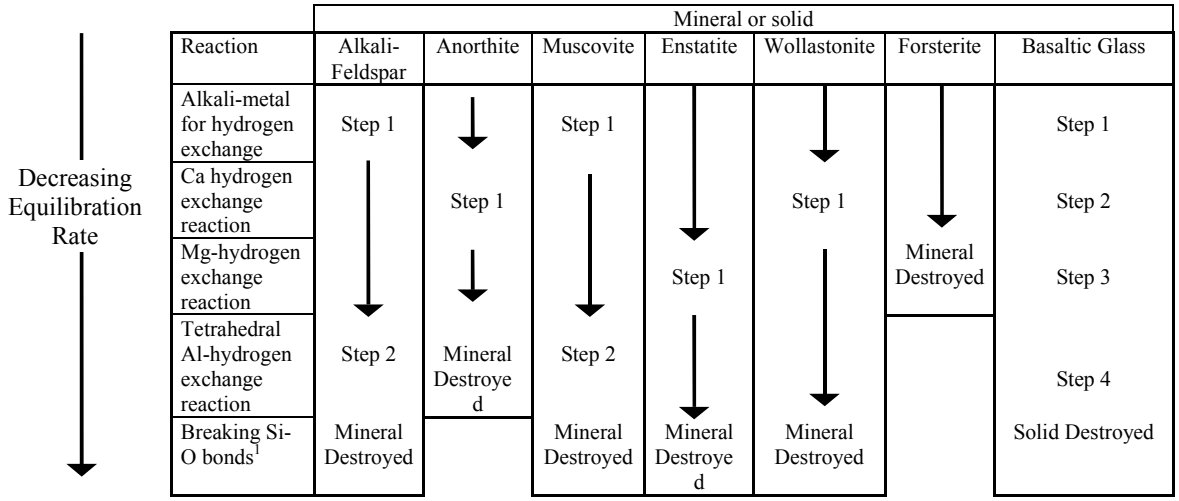

1) The breaking of Si-O bonds may itself be an Si for H exchange reaction. In the reactions described in this table, however, the

The extent to which each metal-hydrogen exchange reaction completely liberates the metal from the near surface can be deduced from the law of mass action of reaction (1) which can be written

$$K_i = \frac{a_{M_i^{z+}} X_{H_{z_i}<}}{a_{H^+}^{z_i} X_{M_i<}} \tag{2}$$

where a_i stands for the activity of the subscripted aqueous species, X_i represents the mole fraction of the indicated species at the mineral surface, and K_i designates the equilibrium constant for the i*th* metal exchange reaction. Assuming that each metal site contains either the original metal or hydrogen ions requires

$$1 = X_{H_{z_i}<} + X_{M_i<} \tag{3}$$

which can be combined with Eqn. (3) to yield

$$X_{H_{z_i}<} = K_i \left(\frac{a_{H^+}^{z_i}}{a_{M_i z_i +}} \right) \Big/ 1 + K_i \left(\frac{a_{H^+}^{z_i}}{a_{M_i^{z_i}}} \right) \tag{4}$$

The degree to which the denominator in Eqn. (4) exceeds unity controls the extent to which the metal M_i is removed from the near surface potentially leading to leached layer formation. For a metal that is dominated by free aqueous ions in solution Eqn. (4) suggests that leached layer formation is favored by low pH and low M_i concentration. The size of the leached layer is, however, related to the rate of diffusion of M_i and H^+ into and out of the mineral structure relative to the dissolution rate of the leached layer itself.

Equations describing dissolution rates consistent with these mechanisms can be deduced considering transition state theory. In accord with this theory, the forward dissolution rate ($\boldsymbol{r}_+$) is proportional to the concentration of the final surface species formed prior to the final irreversible step; this surface species is commonly referred to as the precursor complex. This precursor complex consists of the final partially detached metal oxide of the reaction sequence and in some cases sorbed catalytic species. The concentration of this species can be deduced from the law of mass action for the formation of the precursor complex from the original solid, comprising the exchange reactions (1) and the possible catalytic sorption reaction. The overall dissolution rate ($\boldsymbol{r}$) contains in addition, provision for the reverse reaction(s) ($\boldsymbol{r} = \boldsymbol{r}_+ - \boldsymbol{r}_-$, where $\boldsymbol{r}_-$ refers to the rate of the reverse reaction), which in this case is the reprecipitation of either the original solid or a partially depleted leached surface layer. The degree to which 1) the overall long term dissolution rate depend on the aqueous activity ratio $\left(\frac{\boldsymbol{a}^{\boldsymbol{z}}_{H^+}}{\boldsymbol{a}_{M_i{}^{z+}}}\right)$, and 2) a equilibrium can be attained with a partially depleted leached surface layer that is distinct from the equilibrium of the overall solid is directly related to the degree to which the denominator in Eqn. (4) $\left(1+\boldsymbol{K}_i\left(\frac{\boldsymbol{a}^{\boldsymbol{z}_i}_{H^+}}{\boldsymbol{a}_{M_i^{\boldsymbol{z}_i}}}\right)\right)$ exceeds unity, which itself depends on 1) the pH, 2) the aqueous concentration of the metal M_i, the aqueous speciation of this metal, 4) and the value of the equilibrium constant $\boldsymbol{K}_i$.

Because of its widespread occurrence on the ocean floor and volcanic terrains, its large scale emission during volcanic eruptions, and its relatively rapid dissolution rate, basaltic glass plays a major role in the global flux and cycling of numerous metals and nutrients. Moreover, basaltic glass is the major host rock of the Mururoa Atoll French nuclear test site, and used as an analog for various radioactive waste forms. Consequently, significant efforts have been focused on understanding the dissolution rates and mechanisms of this solid.

A representative chemical formula for basaltic glass is $Si_3AlFe_{0.5}Ca_{0.7}Mg_{0.77}Na_{0.33}K_{0.03}O_{10}$. The structure of this glass is such that the removal of all cations other than Si leads to a viable, though partially detached structure of Si-O bonds. It seems reasonable, therefore to assume that its dissolution consists of the

sequential equilibration of metal-hydrogen exchange reactions leading to the formation of partially liberated Si atoms, which dissolve reversibly to complete the dissolution process (see Table 1). This mechanism is consistent with hydrogen depth profiling and XPS analyses reported by Schott (1990) (see also Berger et al., 1987) which show that dissolving basaltic glass surfaces are depleted in network modifying cations such as Na, Ca, and Mg, which are rapidly and reversibly exchanged with protons. Several other observations which reveal the extent to which the exchanged cations participate in the dissolution rate of the partially leached layer include

- The pH dependence of its dissolution rate mimics that of aluminum oxide mineral solubility: it exhibits a sharp increase with decreasing pH at acidic conditions and a more gentle increase with increasing pH at neutral to basic conditions. The minimum rate is found at ~pH=6 at low temperatures, but this minimum moves to lower pH with increasing temperature (Guy and Schott, 1989).

- At far from equilibrium conditions and at constant pH, basaltic glass dissolution rates are 1) independent of aqueous silica activity, 2) decrease substantially with increasing aqueous aluminum activity, and 3) in mildly acidic solution increase dramatically with increasing oxalic acid concentration (Gislason et al., 1999).

- Its dissolution rates approach zero as the chemical affinity of the overall Al,Fe,Si-oxide structure network hydrolysis reaction approaches zero (Daux et al., 1988).

Taking account of this observations, it seems likely at the solution compositions considered in the laboratory, Na, K, Ca, and Mg depletion from the basalt surface is sufficient (the denominators in Eqn. (4) for their exchange reactions is sufficiently greater than 1) such that the dissolution rate of the outer leached layer is independent of their aqueous concentration and a unique equilibrium can be obtained with this K, Na, Ca, and Mg depleted leached layer. In contrast, it appears that sufficient Al and perhaps Fe are present at the surface to effect the concentration of the partially detached Si-O precursor complex.

Regression of these experimental data indicates that all experimentally measured basaltic glass dissolution rates reported in the literature are consistent with

$$r = k_{+} s \left(\left(\frac{a_{H^{+}}^{3}}{a_{Al^{3+}}} \right) \Big/ 1 + K_{Al} \left(\frac{a_{H^{+}}^{3}}{a_{Al^{3+}}} \right) \right)^{n} \left(1 - exp(-A/RT)\right) \qquad (5)$$

where, k_{+} designates a rate constant, s refers to the glass-solution interfacial surface area, a_i stands for the activity of the subscripted aqueous species, and represents a stoichiometric coefficient A refers to the chemical affinity of the Na, Ca, Mg depleted layer dissolution reaction, R designates the gas constant, T represents absolute

temperature, and ***n*** corresponds to a stoichiometric coefficient of ~ 1/3. Note the pre-exponential part of this equation is identical to that proposed to describe alkali feldspar dissolution rates (see Oelkers et al., 1994). Use of Equation (5) together with an Arrhenius relationship yields an allows the description of the measured rates as a function of temperature, and taking account of solution speciation calculations permits description rates as a function of pH, and the aqueous activities of Si, Al, and organic acids. The role of aqueous Fe on these rates cannot be evaluated with the present data set.

References

Berger, G. Schott, J., and Loubet, M. (1987) Fundamental processes controlling the first stage of alteration of a basalt glass by seawater: an experimental study between 200 and 320° C. Earth Planet. Sci. Let., 84, 431-445.

Daux, V., Guy, C., Advocat, T., Crovisier, J.-L., and Stille (1997) Kinetic Aspects of basaltic glass dissolution at 90° C: Role of silicon and aluminum. Chem. Geol., 142, 109-128.

Gislason S.R., Oelkers, E.H. and Schott, J. (1999) In preparation.

Guy, C. and Schott, J. (1989) Multisite surface reaction versus transport control during the hydrolysis of a complex oxide., Chem. Geol., 78, 181-204.

Oelkers, E.H. (1999) A comparison of enstatite and forsterite dissolution rates and mechanisms. 'Growth, Dissolution and Pattern Formation in Geosystems', B. Jamtveit and P. Meakin , eds., Klwler Academic Publishers (in press).

Oelkers, E.H., Schott, J. and Devidal, J.-L. (1994) The effect of aluminum, pH, and chemical affinity on the rates of aluminosilicate dissolution reactions., Geochim Cosmochim. Acta, 58, 2011-2024.

Oelkers, E.H. and Schott, J. (1995) Experimental study of anorthite dissolution and the relative mechanism of feldspar hydrolysis. Geochim. Cosmochim. Acta, 59, 5039-5053.

Schott, J. (1990) Modeling of the dissolution of strained and unstrained multiple oxides: The surface speciation approach. In Aquatic Chemical Kinetics', W. Stumm ed. John Wiley and Sons, New York, p. 337-366.

What controls mineral dissolution rates: Surface adsorption or ion exchange reactions ?

Oleg S. Pokrovsky[1,2] and Jacques Schott[2]

[1] Laboratory of Environmental Hydrochemistry, Department of Geography, Moscow State University, Vorob'evy Gory, 119899, Moscow, Russia

[2] Laboratoire de Géochimie, CNRS (UMR 5563)-OMP-Université Paul-Sabatier, 38 rue des Trente-Six-Ponts, 31400 Toulouse, France

The chemical weathering of rock-forming minerals is one of the major processes controlling the global cycle of the elements in the hydrosphere. Its modeling requires the accurate description of the structure, energetics and chemistry of the various solid-solution interfaces where it occurs. The surface coordination theory developed by Stumm and coworkers is presently one of the most efficient tool to rationalize this information and derive general rate laws for mineral dissolution. In this approach, the dissolution rate depends on the relative concentration of adsorbed species which promote or retard metal detachment from the surface. As the same conclusion is reached if the reaction sequence is treated according to transition state theory (TST), this species formed from the adsorption of various ligands on surface sites can be viewed as the precursor of the activated complex (Wieland et al., 1988). The stoichiometry and surface concentration of these precursor species can be obtained by combining surface titrations, adsorption experiments, electrokinetic measurements with *in situ* spectroscopic studies (via XPS, XAS, DRIFT, AFM, etc.) of the solid/water interface.

The surface coordination approach, first developed for single (hydr)oxides (FeOOH, AlOOH, SiO_2 ...), was also applied to more complex minerals such as carbonates and multioxide silicates. For example, recent studies of magnesite and dolomite surface speciation and dissolution kinetics in aqueous solutions (Pokrovsky et al., 1999a,b; Pokrovsky and Schott, 1999) show that the dissolution of these minerals is controlled by the protonation of surface carbonate species (>$CO_3H°$) and the hydration of the metal surface centers (>$MeOH_2^+$) in acid and neutral to alkaline solutions, respectively. The following rate equation, consistent with TST, was used to describe carbonate dissolution/precipitation kinetics over the full range of solution composition :

$$R_T = [k^+_{CO_3} \{>CO_3H°\}^i + k^+_L \{>MeL^-\} + k^+_{Me} \{>MeOH_2^+\}^j]\left[1 - \Omega^j\right] \qquad (1)$$

where R_T represents the overall reaction rate (mol/cm^2.s), {>i} stands for surface species concentration (mol/m^2), Ω refers to the solution saturation index with respect to calcite, dolomite or magnesite ; the values of the dissolution rate constants k_i and the reaction orders *i* and *j* for the three investigated carbonates are listed in Table 1. This equation also accounts for the ligand-promoted dissolution via the term k^+_L {>MeL$^-$} and the effect of

inhibitors such as carbonates that adsorb on the metal sites thus decreasing the concentration of the rate-controlling $>MeOH_2^+$ species.

Table 1. Parameters of Eq. 1 for different carbonate minerals (N.D.= non determined)

mineral	$k^+_{CO_3}$	i	k^+_{Me}	j	Reference
calcite	N.D.	2.0	$10^{-5.1}$	1.0	Van Cappelen et al. (1993); Chou et al. (1989)
magnesite	$10^{7.20}$	4.0	$10^{5.38}$	4.0	Pokrovsky and Schott (1999)
dolomite	$10^{1.16}$	2.0	$10^{-3.5}$	1.8	Pokrovsky et al. (1999c)

It should be noted, however, that Eqn. 1 implies, as it is the case for oxides, that carbonates dissolution is stoichiometric and the precursor complex is only formed by adsorption reactions.

The same 'adsorption' concept has been also widely applied to the interpretation of multioxide silicate minerals and glasses dissolution rates despite the fact a) it has long been recognized that the dissolution of these compounds invokes exchanges reactions leading to the formation of surface layers of altered compositions and, b) this concept leads to rate laws that cannot describe the kinetics of dissolution of most multioxides. Besides, determination of initial dissolution stoichiometry, surface titrations and surface spectroscopy analyses have confirmed that important H^+-metal cations exchange reactions occur at the surface of dissolving feldspars, pyroxenes, orthopyroxenes, kaolinite, wollastonite, glasses... and result in the formation of silica-rich, Al-, Mg- or Ca-depleted layers the thickness of which (from few nanometers to several micrometers) depends on the mineral structure and composition, and the reacting solution composition. Whether or not the rate controlling precursor complex is formed by such exchange reactions rather than via protons surface adsorption is still matter of controversy. However, there is ample evidence that the hydrolysis of minerals such as alkali feldspars (Oelkers et al., 1994 ; Gauthier et al., 1994), kaolinite (Devidal et al., 1997), pyroxenes (Oelkers, 1996), kyanite (Oelkers and Schott, 1999), which requires the breaking of at least two types of bonds, is controlled by exchange reactions (Oelkers and Schott, 1995 ; Schott and Oelkers, 1995). On the other hand, protonation of metal sites is believed to control the dissolution of those silicates like, anorthite and olivines, whose hydrolysis requires the breaking of only one type of bonds (Brady and Walther, 1992 ; Oelkers, 1996, 1999). However, proton promoted dissolution of Mg- and Ca-silicates (i.e. olivine or wollastonite) is hard to envision as all surface Ca or Mg sites are protonated ($>MeOH_2^+$) at pH≤8. The unambiguous characterization of the precursor complex reaction formation for such minerals calls for a multitechnique approach combining classic surface complexation measurements, surface spectroscopic observations, and dissolution rate determinations performed in the same solutions.

Such an approach has been taken, for the first time, to characterize forsterite surface speciation and reactivity in aqueous solutions. Surface potentiometric titrations and electrokinetic measurements (streaming potential and electrophoresis techniques) have

been combined with an XPS and DRIFT study of hydrated forsterite surfaces and dissolution kinetics experiments performed in a mixed-flow reactor. The surface chemistry of Fo_{92} in aqueous solutions was investigated using potentiometric titrations, electrokinetic measurements (streaming potential and electrophoresis techniques), and X-ray Photoelectron Spectroscopy (XPS). At pH<9, a Mg-depleted surface layer (< 80 Å in thickness) is formed due to an exchange reaction between a magnesium and 2 protons as confirmed by the preferential release of Mg over Si during the initial stage of dissolution. At pH>9, the surface exhibits a stoichiometric Mg/Si ratio or a slight enrichment in Mg. Electrokinetic measurements yield an isoelectric point or $pH_{i.e.p.}$ of 4.5 which is consistent with the dominance of silica sites at olivine surface for pH<9. In contrast, surface titrations result in a point of zero charge or $pH_{p.z.c.}$ of 10 and the development of a large positive charge (up to 10^{-4} mol/m^2) in acid conditions. This may be explained by penetration of H^+ into the first 3-5 molecular layers of forsterite as confirmed by XPS data that show a distinct increase in the half-peak-height of the O_{1s} peak. Note that such a difference between $pH_{i.e.p.}$ determined by electrokinetic techniques and $pH_{p.z.c.}$ measured from surface titration experiments is a common feature for a wide variety of silicate minerals, from feldspars to pyroxenes, which is likely to indicate a similar mechanism of surface charge development on altered layer.

The dissolution rates of Fo_{92} were measured at 25°C in a mixed-flow reactor as a function of pH (3 to 12), $\sum CO_2$ (0 to 0.05 M) and aqueous silica concentration (0 to 0.001 M). In CO_2-free solutions, the rates decrease with pH at 3≤pH≤8 with a slope close to 0.5 in accord with the results of Blum and Lasaga (1988), Wogelius and Walther (1991) and Oelkers (1999). At 9≤pH≤12, in contrast to the results of Blum and Lasaga (1988) and Wogelius and Walther (1991), the rates continue to decrease with a smaller slope of ~0.2. Olivine dissolution rates are inversely proportional to aqueous carbonate and silica activities at pCO_3^{2-}<4 and pH>8.5, respectively. These results allow to elucidate the mechanism of forsterite dissolution. In acid to weakly alkaline solutions, H^+-promoted dissolution is controlled by the decomposition of a silica-rich, Mg-free, protonated precursor complex formed by a fast exchange reaction of 2 H^+ for one Mg^{2+}, followed by the rate limiting sorption of 0.5 H^+ on each exchanged site. This is consistent with the development of a leached layer where residual hydrated silicate groups are either linked to Mg ions deeper in the mineral structure or which polymerize and link to one another (Casey et al., 1993 ; Schott and Berner, 1985 ; Petit et al., 1989). At pH>9, it is the hydration of surface Mg sites with formation of $>MgOH_2^+$ species which controls dissolution. Preferential Si release, observed at the initial dissolution stage in alkaline solutions, results in the formation of a brucite-like layer on the surface. The breaking of Mg-O-Mg bonds in this partially altered surface layer is thus the critical step for forsterite dissolution at these conditions. Far from equilibrium olivine dissolution is thus controlled by two parallel reactions occuring at silica-rich and hydrated Mg sites in accord with :

$$R_+ = k_{ex} \cdot a_{H^+}^{0.5} + k_{Mg1}\{>MgOH_2^+\} \qquad (2)$$

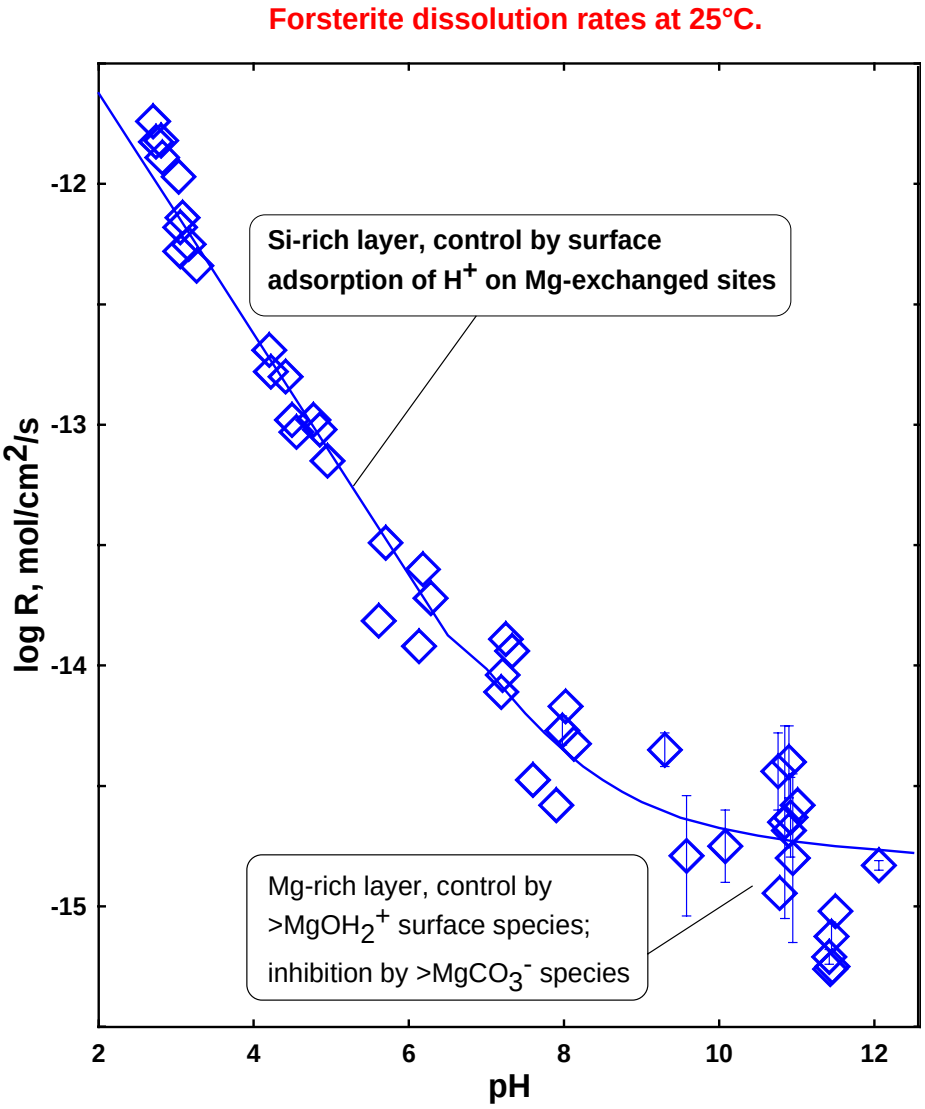

Figure 1: Forsterite dissolution rates at 25°C in 0.1 M NaCl as a function of pH as measured in a mixed-flow reactor (Pokrovsky and Schott, in preparation). The solid line is a model fit to the data (see Eqn. 2 in the text).

The degree to which this equation may be used for describing Fo dissolution rate in carbonate-free solutions is illustrated in Fig. 1. This equation accounts for an ion-exchange reaction in acid to neutral pH conditions, and for the hydrolysis process in alkaline solutions. Moreover, the inhibition of dissolution by carbonate ions is explained in terms of formation of $>MgCO_3^-$ species at the expense of rate-controlling $>MgOH_2^+$. Unlike in Brady and Walther study (1989), no increase of the dissolution rate at alkaline pH, associated with $>SiO^-$ species formation, was detected in the present work.

In conclusion, ion exchange reaction and surface protonation/adsorption should not be viewed as two alternative mechanisms but rather as successive steps involved in the dissolution mechanism of most multioxide silicates. Whether the rate limiting step is the exchange reaction or proton/ligand adsorption depends on the respective values of the thermodynamic exchange constant and of the intrinsic surface adsorption constant. In this regard, the rate of water exchange from the solvent into the hydration sphere of surface metals, and its dependence on pH should be of crucial importance.

References

Brady P.V. and Walther J.V. (1989) Controls on silicate dissolution rates in neutral and basic pH solutions at 25°C. *Geochim. Cosmochim. Acta* **53,** 2823-2830.

Blum A.E. and Lasaga A.C. (1988) Role of surface speciation in the low temperature dissolution of minerals. *Nature*, **331**, 431-433.

Casey W. H., Hochella Jr. M.F. and Westrich H.R. (1993) The surface chemistry of manganoferous silicate minerals as inferred from experiments on tephroite (Mn_2SiO_4). *Geochim. Cosmochim. Acta*, **57,** 785-793.

Chou L., Garrels R.M., and Wollast R. (1989) Comparative study of the kinetics and mechanisms of dissolution of carbonate minerals. *Chem. Geology* **78**, 269-282.

Devidal J.-L., Schott J. and Dandurand J.-L. (1997) An experimental study of kaolinite dissolution and precipitation kinetics as a function of chemical affinity and solution composition at 150°C, 40 bars, and pH 2, 6.8 and 7.8. *Geochim. Cosmochim. Acta*, **61,** 5165-5186.

Gauthier J.-M., Oelkers E. H. and Schott J. (1994) An experimental study of the dissolution rate of K-rich feldspar as a function of chemical affinity at 150°C and pH=9. *Geochim. Cosmochim. Acta*, **58,** 4549-4560.

Oelkers E.H. (1996) Summary of the physical and chemical properties of rocks and fluids for reactive transport calculations. *Reviews in Mineralogy*, **34**, 131-191.

Oelkers E.H. (1999) A comparison of enstatite and forsterite dissolution rates and mechanisms. In *Growth and Dissolution in Geosystems* (B. Jamveit and P. Meakin Eds), 253-257, Kluwer.

Oelkers E.H., Schott J., and Devidal J.-L. (1994) The effect of aluminum, pH, and chemical affinity on the rates of aluminosilicate dissolution reactions. *Geochim. Cosmochim. Acta*, **58,** 2011-2024.

Oelkers E.H. and Schott J. (1995) Experimental study of anorthite dissolution and the relative mechanism of feldspar hydrolysis. . *Geochim. Cosmochim. Acta*, **59,** 5039-5053.

Oelkers E.H. and Schott J. (1999) An experimental study of of kyanite dissolution rates as a function of chemical affinity and solution composition. *Geochim. Cosmochim. Acta*, in press.

Petit J.-C., Dran J.-C., Paccagnella A., and Della Mea G. (1989) Structural dependence of crystalline silicate hudration during aqueous dissolution. *Earth Planet. Sci. Lett.*, **93**, 292-293.

Pokrovsky O.S. and Schott J. (1999) Processes at the magnesium-bearing carbonates/solution interface. II. Kinetics and mechanism of magnesite dissolution. *Geochim. Cosmochim. Acta*, in press.

Pokrovsky O.S., Schott J., and Thomas F. (1999a) Processes at the magnesium-bearing carbonates/solution interface. I. A surface speciation model for magnesite. *Geochim. Cosmochim. Acta*, in press.

Pokrovsky O.S., Schott J., and Thomas F. (1999b) Dolomite surface speciation and reactivity in aquatic systems. *Geochim. Cosmochim. Acta*, special issue W.Stumm, submitted.

Schott J. and Berner R.A. (1985) Dissolution mechanism of pyroxenes and olivines during weathering. In *The Chemistry of Weathering* (J.I. Drever Ed.), 35-53, Reidel.

Schott J. and Oelkers E.H. (1995) Dissolution and crystallization of silicate minerals as a function of chemical affinity. *Pure Applied Chem.*, **67**, 903-910.

Van Cappelen P., Charlet L., Stumm W., and Wersin P. (1993) A surface complexation model of the carbonate mineral - aqueous solution interface. *Geochim. Cosmochim. Acta* **57**, 3505-3518.

Wieland E., Wehrli B., and Stumm W. (1988) The coordination theory of weathering: III. A generalization on the dissolution rates of minerals. *Geochim. Cosmochim. Acta* **52,** 1969-1981.

Wogelius R.A. and Walther J.V. (1991) Olivine dissolution at 25°C: Effects of pH, CO_2, and organic acids. *Geochim. Cosmochim. Acta* **55**, 943-954.

Influence of humic and fulvic acid on the sorption behaviour of Eu(III) on natural hematite

Th. Rabung[1,2], H. Geckeis[2], J. I. Kim[2], H. P. Beck[1]

[1] Universität des Saarlandes, Institut für Analytische und Anorganische Chemie und Radio-chemie, P.O. Box 151150, 66041 Saarbrücken, Germany

[2] Forschungszentrum Karlsruhe, Institut für Nukleare Entsorgungstechnik, P.O. Box 3640, 76021 Karlsruhe, Germany
e-mail: rabung@ine.fzk.de

The solid-water interface reaction is investigated for the sorption of the Eu(III) ion, as a trivalent actinide homologue, onto well-characterized natural hematite at pH $\leq$ 6 in 0.1 M $NaClO_4$ in the presence of humic and fulvic acid (HA/FA) [1].

In the absence of organic ligands sorption of Eu^{3+} onto hematite at coverages < 1% of the surface hydroxyl groups follows the ideal Nernst behaviour (Fig. 1) and can be interpreted in terms of the surface complexation by the following equilibrium reaction [2]:

$$\equiv XOH + Eu^{3+} \Leftrightarrow \equiv XOEu^{2+} + H^{+} \qquad \log K_x^{int} = 2.50 \pm 0.19$$

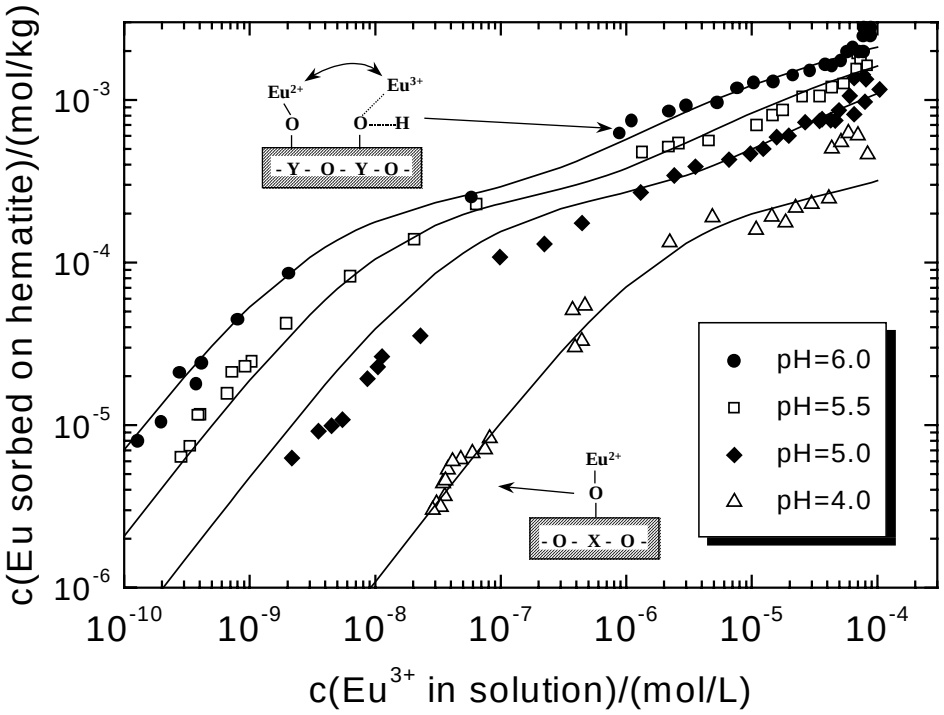

Fig. 1: Isotherms of Eu(III)-sorption on hematite at different pH (I=0.1 M $NaClO_4$). Straight lines are calculated with FITEQL. For the weak site complexation a coulombic interaction was included.

Complexation constants are calculated by either graphically interpretating the sorption isotherms or fitting the data using the code FITEQL [3]. At higher surface coverages a deviation from the Nernst behaviour is observed which can be described satisfactorily by a two-site surface complexation model, taking into account the lateral electrostatic interaction of surface-bound Eu(III) (Fig. 1):

$$\equiv YOH + Eu^{3+} \Leftrightarrow \equiv YOEu^{2+} + H^{+} \qquad \log K_y^{int} = -0.82 \pm 0.11$$

In presence of humic and fulvic acid a pH dependence of the Eu(III) sorption is observed that differs from the sorption of Eu(III) in the absence of ligands (Fig. 2) [4, 5, 6, 7]. At higher pH the sorption is decreased by competition of dissolved ligands with hematite surface sites. At lower pH uptake of Eu(III) increases due to its interaction with surface sorbed ligands (Fig. 3). An attempt is made to describe the reactions by a surface complexation model taking into account the surface complexation constants for Eu(III) onto hematite, the complexation constants for the respective ligands and the experimentally determined solid/liquid distribution of each ligand. However, this simple model is found not suitable to describe the influence of humic and fulvic acid on the Eu(III)-sorption. The divergence of experimental and modelling results is ascribed to blocking of the reactive ("strong") surface hydroxyl groups of the hematite by sorbed humic or fulvic acid and formation of strong ternary surface complexes of the type ≡S-O-Eu=(HA/FA) (Fig. 2 and 3).

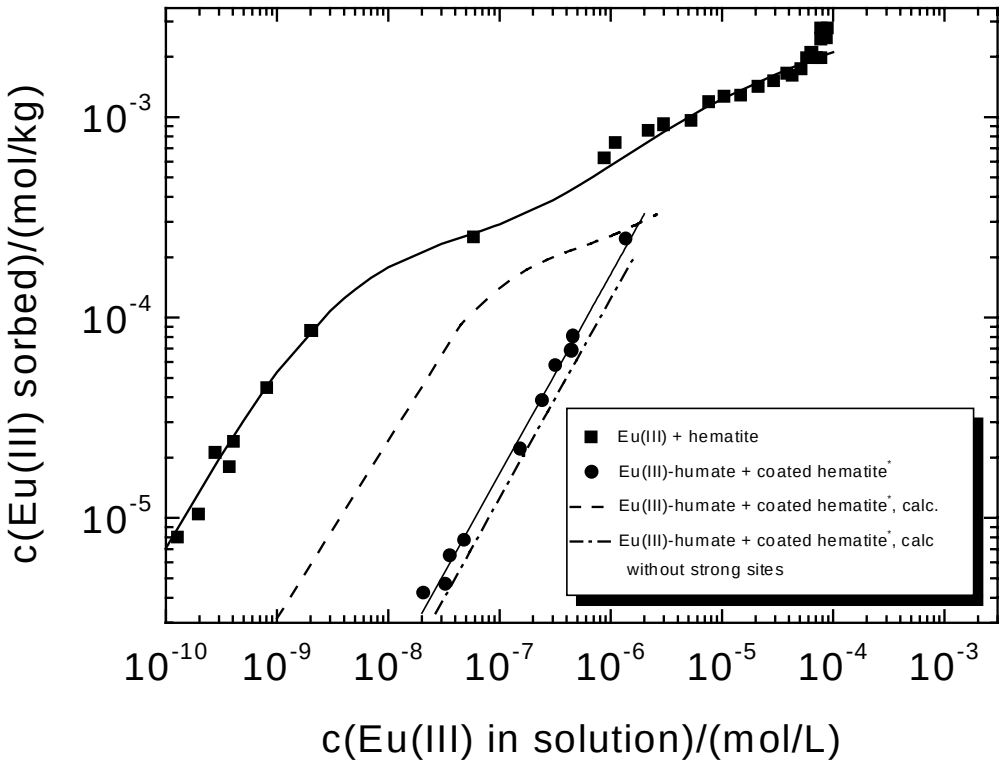

Fig. 2: Eu(III)-sorption onto hematite in the absence and presence of humic acid (pH=6.0, I=0.1 M $NaClO_4$). Comparison between experiment and modelling. *(coated hematite = hematite previously coated with humic acid.)

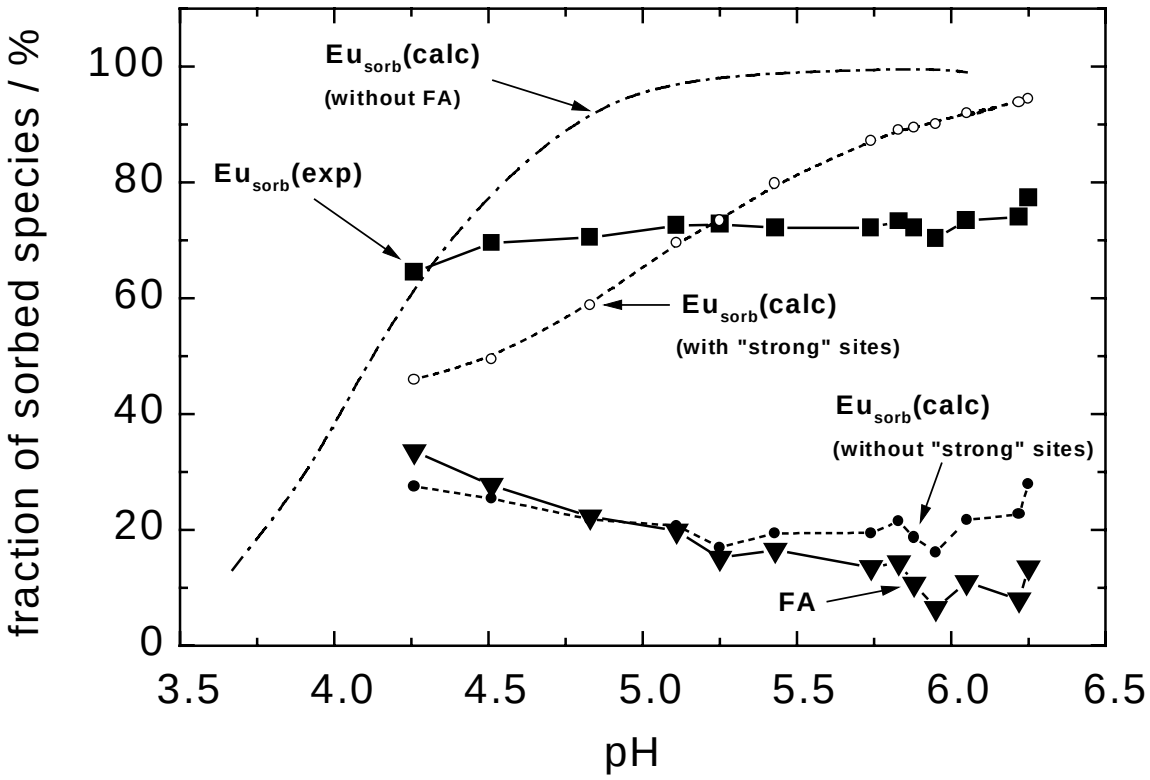

Fig. 3: pH-dependence of Eu(III)-sorption onto hematite in the presence of 30 mg/L fulvic acid. Comparison between experiment and modelling with and without consideration of "strong" complexing binding sites on hematite. The sorption behaviour in the ab-sence of fulvic acid is also shown in the plot.

The results of the present work show that sorption data obtained with homogeneous surfaces have only a limited value for the description of natural systems containing organic material. The sorption behaviour of Eu(III) appears to be predominantly determined by the complexation to sorbed or dissolved organic substances.

References

[1] Rabung, Th.: Der Einfluß von Huminsäure auf die Sorption von Eu(III) auf Hämatit, Dissertation, Anorganische und Analytische Chemie und Radiochemie, Universität des Saarlandes (1998)

[2] Rabung, Th., Geckeis, H., Kim, J.-I., Beck, H. P.: Sorption of Eu(III) on a Natural Hematite: Application of a Surface Complexation Model, J. Colloid Interface Sci. **208**, 153-161 (1998)

[3] Westall, J. C., Morel, F. M. M.: FITEQL: A General Algorithm for the Determination of Metal-Ligand Complex Stability Constants from Experimental Data, Technical Note 18, Ralph M. Parsons Laboratory, Department of Civil Engineering, Massachusetts Institute of Technology, Cambridge, Mass (1977)

[4] Fairhurst, A. J., Warwick, P., Richardson, S.: The Effect of pH on Europium-Mineral Interactions in the Presence of Humic Acid, Radiochim. Acta **69**, 103-111 (1995)

[5] Ledin, A., Karlsson, S., Düker, A., Allard, B.: The Adsorption of Europium to Colloidal Iron Oxyhydroxides and Quartz – The Impact of pH and an Aquatic Fulvic Acid, Radiochim. Acta **66/67**, 213-220 (1994)

[6] Rabung, Th., Geckeis, H., Kim, J.-I., Beck, H.P.: The Influence of Anionic Ligands on the Sorption Behaviour of Eu(III) on Natural Hematite, Radiochim. Acta **82**, 243-248 (1998)

[7] Righetto, L., Bidoglio, G., Azimonti, G., Bellobono, I. R.: Competitive Actinide Interactions in Colloidal Humic Acid - Mineral Oxide Systems, Environ. Sci. Technol. **25**, 1913-1919 (1991)

Modification of the sorption behavior of bentonite by hexadecylpyridinium

B. Riebe [1], S. Dultz [2], J. Bors [1]

[1] Zentrum für Strahlenschutz und Radioökologie,
Universität Hannover, Herrenhäuser Str.2, D-30419 Hannover,
e-mail: riebe@mbox.zsr.uni-hannover.de, bors@mbox.zsr.uni-hannover.de

[2] Institut für Bodenkunde, Universität Hannover, Herrenhäuser Str. 2, D-30419 Hannover,
e-mail: dultz@mbox.ifbk.uni-hannover.de

Introduction

The retardation of radionuclides by engineered clay barriers is primarily controlled by the sorption potential of the mineral constituents, like bentonite clay. Bentonite is characterized by a low hydraulic conductivity and excellent sorption capabilities for cationic radionuclides, but is generally ineffective in adsorbing anionic contaminants. This is especially of concern in the case of the long-lived ^{129}I and ^{99}Tc, which exist predominantly as anions in aqueous environments.

Extensive studies have shown, however, that the sorptive capabilities of clay minerals for anionic radionuclides can be improved substantially by replacing natural inorganic interlayer cations with quaternary alkylammonium ions of the form $[RN(CH_3)_3]^+$, where R is an alkyl or aromatic hydrocarbon. The resulting organo-clays are capable of sorbing non-ionic organic compounds (Mortland et al., 1986) as well as iodide (Bors, 1990, Bors et al., 1998).

In the present work sorption and diffusivity of the anionic radionuclides iodide, technetium, and of the cations cesium and strontium on MX-80 bentonite with different hexadecylpyridinium ($HDPy^+$) loadings, were studied using synthetic ground water (SGW) as equilibrium solution. It was of particular interest to obtain more information on sorption mechanisms and optimizing of engineered clay barriers by mineralogical and chemical characterization of the organo-bentonite samples.

Methodology

Sorption (R_d-values) of the elements in concern was carried out using the batch technique with ~37 kBq of ^{125}I, ^{95m}Tc, ^{134}Cs and ^{85}Sr (~$5 \cdot 10^{-12}$ mol·l^{-1}) and the corresponding carriers KI, CsCl and $SrCl_2$ in concentrations ranging between 10^{-8} and 1 mol·l^{-1}. As no stable isotope of technetium exists, ReO_4^- was used as carrier for TcO_4^- in the same

concentrations. According to experimental results, size, structure and sorption behavior of ReO_4^- are similar to those of TcO_4^- (Kang et al., 1998).

The uptake of $HDPy^+$ was determined by measuring the C-content with a LECO C-determinator (IR 12) and, for comparison, by calculations from the chemically analysed (atomic absorption spectrometry) contents of Na^+, K^+, Mg^{2+} and Ca^{2+} of the organo-bentonite samples.

Diffusion experiments have been carried out with iodide, pertechnetate, cesium and strontium using diffusion cells developed at and provided by KTH, Stockholm. The diffusion cell and experimental arrangement is described in more detail by Eriksen and Jansson (1996). Original bentonite and HDPy-bentonites were compacted in the diffusion cylinders (internal diameter = 10 mm, length = 5 mm) to a dry density of 1.8 $kg \cdot dm^{-3}$.

The samples were preconditioned with synthetic ground water (SGW) for 2 weeks. After that the diffusion tests with the radioactive tracers ^{125}I, ^{95m}Tc, ^{134}Cs and ^{85}Sr were started and terminated after 4 weeks.

Results and discussion

Sorption experiments

The different sorption behavior of anions (I^-, TcO_4^-) and cations (Cs^+, Sr^{2+}) as influenced by the concentrations of $HDPy^+$ applied is illustrated in Fig. 1. It can be seen that iodide and pertechnetate sorption increases, while cesium and strontium sorption decreases with increasing $HDPy^+$ saturation. Considering the construction of engineered barriers, it is important to realize that bentonite saturated with $HDPy^+$ to about 70-90% of the CEC is capable to sorb both anions as well as cations in comparable amounts.

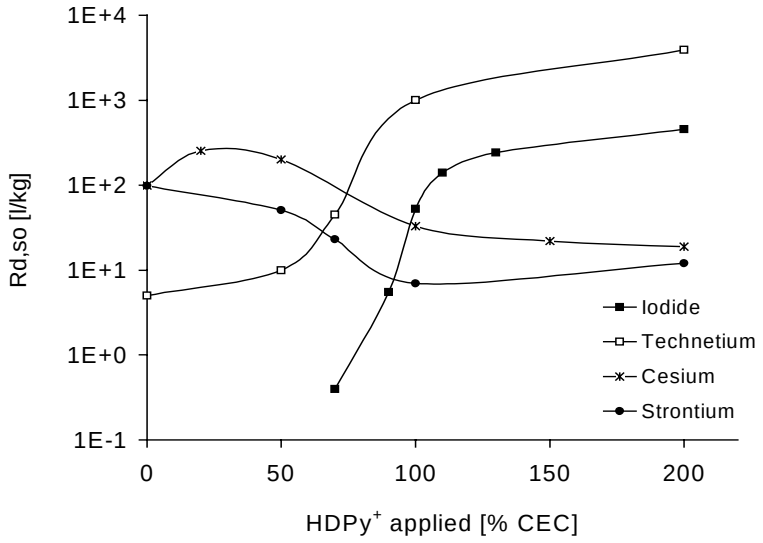

Fig. 1: Sorption, $R_{d,so}$-values for I^-, TcO_4^- (ReO_4^-), Cs^+ and Sr^{2+} using synthetic ground-water on MX-80 bentonite as a function of the amounts of hexadecylpyridinium ($HDPy^+$) applied.

The apparent diffusivities (D_a) and R_d-values are summarized in Table 1 for iodide and for pertechnetate. Generally, the data of the diffusion experiments confirm the implications of the results of the sorption tests that the retardation capability of bentonite for anionic fission products increase with increasing content of alkylammonium ions.

Tab. 1: Diffusivity of iodide and pertechnetate in compacted bentonite of different $HDPy^+$-loadings

		Iodide		Pertechnetate	
$HDPy^+$ applied [% CEC]	porosity	$R_{d,so}$ [l/kg]	D_a [cm^2/s]	$R_{d,so}$ [l/kg]	D_a [cm^2/s]
0	0.19	2.0 E+00	2.10 E-09	9.0 E+00	1.60 E-08
20	0.20	7.0 E+00	4.15 E-08	1.1 E+01	1.70 E-08
50	0.16	2.1 E+02	3.25 E-08	2.1 E+01	8.57 E-09
100	0.10	1.0 E+03	3.20 E-09	8.2 E+02	6.61 E-10
200	0.04	1.1 E+03	3.94 E-10	2.8 E+03	1.10 E-10

Mineralogical and chemical charakterization

Mineralogical characteristics of the organo-bentonite samples investigated by powder X-ray diffraction (XRD), by thermogravimetric (TG) and by calorimetric (DTA) measurements and by IR spectral analysis, as well as the dependence of surface charge on the degree of organophilicity are described elsewhere (Bors et al.,1998). The exchange behaviour of $HDPy^+$ is shown in Table 2.

The total quantities of adsorbed $HDPy^+$ differ considerably depending on the two different analytical approaches. The best explanation for this discrepancy is that part of the exchangeable inorganic cations (Na^+ and Ca^{2+}) remain unexchanged in the interlayer space in spite of the fact that $HDPy^+$ loading has reached CEC. This is important, inasmuch as these cations may account for the sorption of cationic radionuclides in partially organophilic bentonites (Fig. 1).

On the basis of chemical and mineralogical analyses it was concluded that the alkylammonium ions are adsorbed as 1. $HDPy^+$ cations, 2. HDPyCl molecules and 3. micelles with decreasing binding intensities in this order. As the organo-bentonites possess a fairly sufficient thermal stability up to 200°C, their use in engineered barriers for heat generating pollutants like nuclear waste should be taken into consideration.

Tab.2: Comparison of $HDPy^+$-content of MX-80-bentonite, calculated from Na^+-, K^+, Mg^{2+}- and Ca^{2+}-contents and from C_{org}-determination (values in $mol_c \cdot kg^{-1}$)

$HDPy^+$ applied [% CEC]	Na^+	K^+	Mg^{2+}	Ca^{2+}	$HDPy^+$ calculated	$HDPy^+$ [% CEC]	$HDPy^+$ [% CEC]*
0	0.35	0.13	1.07	0.46			
20	0.29	0.12	1.10	0.45	0.05	7	20
70	0.18	0.11	1.00	0.33	0.39	51	67
100	0.16	0.1	0.95	0.22	0.58	76	96
130	0.17	0.1	0.9	0.2	0.64	84	123
150	0.16	0.1	0.89	0.18	0.68	90	137
200	0.15	0.1	0.91	0.18	0.67	88	147
400	0.14	0.1	0.91	0.16	0.7	92	136

* $HDPy^+$-content calculated from C_{org}-determination

Concluding remarks

In HDPy-modified MX-80 bentonite, iodide and pertechnetate ions exhibited increasing sorption while cesium and strontium showed decreasing sorption with increasing organophilicity. In case of medium saturation levels, the simultaneous sorption of anions (I^- and TcO_4^-) and cations (Cs^+ and Sr^{2+}) were observed. These results tend to be confirmed by the data of the diffusion experiments carried out.

Anion adsorption can be explained by the uptake of $HDPy^+$ in excess of the CEC and/or the uptake as HDPyCl molecules, and by the change of the particle surface charge from negative to positive values (Bors et al., 1998). With respect to adsorption of cationic radionuclides in HDPy-MX-80-bentonites it is remakable that part of the inorganic cations remain unexchanged even when $HDPy^+$ is incorporated in amounts equal to or higher than the CEC.

References

Bors, J., 1990. Sorption of radioiodine in organo-clays and soils. Radiochim. Acta **51**: 139-143.

Bors, J. Dultz, St. and Gorny, A., 1998. Sorption of iodide, cesium and strontium on organophilic bentonite. Radiochim. Acta **82**, 269-274.

Eriksen, T. and Jansson, M., 1996. Diffusion of I^-, $Cs^+$and Sr^{2+}in compacted bentonite-Anion exclusion and surface diffusion. SKB Technical Report 96-16.

Kang, M. J., Chun, K. S., Rhee, S. W., Moon, H., Fanghänel, Th. and Neck, V., 1998. Sorption of MO_4^- (M=Tc, Re) on Mg/Al Layered Double Hydroxide and Characterization of Reconstructed LDH with ReO_4^-. Radiochim. Acta, in press.

Mortland, M. M., Shaobai, S. and Boyd, S. A., 1986. Clay-organic complexes as adsorbents for phenol and chlorophenols. Clays Clay Miner. **34**: 581-585.

A comparison of different phosphonate growth inhibitors for sulfates: AFM study on barite and celestite

Risthaus Peter [1], Bosbach Dirk [1], Coveney Peter V. [2]. and Putnis Andrew [1]

[1] Institut für Mineralogie, Universität Münster, 48149 Münster, Germany

[2] Schlumberger Cambridge Research, High Cross, Cambridge CB3 0EL , UK

Understanding the inhibition of crystal growth by organic additives has wide application both in natural mineralisation in sedimentary environments and in industrial processes. One important example is the scaling problem in off-shore oil-wells: Seawater injection is common in off-shore oilfields. The chemical incompability between injected seawater and formation water makes $BaSO_4$ and related scale deposition possible at various producing wells and facilities. Injected water may also mix with formation water in the near-wellbore area, reducing the permeability of the rock. Phosphonate inhibitors have been used for some years to prevent the build-up of barite scale in off-shore oil-wells. However, the mechanism of inhibition is largely unknown. In this paper we demonstrate that it is possible to study the growth of barite and celestite at molecular resolution *in situ* in a fluid cell of an atomic force microscope (AFM) and hence to make inferences about the attachment of inhibitor molecules on specific surface sites.

In the absence of inhibitor, the advancement of molecular steps as well as two-dimensional nucleation can be observed. Specific features of the process, such as the shape of the nuclei and the growth rate in different crystallographic directions can be measured by direct observation. This provides the basis for understanding modifications to the growth process introduced by the presence of inhibitor molecules in the solution.

The phosphonic acids described here include small molecules such as HEDP (Hydroxyethane diphosphonic acid) which have been used as inhibitors for some years, as well as new ‘molecular-engineered’ molecules with a larger number of binding motifs, and hence presumably a more efficient inhibition under higher supersaturation conditions. One such example is a macrocyclic aminomethylphosphonate, (hexaza-18-crown-6). All phosphonic acids, when added to the supersaturated sulphate solution in the fluid cell, first attach to the molecular-height cleavage steps on the surface. As the concentration of the inhibitor increases, the organic molecules also attach to flat terraces and build a complete monomolecular coating. With small phosphonate molecules such as HEDP it is not possible to observe this directly, but the attachment of molecules on kink sites can be inferred from the development of serrated step morphologies. Larger phosphonate molecules can be imaged directly by changes in the height of steps.

HEDP inhibits growth by attaching to the growth steps. Further growth is inhibited unless the supersaturation of the sulphate solution is increased, or the inhibitor is removed. The effectiveness of the inhibitor depends on its concentration, and the supersaturation of the fluid. Passing an inhibitor-free solution over the surface can remove HEDP, indicating a

rather weak attachment to the surface. On the other hand the larger macrocyclic molecules with up to 6 binding phosphonate motifs attach very strongly to step edges and surfaces and completely inhibit growth, even at low inhibitor concentrations where HEDP is less effective. This inhibitor cannot be removed by passing inhibitor-free fluid over the crystal surface, and continues to be effective at high supersaturations.

The effectiveness of the inhibitors and the mechanism of inhibition will be defined as a function of both inhibitor concentration and fluid supersaturation and can therefore be used to predict the range of the minimum effective dosage for scale inhibitors to optimize treatment levels in field applications.

Water-bearing fluid during formation of the diamond-bearing eclogitic rocks

S. K. Simakov

Geol.Dep., St.-Petersburg Univ., Russia, simakov@vap.usr.pu.ru

By nowadays there are many fluid inclusions data of granulitic and pelitic rocks. But there is a lack of reliable oxygen barometers for this rocks.

Model of garnet-clinopyroxene oxygen barometer for granulitic and eclogitic rocks was developed on the basis of the reaction:

$$2Ca_3Fe_2Si_3O_{12} + 2FeSiO_3 + 4SiO_2 = 6CaFeSi_2O_6 + O_2$$

The model was checked on Carroll and Wyllie (1989) experimental data for tonalite-peridotite system synthesised at 900-1030^o C, 15 kbar and nearly QFM buffer. By this method oxygen fugacity and equilibrated fluid compositions in the C-O-H system were calculated for Alpine, Norwegian, Indian and another granulites, pelitic shifts and eclogitic rocks. Calculated fluid compositions mainly closed to yearly extracted. This method was applied to diamond-bearing and -free Kokchetave eclogites. By the calculations diamond-free rocks have mainly CO_2 fluid meanwhile diamond-bearing ones - mainly H_2O-CH_4 fluid.

Kinetics, steady state or equilibrium ? Reversibility or irreversibility in chemical weathering rate modelling

Harald Sverdrup and Johan Holmqvist
Chemical Engineering, Lund University, Box 124, 221 00 Lund, Sweden
E-mail: harald.sverdrup@chemeng.lth.se

Introduction

The road to a functioning model for chemical weathering in soils that is based in first principles, has been long and winding. The mechanisms behind chemical weathering are dissolution reactions that take place at the mineral-solute interface, and conditions at the interface affecting the weathering rate. As aqueous solution concentrations rise, several different models have been used to limit the dissolution rate. There are important differences in the basic philosophy behind different weathering kinetics models. The differences lead to different behaviour in soil systems, making the selection of basic principles important. Great emphasis was put on developing models based in fundamental research that still would be easily applicable under field conditions (Sverdrup and Warfvinge, 1993; Sverdrup and Warfvinge, 1995).

Historically, there has not been rate laws available that have made it possible to link solute concentration to mineral dissolution, and no scheme for how the mineral phase should be characterised. Despite the lack of scientific support, soil and catchment modellers have been forced to assess weathering rates.

Hypothesises

The presently existing models estimate mineral weathering based on one of the following basic principles, implying that weathering under soil conditions is controlled by:

1. Reversibility and fast approach towards equilibrium.

2. Reversibility and approach towards equilibrium, limited by slow kinetics.

3. Irreversible and slow kinetics, affected by product inhibition, but no equilibrium exist between the reacting mineral and the aqueous solution.

Assumption (1) is widely used in geochemical models applied to deeper groundwater. The assumption is correct under conditions with high temperature or pressure, when the reactions are really fast and fully reversible. It is not correct for low temperature conditions on the earth surface, except for certain carbonates and simple very soluble

salts. Assumption (2) was the foundation for a large number of models (Aagaard and Helgesson, 1992; Brantley and Stillings, 1996; Gautier et al., 1994; Helgeson et al., 1984; Murphy and Helgeson, 1987). The assumption is dependent on the reversibility of the reactions for the equilibrium assumption to be applicable. This is the most widely applied assumption, according to our survey of the literature. Assumption (3) is the basis for some of the first models to be successful in calculating field weathering rates in forest soils and catchments. Assumption (3) imply that there is no equilibrium that can be reached, but that the system may have different types of steady states established after some time (Sverdrup and Warfvinge, 1993; Sverdrup and Warfvinge, 1995).

Theory

The use of saturation state to limit dissolution rates is well known for simple salts. Plummer et al. (1978) and Sjöberg (1979) developed rate laws and tested simple models for calcite dissolution and precipitation that involved several chemical reactions, the approach of equilibrium saturation with respect to calcite and reversibility. Calcite dissolution is fully reversible, and once the solution become oversaturated, it is known that calcite will precipitate as a solid mineral. Working with silicate minerals, Lasaga (1995) states that *"$f(\Delta G_r)$ must be a part of any kinetic rate law, as it is required that "$f(\Delta G_r) = 0$ at equilibrium when the dissolution reaction must come to a standstill"*. Aagaard and Helgeson (1992), Helgeson et al., (1984), Lasaga (1995) and Murphy and Helgeson (1987) formalised the transition theory for dissolution of one alumino-silicate mineral occurring through one elementary reaction into a rate equation per unit area:

$$r_W = k_0 \cdot e^{-E_a / RT} \cdot \prod_{i=1}^{n} a_i^{-n_i} \cdot f(\Delta G_r) \qquad (1)$$

R_w is the amount of ion released due to weathering of the mineral, k the specific rate coefficient, a_i he activity of the i-th species, n_i the reaction coefficient of the i-th reactant species in the reversible reaction corresponding to the formation of one kmole of activated complex on the surface of the mineral. For feldspars, in reality, a fully reversible reaction has been suggested (Lasaga, 1995); (Aagaard and Helgesson, 1992); (Helgeson et al., 1984); (Murphy and Helgeson, 1987); (Gautier et al., 1994); (Blum and Stillings, 1995); and (Brantley and Stillings, 1996). The reaction inherently assumes that the primary mineral albite feldspar may form from an aqueous solution, if only the solution is oversaturated. Simplified, we have:

$$r_W = f(chemistry) \cdot (1 - \Omega^m) \qquad (2)$$

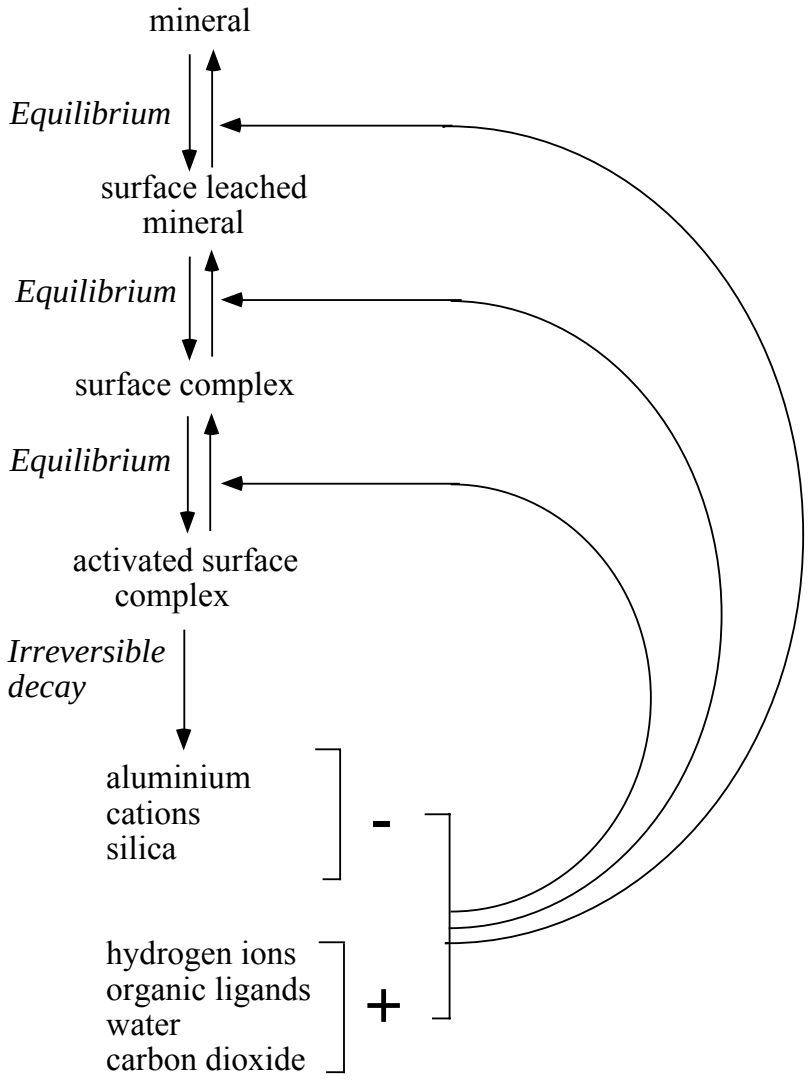

Figure 1: Schematic view of the dissolution process. It is not possible to move from dissolved back to the native mineral because of the irreversible steps.

Ω is the saturation quotient. A schematic view of the weathering process under soil conditions and in low temperature is shown in Fig 1. Reactants form an activated surface complex at the mineral surface, reaction products in the soil solution affect the formation process. The formation process for the activated surface complex from the leached parent mineral surface is considered to be reversible. The activated surface complex decays irreversibly, proportionally to the number of activated surface complexes existing. Reaction products may interfere with the formation process for the activated surface complex, but take care to note that the decay reaction products are not in equilibrium with the parent mineral. The solution composition is not controlled by the mineral surface reactions, but by the balance between this process and all the other soil processes. Secondary mineral phases may be formed either as solid residuals or from the soil solution when aluminium and silica concentrations increase, either irreversibly or reversibly. The structural lattice of such minerals can only dissolve through the same

kinetic processes as for the primary mineral. We consider the rate of formation of the activated complex to be much faster than the decay reaction for the activated complex. The formation of the complex will thus be at equilibrium, and $f(\Delta G_\psi)=0$ for the activated complex at all times. But $f(\Delta G_r)$ for the decay reaction is always different from zero and the decay reaction is never at equilibrium with the decay products. The implication is that most primary minerals are thermodynamically unstable phases in the presence of aqueous solutions. The reaction products may be in equilibrium with the surface concentration of activated surface complex at all times, affecting the rate of decay by determining the amount of complexes that can decay, despite that the decay mechanism itself is totally unaffected by any of the solution concentrations. No type of solution composition can actually stop the complex decay process which solely depend on quantum mechanisms and internal structural energy distributions within the activated complex.

Chou and Wollast (1985) combined the transition state theory combined with surface co-ordination chemistry in a number of elementary reactions. A number of weathering reactions was experimentally identified to take place in parallel at the mineral surface: (1) hydrogen ion, (2) water, (3) hydroxyl ion, (4) carbon dioxide and (5) organic acids. Sverdrup (1990) expanded the model of Chou and Wollast (1985) to include the different reactions and including both base cations and aluminium in the retarding mechanism. A modified version is incorporated in the integrated soil models SAFE and PROFILE (Sverdrup and Warfvinge, 1995).

It is important to distinguish between true equilibrium and apparent equilibria created by steady states. A steady state represents the apparent stable balance between different mechanistically independent rates. Equilibrium is a balance between rates, which are mechanistically dependent in a closed system or in an open system where these rates are dominating over other rates of mass transfer in the system. For explanations, we must look at the expression for the observed release of ions caused by the chemical weathering rate, using cation release from feldspar as example:

$$r_W = \sum^{\text{Dissolution reaction}} \vec{r}_{feldspar} - \sum^{\text{Precipitation reaction}} \overleftarrow{r}_{secondary} \qquad (3)$$

where $\vec{r}$ is the forward reaction rate and $\overleftarrow{r}$ is the formation rate of a secondary phase. The equilibrium constant for a chemical reaction is derived from the situation where the forward reaction is equal to the backward rate with a final result equal to the start of the forward reaction (Denbigh, 1955), from which the equilibrium constant can be derived as a ratio of the rate coefficients. Murphy and Helgeson (1987), Helgeson et al. (1987), Lasaga (1995), Oelkers et al. (Oelkers et al., 1994) all utilise the reversibility of the reaction to estimate the backward rate from the equilibrium coefficient and the forward rate. This makes it of paramount importance that the equilibrium is really taking place in a mechanistical sense. If the backward reaction does not exist or is vanishingly small, then the total rate will become equal to the forward rate, and the whole affinity term will vanish and the function $f(\Delta G_r)$ become unity.

It is, however, evident that this condition is not fulfilled for the primary mineral experiments at 20°C and 1 atm, and that an apparent equilibrium is used by Murphy and Helgeson (1987), Helgeson et al. (1984), Lasaga (1995) and Gautier et al. (1994) as well as many others. For most primary minerals, the true back reaction is zero, and the apparent equilibrium coefficient corresponding to the steady state "equilibrium" is taken to be the balance between the rate of forward reaction for feldspar and the rate of backward reaction for kaolinite, a completely different mineral:

$$f(\Delta G)_{Steady\ state} = (1 - \frac{\overleftarrow{r}_{kaoline}}{\Sigma_{i=1}^{n} \overrightarrow{r}_{feldspar}}) \tag{4}$$

Eq. 4 describe the approach to steady state between dissolution of a primary mineral, feldspar, and precipitation of different mineral, kaolinite, to be distinguished from equilibrium with one feldspar mineral phase only. It is only valid under that conditions which preserves the conditions for the steady state, and it is not transferable to any other open system such as a natural soil. The formal definition of equilibrium states that the affinity function must be expressed by the forward reactions having a startpoint corresponding to the endpoint of the reverse reactions (Denbigh, 1955):

$$f(\Delta G)_{Eq} = (1 - \frac{\Sigma_{i=1}^{n} \overrightarrow{r}_{i,feldspar}}{\Sigma_{j=1}^{n} \overleftarrow{r}_{j,feldspar}}) \tag{5}$$

Eq. 4 is nowhere near Eq. 5. As long as all reactions in the reaction chain are reversible, it a matter of convention if the equilibrium is expressed for one elementary reaction or a sum of several elementary reactions. But as soon as only one of the reactions in the chain is irreversible, then equilibrium between start and end will be impossible because of the lack of back-adjustment. If there is no equilibrium, limiting the rate of feldspar dissolution with approach to equilibrium cannot be correct. To substitute the feldspar back reaction with the reaction of another totally different mineral, is not making the reaction reversible; it merely creates an illusion of equilibrium. Most colleagues would agree that most primary silicate minerals dissolve irreversibly under the low temperature, low-pressure conditions found in the laboratory experiments and in the natural soil. It is almost everywhere accepted that most of the primary silicate mineral phases are thermodynamically unstable at standard temperature and pressure with respect to water. They have no back reaction going from dissolved in water to original primary mineral at such conditions. Still, the hypothesis usually adopted, imply that this is assumed to be possible, denying what we just said. Primary minerals can only enter the solution by following the overall irreversible dissolution process path. The mineral may appear to be in equilibrium with the dissolved components of the solution at high aqueous solution concentrations, as concentrations seem to stabilise at constant levels. The rate of primary mineral dissolution at that point equals the precipitation reactions that form secondary minerals. This steady state has often been mistaken to for an equilibrium. In this situation $f(\Delta G_r) << 0$, and there is still a driving factor on the reaction. Interpreting this

steady state as a thermodynamic equilibrium is false, and it cannot used to calculate Gibb's free energies. If the mass of the dissolving mineral is decreasing in the reactor, when the solution concentrations are stationary, then equilibrium is with certainty excluded. It appears that the basic assumptions for applying the chemical affinity for limiting the rate of silicate dissolution is not fulfilled in most cases where it has been applied.

Conclusions

The hypothesis of equilibrium limiting the kinetic rate of irreversible dissolution of primary silicate minerals must be rejected. Much stricter distinction must be made between minerals that dissolve in irreversible reactions such as feldspars, garnets, olivines, amphiboles, pyroxenes and crystalline mica minerals versus reversible reactions involving minerals such as soluble salts, newly formed amorphous alumino-silicates and carbonates. More stringency is required to distinguish true equilibria from steady state conditions that appear to be equilibria. This put into question the validity of equilibrium models utilising thermodynamic stability diagrams for soil weathering calculations in geochemical systems with primary silicate minerals present, as the apparent equilibria used are in reality multiple steady states of both irreversible and reversible reactions that may change with time.

References

Aagaard P. and Helgesson H. (1992) Thermodynamic and kinetic constraints on reaction rates among minerals and aqueous solutions: I. Theroetical considerations. *American Journal of Science* **282**, 237-285.

Blum A. and Stillings L. (1995) Feldspar dissolution kinetics. In *Chemical weathering rates of silicate minerals*, Vol. 31 (ed. A. F. White and S. L. Brantley), pp. 291-353. Mineralogical Society of America.

Brantley S. L. and Stillings L. (1996) Feldspar dissolution at 25°C and low pH. *Amer. J. Sci.* **296**, 101-127.

Chou L. and Wollast R. (1985) Steady-state kinetics and dissolution mechanisms of albite. *Amer. J. Sci.* **285**, 963-993.

Denbigh K. (1955) *The principles of chemical Equilibrium*. Cambridge University Press.

Gautier J. M., Oelkers E., and Schott J. (1994) Experimental study of K-feldspar dissolution rate as a function of chemical affinity at 150°C and pH 9. *Geochimica et Cosmochimica Acta* **48**, 4549-4560.

Helgeson H., Murphy W., and Aagaard P. (1984) Thermodynamics and kinetic constraints on reaction rates among minerals and aqueous solutions: II. Rate constants, effective surface area and the hydrolysis of feldspar. *Geochimica et Cosmochimica Acta* **48**, 2405-2432.

Lasaga A. (1995) Fundamental approaches in describing mineral dissolution and precipitation rates. In *Chemical weathering rates of silicate minerals*, Vol. 31 (ed. A. F. White and S. L. Brantley), pp. 23-86. Mineralogical Society of America.

Murphy W. and Helgeson H. C. (1987) Thermodynamic and kinetic constraints on reaction rates among minerals and aquepus solutions. III. Activated complexes and the pH-dependence of the rates of feldspar, pyroxene, wollastonite, and olivine hydrolysis. *Geochimica et Cosmochimica Acta* **51**, 3137-3153.

Oelkers E. H., Schott J., and Devidal J. L. (1994) The effect of aluminum, pH, and chemical affinity on the rates of aluminosilicate dissolution reactions. *Geochimica Cosmochimica Acta* **58**, 2011-2024.

Plummer N., Wigleu T., and Parkhurst D. (1978) The kinetics of calcite dissolution in CO_2-water systems at 5°C to 60°C and 0.0 to 1.0 atm CO_2. *American Journal of Science* **278**, 179-216.

Sjöberg L. (1979) Kinetics and mechanism of calcite dissolution in aqueous solutions at low temperatures, Stockholm University.

Sverdrup H. (1990) *The kinetics of chemical weathering*. Lund University Press.

Sverdrup H. and Warfvinge P. (1993) Calculating field weathering rates a mechanistic geochemical model PROFILE. *Applied Geochemistry* **8**, 273-283.

Sverdrup H. and Warfvinge P. (1995) Estimating field weathering rates using laboratory kinetics. In *Chemical weathering rates of silicate minerals*, Vol. 31 (ed. A. F. White and S. L. Brantley), pp. 485-541. Mineralogical Society of America.

Experimental investigation of the effect of high pH solutions on the Opalinus shale and the Hammerschmiede smectite

Heinrich Taubald[1)] and Andreas Bauer[2)]

[1)] Universität Tübingen, Institut für Mineralogie, Petrologie und Geochemie, Lehrstuhl für Geochemie, Wilhelmstr. 56, D-72074 Tübingen, e-mail: taubald@uni-tuebingen.de

[2)] Forschungszentrum Karlsruhe, Institut für Nukleare Entsorgungtechnik, PO Box 3640, D-76021 Karlsruhe, e-mail: bauer@fzk.ine.de

Introduction

High pH solution-mineral reactions occur in a variety of geological environments as well when the environment has been modified by human activty in various engineering projects, including emplaced concrete. Concrete and cement are proposed as matrix material, backfill material and as structural components of radioactive waste repositories with an high amount of concrete (e.g. 8.2 10^5 m^3, Karlson et al., 1986), especially in low-level waste facilities. Solidification or disaggregation of concrete in natural environment will produce high pH solutions, with pore fluids ranging in pH from 12.5 to 13.5 and high ionic strenght, dominated by Na and K in concentrations ranging from 300-4200 ppm and from 100-7500 ppm respectivly (Andersson et al., 1989, Lunden and Andersson, 1989). Ca concentrations in these pore fluids are much lower and range from 20-130 ppm. The release of this alkaline plume has been modelled (Haworth et al., 1989; Reardon, 1990; Jeffries et al., 1988; Berner, 1990; Vieillard and Rassineux, 1992) showing a first period of NaOH and KOH release (pH > 13), followed by a solution composition controlled by portlandite $Ca(OH)_2$ and finally a solution composition controlled by calcium-silicate-hydrate (CSH) gels (pH to 9-10).

Materials and Methods

In this study we present the long term behaviour (two years) of two natural clays in an alkaline solution. For our study we used column experiments (cylindrical samples 8 cm high, 9 cm in diameter). The clays are the Jurassic Opalinus Shale **(OP)** and the Tertiary Hammerschmiede smectite **(HS)**. In the beginning the hydraulic gradient was i = 20 for both materials. After 40 weeks the hydraulic gradient was changed to i = 1 for the Opalinus Shale and i = 90 for the Hammerschmiede smectite. During the experiments the permeability as well as pH and Ca^{2+}, Mg^{2+}, Na^{+}, K^{+}, and Si^{4+} solution concentrations were monitored as a function of time. After the experiment the columns were cut into 5-6 horizontal segments and the mineralogy, the chemical and the isotopic ($\delta^{18}O$ and $\delta^{13}C$ of carbonate phases) composition were studied.

As starting fluid we used the Simple Young Fluid (SYF). The chemical composition of this fluid is supposed to be typical for solutions resulting from the initial stages of cement alteration (NAGRA, internal report). The starting solutions were prepared from analytical reagent grade salts with NaOH = 2.606 g/l, KOH = 9.033 g/l, $Ca(OH)_2$ = 0.166 g/l. The initial was pH = 13.22.

Results

Fluids - hydraulic conductivity

In the beginning of the experiment both materials showed the same hydraulic conductivity of around 5 x 10^{-10} m/s. In case of the Opalinus Shale the hydraulic conductivity stayed more or less constant for 40 weeks, whereas for the HS the hydraulic conductivity decreased in the same time by two orders of magnitude to increase then slowly again till the end of the experiments. After 40 weeks the hydraulic conductivity started to increase for the Opalinus Shale. This increase of permeability continued till the end of the experiment where the permeability increased by more than two orders of magnitude. The total amount of percolated SYF fluid is around 900 ml for HS and around 2400 ml for OP.

Fluids – pH

For the two different clays the evolution of the pH with time is not the same. In first 40 weeks the pH showed only a slight increase for the Hammerschmiede clay (8.5 to 9.23). The pH increased then continuously to 12.42 where it remains constant till the end of the experiments. In case of the Opalinus shale the pH showed no change for the first 6 weeks. This period was followed by a increase of the pH from 7.31 to 12.74 within 5 weeks. The pH showed then only a slight increase and reached a maximum after 45 weeks (13.21).

Fluids - salt concentrations

The evolution of the salt concentrations in the percolating fluids mirror the evolution of pH. Na^+ and K^+ increase, while Ca^{2+} and Mg^{2+} decrease with increasing pH, indicating the breakthrough of the high pH plume through the column. This is especially true for HS, where pH and kation concentration correlate perfectly. For OP a second decrease in Ca^{2+} and Mg^{2+} concentration can be observed in the percolated fluids after 28 weeks. The concentrations for Si^{4+} increase slightly with time, however no direct dependency on pH can be observed.

Solids - main elements

CaO and K_2O, Na_2O are enriched on the top of the columns. In the Hammerschmiede clay this enrichment is more obvious for the first 20 mm than for the Opalinus shale. In this zone a white veil of carbonates, portlandite and Ca-Al-Si-hydroxide phases (CASH) covered the surface of the Hammerschmiede smectite. In the lower part of the column no significant trend can be observed for CaO and K_2O while Na_2O was depleted in the lower part of the Hammerschmiede column. SiO_2 showed for both clays only a slight decrease in the top of the columns but showed no change with increasing depth. Fe_2O_3, MgO and Al_2O_3 are depleted in the first 20 mm of the column in both clays but showed for the lower part no significant change. In case of the Hammerschmiede sample CaO and MgO concentrations increase at the bottom of the column again where XRD showed the presence of carbonates, portlandite and brucite.

Rare Earth Elements (REE)

For the two clays a different trend of the distribution of the REE was observed. In case of the Opalinus shale in all segments the REE are depleted compared to the starting clay except in the 5-10 mm level. Only Sm, Eu and Tb showed here a slow depletion. The greatest loss can be observed in the surface layer, followed by a an enrichment in the 5-10 mm level. In the next layers the REE are depleted but the loss becomes less important with increasing depth (Fig. X). In case of the Hammerschmiede smectite the REE were depleted in the upper part. In the last two segments (30-60 mm and 60-90 mm) the REE are concentrated or show only a minor depletion (Ce, Sm, Eu and Tb).

Solids - carbonate concentration and isotopic composition

A profile through the sample from top to bottom shows higher carbonate contents in the upper parts (0-20mm) and lower carbonate contents in the lower parts compared to the average composition of untreated raw material (9.7 % for OP, 16.1 % for HS). For OP carbonate content falls continuously from 13.9 % to 8.9 % and for HS from 17.5 % to 13.4 % with increasing depth. This is due to precipitation of secondary carbonates in the upper parts in HS and OP. The CO_2 for carbonate precipitation is of atmospheric origin with a $\delta^{13}C$ value of around -9‰. Depending on the grade of equilibrium between CO_2 and the carbonate the secondary carbonate should have a $\delta^{13}C$ value between -9‰ and +1‰. The $\delta^{18}O$ of newly formed carbonate is dominated by DI water with $\delta^{18}O$ of around -41‰$_{PDB}$. Under equilibrium conditions at 20°C, which are assumed for oxygen, the resulting carbonate should then have a $\delta^{18}O$ value of around -11‰. Compared to the original isotope values of the untreated raw material for OP and HS (for HS: $\delta^{13}C$ = -8.6‰, $\delta^{18}O$ = -5.3‰, for OP: $\delta^{13}C$ = -2.1‰, $\delta^{18}O$ = -7.0‰) $\delta^{18}O$ in OP and HS shows shifts to more negative values in those segments with secondary carbonate precipitation.

However, the $\delta^{13}C$ values for OP are between 1‰ and 1.7‰ more negative througout the core whereas for HS they don´t show any significant variation, execpt the uppermost sample which gave a value 0.4‰ more positive. This a) is evidence for a $\delta^{13}C$ value of the newly formed carbonate of around -5.5‰, indicating a disequilibrium precipitation process and b) shows, that in OP in all segments a possible recrystallisation of carbonate phases may be the reason for the rising permeability of OP during the end of the experiment.

XRD - bulk samples

Throughout the whole sample no significant appearance of new peaks or disappearance of diffraction peaks could be observed for OP within a 2θ range of 2° and 56°.

References

Andersson K., Allard B., Bengtsson M. and Magnusson B. (1989) Chemical composition of cement pore waters. Cement Concrete Res. 19, 327-332.

Berner U. (1990) A thermodynamic description of the evolution of porewater chemistry and uranium speciation during the degradation of cement [rep.]. Nagra NTB, 90-12, Baden, Switzerland.

Day, P. R. (1965) Particle fractionation and particle size analysis. In Methods of Soil Analysis (ed. C. A. Black), 545-567, Amer. Soc. Agron. Inc.

Haworth A., Sharland S. M. and Tweed C. J. (1989) Modelling of the degradation of cement in a nuclear waste repository. Material Research Society Symposium Proceedings 127, 447-454.

Jeffries N. L. Tweed C. J. and Wisbey S. J. (1988) The effects of changes in pH in a clay surrounding a cementitious repository. Material Research Society Symposium Proceedings 112, 43-52Karlson L. G., Hˆglund L. O. and Pers K. (1986) Nuclide release from the near-field of a L/ILW repository [rep.]. Narga NTB, 85-33, Baden, Switzerland.

Lunden I. and Andersson K. (1989) Modelling the mixing of cement pore water and groundwater using the PHREEQE code. Mat. Res. Soc. Symp. Proc. 127, 949-956.

McCrae, J.M. (1950): On the Chemistry of Carbonates and a Paleotemperature Scale. The Journal of Chemical Physics, 18, 849-857.

Nagra (1995): internal report.

Reardon E. J. (1990) An ion interaction model for the determination of chemical equilibrium in cement/water systems. Cement and Concrete Research 20, 175-192.

Richter, U. (1994): Vergleichende mineralogische und geochemische Untersuchungen an Tonen der Oberen S¸?wassermolasse. Ph.D. thesis, Technical University Munich.

Vieillard P. and Rassineux F. (1992) Thermodynamic and geochemical modelling of the alteration of two cement matrices. Applied Geochemistry 1, 125-136.

Sr uptake during CSH phase formation: Adsorption versus co-precipitation

J. Tits, E. Wieland, C. Poinssot* and J. P. Dobler

Paul Scherrer Institute, Laboratory for Waste Management, CH 5232 Villigen PSI, Switzerland

* CEA de Saclay, DCC/DESD/SESD, Laboratory for Migration and Solid Geochemistry, BP 11, 91191 Gif-sur-Yvette, France

Introduction

For disposal options involving the isolation of low- and intermediate-level radioactive waste (L/ILW) in a cementitious repository, uptake by Calcium silicate hydrate (CSH) phases will play an important role in retaining the migration of radionuclides in both the near field and the far field. In the near field, CSH phases are major components of hardened cement paste, and the interaction of hyperalkaline fluids from the repository (pH plume) with the mineral components of sedimentary rocks produces a range of CSH-type secondary minerals in the far field (see for example CRAWFORD and SAVAGE, 1994). Studies concerning the retention of trace concentrations of radionuclides by CSH phases have mainly focused on adsorption as the dominating uptake mechanism (EWART et al., 1990; MARX et al., 1995; TITS et al., 1996). However for some radionuclides, other uptake mechanisms such as co-precipitation may play an additional important role. Especially when adsorption is weak, other uptake mechanisms might become important for the immobilisation of radionuclides. Co-precipitation with calcite is a well documented example (e.g., CURTI, 1997 and references therein). Previous co-precipitation studies with CSH phases were mostly performed using radionuclide concentrations far above the levels expected in a L/ILW repository and, frequently, also above the solubility of the radioelements under highly alkaline conditions (e.g., KOMARNENI, et al.,1986; LAMEILLE, et al., 1987; KOMARNENI, 1988). This paper reports the formation of CSH phases in quartz - portlandite mixtures under high pH conditions and its effect on Sr retention. The purpose of the present study was to elucidate the role of adsorption and co-precipitation as possible retention mechanisms on CSH phases at trace concentrations of Sr. Sr is an important component of different types of radioactive waste. Moreover, Sr adsorption on CSH phases is relatively weak compared to the stronger sorbing actinides, so that co-precipitation in addition to adsorption would have a favourable effect on the overall immobilisation.

Materials and methods

Solutions were prepared from reagent (or higher) grade chemicals in de-ionised water. All experiments were conducted in an artificial cement pore water (ACW) to simulate high

pH conditions. The ACW contained 0.18 M KOH and 0.114 M NaOH and was equilibrated for at least 2 weeks with 2 g L^{-1} $CaCO_3$ and 2 g L^{-1} $Ca(OH)_2$. An acidic source radionuclide solution of ^{85}Sr was purchased from Amersham International Plc. This source solution was diluted in 50 ml de-ionised water.

The quartz used in this study was MIN-U-SIL 30 obtained from U.S. Silica company, Berkeley Springs, USA. 97.5 % of the quartz material was finer than 30.0 μm according to specifications. Prior to use in the sorption experiments, the material was treated following a procedure described by O'DAY (1992) to remove organic, and inorganic contaminants and rapidly dissolvable material. Portlandite ($Ca(OH)_2$) was purchased from Merck and used without further pre-treatment. A fully characterised CSH-gel was obtained from the University of Aberdeen. The $CaO:SiO_2$ (C:S) ratio was 1.4 and the specific surface area, determined from single point N_2-BET measurements, was 128 m^2 g^{-1} (GLASSER, pers.comm). This CSH phase was equilibrated with ACW for one month prior to use.

In order to simulate the conditions in a disturbed far field, pure quartz was dissolved in ACW at pH 13.3 in the presence of portlandite. As a result, secondary CSH phases were precipitating (SAVAGE et al., 1992). The effect of an eventual co-precipitation on the overall retention of Sr in the mixture was evaluated from a comparison of two experimental set-ups: In the first set-up, Sr was added to the mixture after an equilibration period of 3 months. During this equilibration, quartz and portlandite were allowed to dissolve and CSH phases to precipitate. After 3 months, significant amounts of CSH were formed, and, adsorption on these CSH phases was the controlling uptake mechanism for Sr. In a second set-up, Sr was added to the mixture at the beginning of the equilibration period. Sr was then removed from the fluid due to either co-precipitation with the CSH or adsorption on the CSH surface (sorption on portlandite and quartz was negligible). Comparison of the Sr distribution ratios (R_d) obtained from the two set-ups allowed co-precipitation to be distinguished from adsorption as possible uptake mechanisms for Sr.

All experiments were performed in controlled atmosphere glove boxes (O_2 and CO_2 levels were ~ 5 ppm or lower). Sorption of ^{85}Sr was determined using the batch technique in suspensions of quartz (40 g L^{-1}), portlandite (40 g L^{-1}), CSH-gel (5.3 g L^{-1}) or mixtures of quartz and portlandite in ACW. CSH suspensions were prepared by appropriate dilution of the pre-equilibrated CSH phases. The mixtures were made up by mixing 4 g of portlandite and 4 g of quartz with 200 ml ACW (overall S:L ratio = 40 g L^{-1}). Phase separations were carried out by centrifugation (1 hour at 95000*g* max). Radio assays were performed using a Canberra Minaxi 5530 auto γ-counter. Wall sorption artefacts were avoided by counting the total activities in the suspensions before phase separation and in the corresponding supernatant solutions after phase separation. The solid phases were characterised by Scanning Electron Microscopy (SEM) combined with Energy Dispersive Spectrometry (EDS). Analytical conditions (15 kV, 10 μA) were optimised so that the sample damage was reduced. The solution compositions were analysed by plasma emission spectrometry (ICP-AES).

Results and discussion

Si resulting from the dissolution of quartz in the alkaline quartz - portlandite - ACW mixture precipitates together with Ca, from the portlandite, to form CSH phases (Fig. 1a and b). Figure 1b shows CSH precipitates as flaky amorphous structures around a quartz particle. In a Ca-free quartz suspension at pH 13.3, no secondary precipitates were observed (Fig. 1a). An estimate of quantity of CSH precipitated in the mixture was made assuming that the dissolution rate of Si in the mixture was similar to the dissolution rate of Si in a Ca-free quartz suspension (0.3 M NaOH at pH 13.3) (Fig. 2a). The increase in Si concentration with time in the Ca-free quartz suspension was described by a fast initial and a subsequent slower Si release (Fig. 2a).

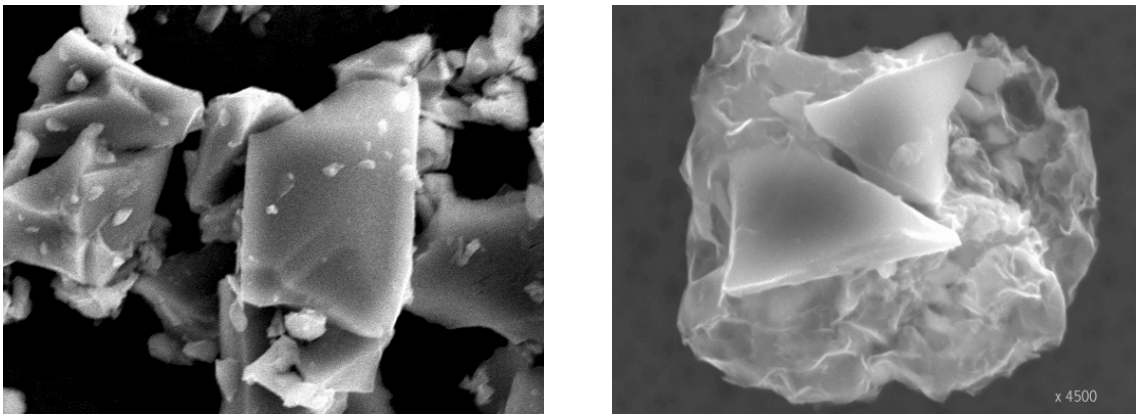

Figure 1: Formation of CSH in a quartz - portlandite - ACW suspension: a) Quartz particles in 0.3 M NaOH (pH 13.3) in the absence of Ca.
b) Quartz particles in the presence of portlandite in ACW (pH 13.3). Both pictures are taken after an equilibration time of 3 months.

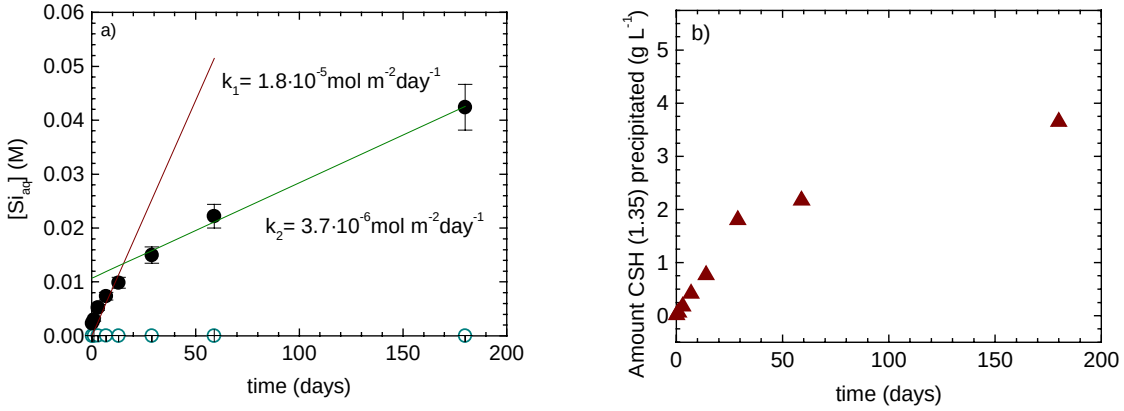

Figure 2: CSH formation as a function of time in a quartz - portlandite mixture. a) Aqueous Si concentration in a quartz - ACW suspension (●) and in a quartz - portlandite - ACW suspension (○). $k_1$and k_2 are the dissolution rate konstants. b) Calculated amount of CSH (C:S = 1.35) precipitated as a function of time.

The C:S ratio of the precipitating CSH phase was measured by EDS to be 1.35±0.15. Knowledge of the CSH composition and the total concentration of dissolved Si allowed the quantity of precipitated CSH phases to be estimated. Figure 2b shows the calculated amount of CSH phases formed as a function of time in an ACW suspension containing 20g L^{-1}quartz and 20g L^{-1} portlandite. The break in the curve is a result of the two-rate dissolution process.

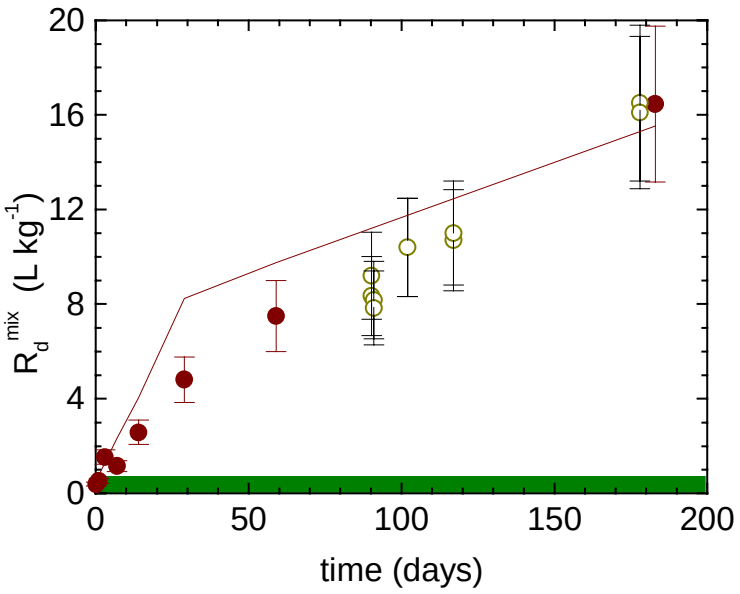

Figure 3: Sr R_d values in a mixture containing quartz, portlandite and CSH phases: Circles indicate experimental data: (●) Sr added at the beginning of the equi-libration period; (○) Sr added after 3 months equilibration. The solid line represents estimated R_d values assuming sorption on quartz, portlandite and precipitated CSH phases (C:S = 1.35). The shaded area represents calculated R_d values assuming that sorption occurs only on the quartz and portlandite fraction.

Figure 3 shows the time-dependent uptake of Sr in the quartz - portlandite - ACW mixture. The shaded area at the bottom of the figure indicates R_d values for Sr sorption on quartz and portlandite alone, i.e. before CSH phase formation. The experimental results (circles) show that the R_d value increased with time indicating that the precipitating CSH phases enhance Sr uptake through adsorption or co-precipitation. Open circles represent sorption values for the case where the quartz - portlandite - ACW mixture was allowed to equilibrate for 3 months prior to the addition of Sr (first experimental set-up). The filled circles indicate sorption data for the case where Sr was added at the beginning of the equilibration period (second experimental set-up). As mentioned above, Sr can either co-precipitate with the CSH phases or adsorb on the surface of the CSH phases in the second set-up. In the first set-up, Sr can only adsorb on CSH phases which were formed during

the preceding equilibration period. If co-precipitation were important, the combination of adsorption and co-precipitation in the second set-up would result in higher R_d values compared to the first set-up. This is clearly not the case. When Sr was added after the equilibration period (first set-up), the R_d value immediately attained the same level as in the set-up where Sr was present during CSH phase formation. Hence Sr retention can be interpreted in terms of an adsorption-controlled process on the surface of CSH phases rather than co-precipitation.

Sr sorption in the quartz - portlandite - ACW mixture was estimated from the amount of CSH formed and the R_d values of the individual components (quartz, portlandite and a CSH phase with C:S ratio of 1.4, respectively). These R_d values were determined in separate sorption experiments (Table 1). The overall R_d value in the mixture (R_d^{mix}) was calculated as follows:

$$R_d^{mix} = \left(\frac{G_q}{G_q + G_P + G_{CSH}}\right) \cdot R_d^q + \left(\frac{G_p}{G_q + G_p + G_{CSH}}\right) \cdot R_d^p + \left(\frac{G_{CSH}}{G_q + G_p + G_{CSH}}\right) \cdot R_d^{CSH}$$

were G_p, G_q, G_{CSH} are the masses of portlandite, quartz and CSH phases in the mixture and R_d^p, R_d^q, R_d^{CSH} as the R_d values (L kg^{-1}) of the individual components. By adopting this approach, it is assumed that the total sorption on the mixture is a linear addition of the sorption on the individual components.

Table 1: R_d values for Sr on solid phases under high pH conditions (ACW, pH 13.3)

	quartz	portlandite	CSH (1.4)
R_d (L kg^{-1})	0.02	0.8	110

Estimated R_d values of the mixture (solid line in Figure 3) agree fairly well with the measured sorption values. It clearly confirms the hypothesis that adsorption was the dominating uptake mechanism for Sr in the mixture, and that Sr was not co-precipitated with the CSH phases.

Conclusions

This study shows that the dissolution of quartz in ACW in the presence of portlandite results in the precipitation of secondary CSH phases with a C:S ratio of approximately 1.35. The formation of CSH phases enhances the R_d values of Sr in the mixture compared to the sum of the R_d values of the original mixture (quartz + portlandite). Moreover, the R_d value for Sr increases with time due to a continuous formation of CSH in the quartz -

portlandite mixtures. The results clearly demonstrate that Sr uptake by CSH phases is controlled by adsorption on the surface rather than co-precipitation of Sr with CSH.

Acknowledgements

The authors like to thank M. H. Bradbury for the many helpful discussions and Nagra for partial financial support

References

CRAWFORD, M.B. and SAVAGE, D. (1994): The Effects of Alkaline Plume Migration from a Cementitious Repository in Crystalline and Marl Host Rocks. Technical Report, WE/93/20C, British1 Geological Survey, Nottingham, UK.

CURTI, E. (1997): Co-precipitation of Radionuclides: Basic Concepts, Literature Review and first Applications. PSI Bericht, Nr. 97-10, Paul Scherrer Institut, Würenlingen und Villigen, Switzerland and Nagra Technical Report, NTB 97-08, Nagra, Wettingen, Switzerland.

EWART, F.T., GLASSER, F., GROVES, G., JAPPY, T., McCROHON, R., MOSELEY, P.T., RODGER, S., and RICHARDSON, I. (1990): Mechanisms of Sorption in the Near Field. UKDoE Report, DOE/RW/90/065.

KOMARNENI, S., ROY, R., and ROY, D.M. (1986): Pseudomorphism in Xonotlite and Tobermorite with Co^{2+} and Ni^{2+} exchange for Ca^{2+} at 25.C. Cem. Conc. Res. 16, 47 - 58.

KOMARNENI, S., BREVAL, E., ROY, D.M., and ROY, R. (1988): Reactions of some Calcium Silicates with Metal Cations. Cem. Conc. Res. 18, 204 - 220.

LAMEILLE, J.M., GOUTIERE, G., PETIT, J.L., and REGOURD, M. (1987): Retention of Cobalt, Caesium, and Strontium in the Hydrates of C_3S, C_3A, and Gypsum. J. Am. Ceram. Soc. 70, 604 - 614.

MARX, G., ALTENHEIM-HAESE, C., and BISCHOFF, H. (1995): Adsorption of Actinides on Cementitious Material under the Influence of Complexing Organics at various Temperatures. Proceedings of the Fifth International Conference on Radioactive Waste Management and Environmental Remediation, ICEM '95, Volume 2. Management of Low-Level Waste and Remediation of Contamined Sites

and Facilities, Berlin, Germany, S. Slate, R. Baker, and G. Benda (eds.): , The American Society of Mechanical Engineers.

O'DAY, P.A. (1992) Structure, Bonding, and Site Preference of Cobalt(II) Sorption Complexes on Kaolinite and Quartz from Solution and Spectroscopic Studies. Ph.D. Thesis, Stanford University, Stanford, USA.

SAVAGE, D., BATEMAN, K., HILL, P., HUGHES, C., MILODOWSKI, A., PEARCE, J., RAE, E., AND ROCHELLE, C. (1992): Rate and Mechanism of the Reaction of Silicates with Cement Pore Fluids. Applied Clay Science 7, 33 - 45.

TITS, J., BAEYENS, B., and BRADBURY, M.H. (1996): Sorption Measurements for Eu and Th on Calcite and a CSH-gel in the Absence and in the Presence of Na-gluconate. 4th international conference on nuclear and radiochemistry, NRC4, Volume 2, St. Malo, France, F. David and J. C. Krupa (eds.): Institut de Physique Nucléaire, Orsay, France.

In situ X-ray techniques and related developments in mineral surface analysis

R.A. Wogelius[1], M.L. Farquhar[2], and C.C. Tang[3]

[1]Department of Earth Sciences, University of Manchester, Oxford Road, Manchester M13 9PL, UK. Roy.Wogelius@man.ac.uk

[2]Department of Petroleum Engineering, Heriot-Watt University, Riccarton, Edinburgh EH14 4AS, UK. morag@pet.hw.ac.uk

[3]Daresbury Laboratory, Warrington, Cheshire WA4 4AD, UK. C.C.Tang@dl.ac.uk

One of the most rapidly growing research areas in the geosciences is mineral surface science. Specific mechanisms govern the kinetics of overall reactions and, therefore, to be able to predict reaction paths and reaction rates between mineral surfaces and aqueous fluids, detailed measurements must be completed which will give insight into how configurations of atoms adjust during reaction. Research has been impeded by the difficulties presented in analyzing these quasi-two-dimensional systems, but recent advances in analytical techniques are making it more convenient to gather data pertinent to mineral surface chemistry. In particular, the ability to perform analyses *in situ* (i.e. with the reactant fluid present) is a key advance. Synchrotron X-ray techniques, especially glancing incidence X-ray measurements of the reflected and diffusely scattered components of the beam, are particularly useful for describing the structural adjustments that occur during reaction even if the surface layer becomes amorphous. As in high-angle experiments, the glancing incidence beam can also be used to fluoresce elements present at the mineral surface (van der Hoogenhof and Ryan, 1993). Because the penetration depth of X-rays is a known function of incident angle, the fluorescence signal can therefore be used as a depth sensitive probe. (When the characteristic radiation is excited by X-rays, this is known as Total external reflection X-Ray Fluorescence or TXRF; an identical technique which uses protons to excite the target is referred to as Total external reflection Proton Induced X-ray Emission or TPIXE). TPIXE and TXRF allow extremely low concentrations of adsorbates to be depth profiled. Also, at a synchrotron the energy of the incident beam can be varied by the use of a monochromator. This allows X-ray Absorption Spectroscopy (XAS) to be performed as well. In the work presented here we will discuss the related measurements of reflectivity and diffuse scatter along with some TPIXE, XPS, and AFM analyses as applied to silicate minerals.

Oligoclase Feldspar Cation Loss- Case study in Reflectivity

A (001) surface of an oligoclase wafer was exposed to de-ionised water. While this reaction proceeded, reflectivity measurements were taken *in situ.* The altered layer was characterised in terms of its density, thickness, surface roughness, and the interfacial roughness of the buried interface between the altered layer and bulk feldspar. Although the error bars on some of the fitted parameters are relatively large, important information can unambiguously be extracted from them. The unreacted oligoclase surface had a

starting r.m.s. roughness of 6.1 Å (+/-0.35). Figure 1 shows the corrected experimental data with errors (vertical bars) and fit (smooth curve) for the sample after 30 minutes in de-ionised water. As shown, within 30 minutes of being in contact with de-ionised water a low density (79 % ρ oligoclase) layer approximately 32 Å (+/-11 Å) thick forms at the oligoclase-water interface. During this 30 min exposure time there has been no significant roughening of the solid-fluid interface. The best fit interfacial roughness between oligoclase and the altered layer is calculated to be high at 14.9 Å (9.8<roughness<29.0 Å). Note that without an altered layer in the simulation it is not possible to adequately fit the experimental data; the best fit without an altered layer is also shown in Figure 1 as the dashed line. This dashed curve corresponds to a simulation of the unreacted surface and is clearly different from the reacted surface.

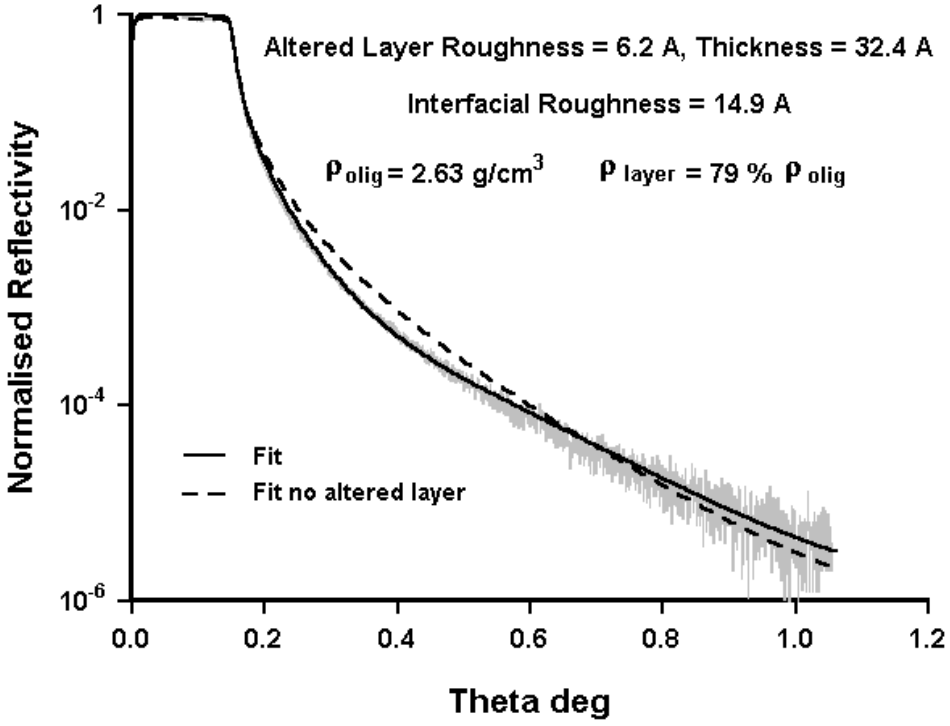

Figure 1. *In-situ* corrected experimental reflectivity data with errors for oligoclase (001) plane in contact with de-ionised water for 30 minutes. The best fit to the data is shown as a continuous line. Best fit without an altered layer is shown as the dashed line.

In order to verify the interpretation of the X-ray analyses, XPS analyses were completed on identically prepared (and reacted) oligoclase samples. The reacted sample showed clear depletion of Na in the near surface down to a depth between 25 and 30 Å. This phenomenon has been noted in many other studies, e.g. Casey et al. (1989). Average composition of the altered layer determined from the XPS results indicates that the density of that layer is 80 % (± 5) of oligoclase. These *ex situ* results are in excellent agreement with the reflectivity analysis, clearly showing the ability of X-ray reflectivity to follow such reactions *in situ*. (Full details are in Farquhar et al., 1999).

Forsteritic Olivine Surface Roughening- Diffuse Scatter Case Study

Two (010) Fo_{90} surfaces were reacted with pH 4 nitric acid, one for 10^4 seconds and another for 10^6 seconds. Surface roughness values as determined by X-ray reflectivity were 8.5 Å (+/- 0.5) for the 10^4 s sample vs. 19.0 Å (+/-1.5) for the 10^6 s sample. Along with the specular reflectivity measurement, measurement of the diffusely scattered portion of the beam allows a complete mathematical description of the surface topography to be constructed.

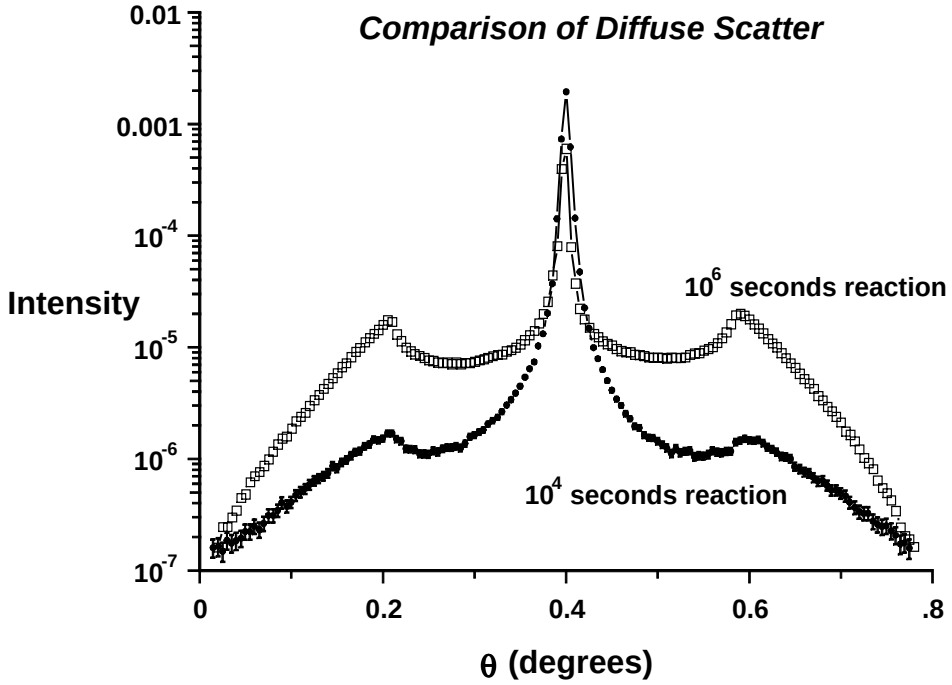

Figure 2. Comparison of the diffuse scatter component as measured by rocking curve scans for the 10^4 s (solid circles with error bars) and 10^6 s samples (open squares, symbol size equals error). The detector angle was held fixed at 0.8^o. Central peak is the specular reflectivity peak while the symmetric features with lower intensity peaks are the Yoneda wings. Locations of the Yoneda peaks correspond to the critical angle for the incident (0.21^o) and the scattered (0.8^o - 0.21^o = 0.59^o) beam.

Figure 2 shows the data for diffuse scatter (rocking curve) scans taken from each of these two samples. Error bars are clearly shown at the start of the 10^4 s sample scan (solid symbols) and the errors become equal to or smaller than the symbol size at the center of the figure (between the Yoneda peaks at 0.21^o and 0.59^o). Symbol size for the 10^6 s sample (open symbols) is approximately equal to the maximum error. Two clear developments should be noted. First of all, the specular peak in the sample reacted for 10^6 s (square symbols) has decreased in intensity by a factor of 5 (0.6 log units) relative to the 10^4 s sample. This is the result of the increase in surface roughness. Secondly, the intensity of the diffuse scatter out in the Yoneda wings has dramatically increased by over an order of magnitude as the reaction time increased. The shapes of these wings in the

rocking curve scans can be used to constrain the height-height correlation function for each of the samples. Simulation of the 10^4 s data resulted in the following values: correlation length (ξ) = 16 mm (+/- 6), fractal parameter (***h***)= 0.23 (+/- 0.02), and surface roughness (σ) = 7.8 Å (+/- 1). As seen in Figure 2, the diffuse component changes significantly after reaction for 10^6 s. Here, the model parameters are: ξ = 2750 Å (+/- 260) , ***h*** = 0.195 (+/- 0.03), and σ = 20.2 Å (+/- 1.5). Surface area changes can be calculated from these data in either a fractal or Euclidean manner. Euclidean calculations, using the robust change in ξ, give a 3% surface area increase. For comparison, a fractal analysis using the change in ***h*** (assuming that the errors were smaller and that the x-y plane is isotropic) gives the fractal dimension of the surface plane as: **D=3-*h*** (Turcotte, 1992). A 5.8 % increase in surface area, similar to the Euclidean result, is calculated by this approach. Knowledge about such subtle changes in surface topography, which are nearly impossible to resolve by standard techniques, will help us understand the changes in the rates of surface-controlled reactions as they proceed. (Full details are in Wogelius et al., 1999.)

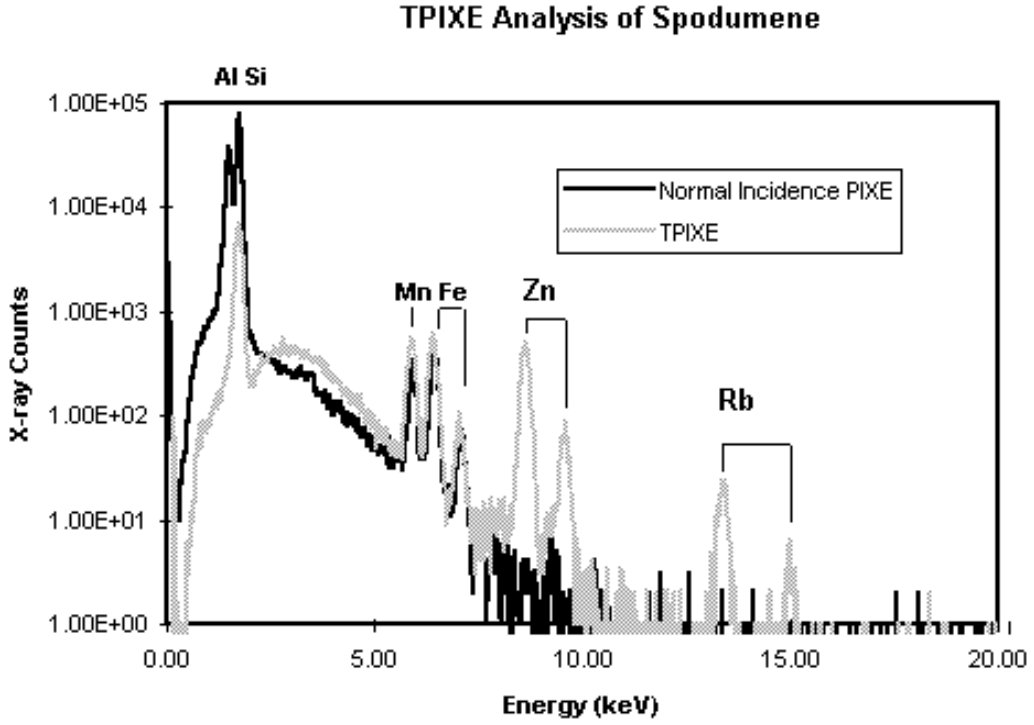

Figure 3 shows a comparison between normal incidence PIXE and glancing incidence TPIXE for the spodumene sample. The normal incidence measurement was completed without a Be filter on the detector and therefore characteristic X-radiation for Al and Si is much more intense. Adsorbed Zn at the mineral surface and the thin region where Rb has been exchanged for Li are clearly visible in the TPIXE analysis.

Cation uptake by Spodumene- Case Study in TXRF/TPIXE

A spodumene (010) sample was reacted with solutions spiked with first Zn and then Rb. Surface roughness as measured by reflectivity did not change during reaction, staying constant at 7.9 Å (+/-0.2). However, the uptake of both Zn and Rb by the sample surface was clearly shown by the appearance of characteristic peaks for each element in the TXRF spectra taken after exposure to each solution. This sample was re-analyzed within 7 days by the TPIXE method at the Oxford SPM unit. Figure 3 shows a comparison between normal incidence PIXE and glancing incidence TPIXE. Analysis time in each case was 15.1 minutes. Peak intensities for Mn and Fe, both trace elements present in the substrate, are similar in both analyses. However, the adsorbed Zn at the mineral surface and the thin region where Rb has been exchanged for Li are not detectable in the standard geometry but show up clearly via TPIXE. Further work to convert the X-ray intensity to absolute concentration is ongoing, however our preliminary estimate of the Zn concentration at the surface is 1 atom per 100 $Å^2$. The Rb concentration is also less than a monolayer. The Rb signal was below the limit of detection for XPS, indicating that glancing incidence chemical analysis may prove to be an extremely useful addition to our array of surface analysis techniques. AFM analysis of the reacted sample was also completed. AFM rms roughness values taken from various portions of the sample surface ranged from 5.50 to 8.54 X, in good agreement with the reflectivity results.

References

Casey W.H., Westrich H.R., Arnold G.W. and Banfield J.F. (1989) The surface chemistry of dissolving labradorite feldspar. *Geochim. Cosmochim. Acta*, **53**, 821-832.

Farquhar M.L., Wogelius R.A., and Tang C.C. (1999) *In situ* Synchrotron X-ray Reflectivity Study of the Oligoclase Feldspar Mineral-Fluid Interface. *Geochim. Cosmochim. Acta*, in press.

Turcotte D.L. (1992) *Fractals and Chaos in Geology and Geophysics.* Cambridge University Press.

van der Hoogenhof W.W. and Ryan T.W. (1993) Structural characterization of Au/Co multi-layers by X-ray diffraction, X-ray reflectivity, and glancing incidence X-ray fluorescence. *Journal of Magnetism and Magnetic Materials* **121**, 88-93.

Wogelius R.A., Farquhar M.L., Fraser D.G., Tang C.C. (1999) Structural evolution of the mineral surface during dissolution probed with synchrotron X-ray techniques. In: *Growth and dissolution in Geosystems*. Eds. B. Jamtveit and P. Meakin, in press.

Modelling Sorption of uranyl onto quartz and muscovite

T. Arnold, T. Zorn , G. Bernhard

Forschungszentrum Rossendorf e.V., Institute of Radiochemistry, Postfach 510119,
D-01314 Dresden, e-mail: T.Arnold@fz-rossendorf.de

Introduction

Quartz and muscovite are common rock forming minerals and present in many rocks such e.g granite. The prediction of the long term migration of uranium in the environment, especially in the vicinity of uranium mining sites and in the far field of proposed nuclear waste disposals is, among other parameters, related to the the mineralogical composition of the surrounding rocks. At present, surface complexation models provide the best concept to interprete sorption results. In this study surface complex formation constants for uranyl sorbing onto quartz and muscovite are determined by using batch sorption data, the Diffuse Double Layer Model, and the computer program FITEQL /1/.

Experimental

Batch sorption experiments with uranyl and the minerals quartz and muscovite were carried out under ambient pressure in the pH range from 3.5 to 9.5 in 0.1 M $NaClO_4$ using an uranium concentration of 1×10^{-6} M, a size fraction of 63-200 µm and a solid solution ratio of 0.5 g/40 mL.

Also, potentiometric titrations with quartz and muscovite were carried out under Nitrogen atmossphere under the same experimental conditions. The titrations were performed using CO_2 free NaOH and CO_2 free deionized water. The acidity constants for quartz and muscovite were calculated with the computer code FITEQL.

Results and Discussion

The point of zero charge of quartz is reported in the literature to range between pH 2.0 /2/ and pH 2.9 /3/. This indicates that the quartz surface in the pH range of our sorption experiments is negatively charged and QO^- surface species predominate. Therefore, only one acidity constant for the reaction $QO^- + H^+ = QOH$ is required. By using the titration data and FITEQL the acidity constant for quartz was determined to be log K = -7.43.
In contrast to quartz, the point of zero charge of muscovite is in the neutral range at about pH 6.6 /4/. This indicates that both positively and negatively charged surface species exist on the muscovite surface and thus two acidity constants were determined. Again, titration data and FITEQL were used to calculate these constants.

The obtained log K values for muscovite are listed below.

$$MO^- + H^+ = MOH \qquad \log K = -10.10$$

$$MOH_2^+ = MOH + H^+ \quad \log K = 7.79$$

Using these acidity constants together with the sorption data obtained in batch experiments and the computer code FITEQL, surface complex formation constants for uranyl sorbing onto quartz and muscovite were calculated.

For quarz two surface species were postulated. For the first one, $QOUO_2^+$, there are already some evidence from EXAFS analysis /5/ which indicate that uranyl is sorbing as a mononuclear bidentate surface complex. The equation for the first surface species is:

$$QOUO_2^+ + H^+ = QOH + UO_2^{2+}$$

The second uranium-quartz surface species, $QOUO_2OH$, was also modelled as a mononuclear bidentate surface complex.

$$QOUO_2OH + H^+ = QOH + UO_2OH^+$$

Based on the experimentally obtained sorption data, the following surface complex formation constants for uranyl sorbing onto the quartz surface were calculated with FITEQL. The value of WSOS/DF represents "weighted sum of squares divided by degrees of freedom" and is an indicator of the goodness of fit.

Tab. 1: Surface complex formation constants for uranyl sorbing onto quartz

Surface species	**Log K**	**WSOS/DF**
$QOUO_2^+$	5.87	0.056
$QOUO_2OH$	0.80	0.056

The fitted data together with the experimental sorption results are shown in Fig. 1. The sorption data for muscovite were also modelled using the same two surface species as for quartz..

$$MOUO_2^+ + H^+ = MOH + UO_2^{2+}$$

$$MOUO_2OH + H^+ = MOH + UO_2OH^+$$

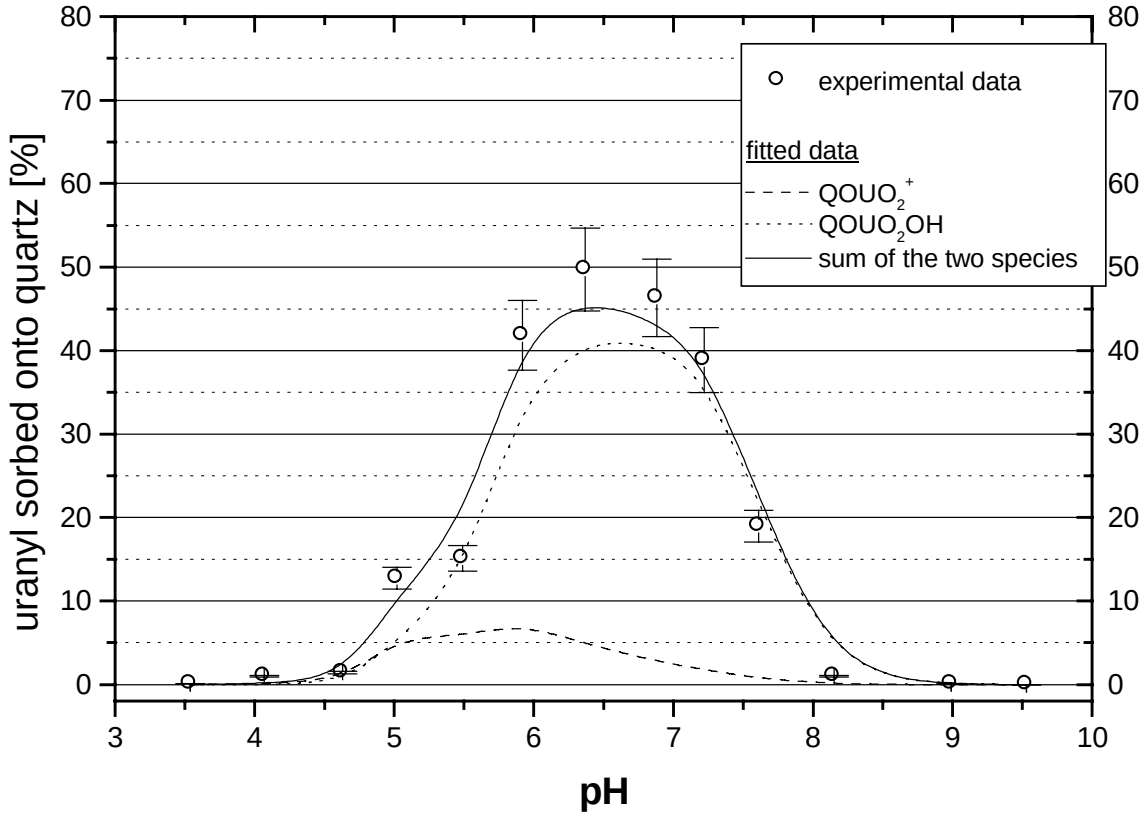

Fig. 1: Experimental and calculated sorption data of uranyl sorbed onto quartz, relative error of ± 5 % are included.

The appropriate surface complex formation constants are listed in Tab.2 and the experimental batch sorption data together with the calculated sorption data are shown in Fig. 2.

Tab. 2: Surface complex formation constants for uranyl sorbing onto muscovite

Surface species	**Log K**	**WSOS/DF**
$MOUO_2^+$	6.91	0.206
$MOUO_2OH$	-0.26	0.206

However, these postulated surface complexes on quartz and muscovite require further spectroscopic evidence. The verified surface complexes with the appropriate constants could then be included in the appropriate data enabling improved uranium related risk assesments.

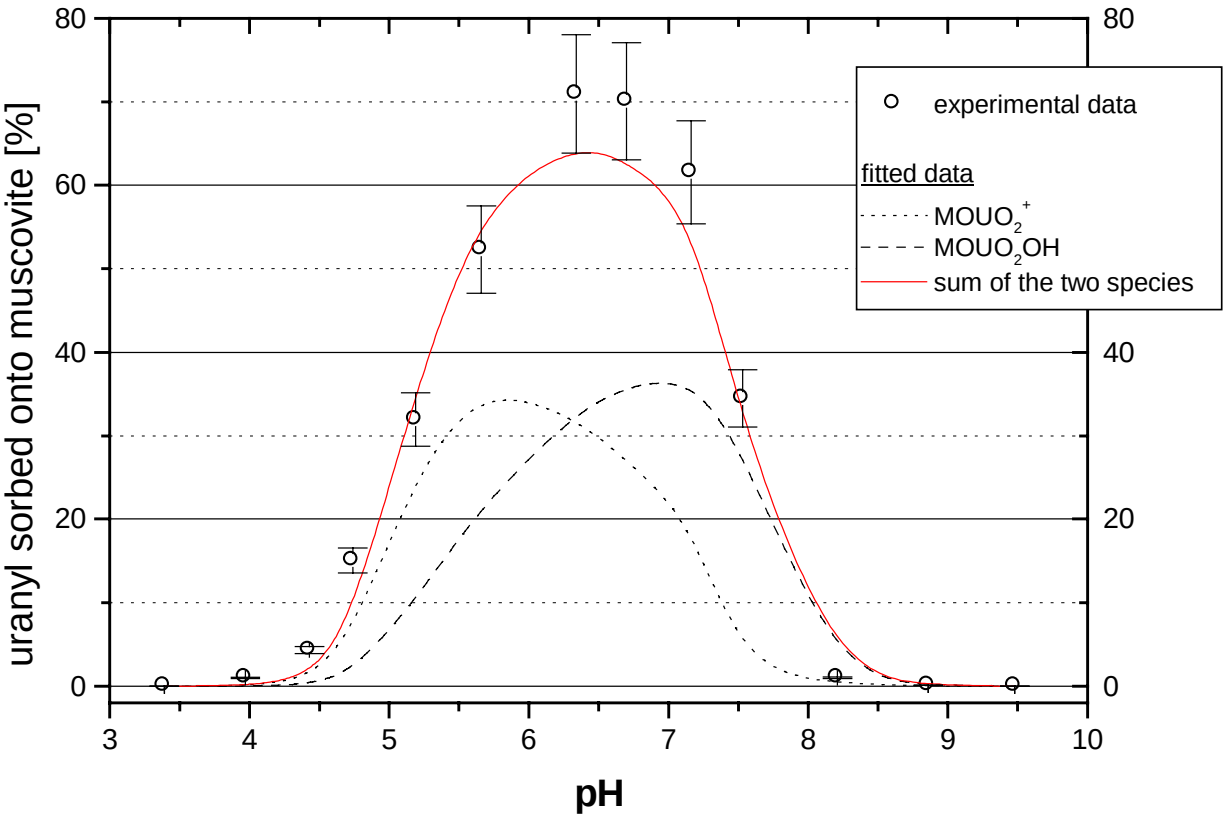

Fig. 2: Experimental and calculated sorption data of uranium sorbed onto muscovite, relative error of ± 5 % are included.

References

/1/ Herbelin, A. and Westall, J. (1996) FITEQL A Computer Program for Determination of Chemical Equilibrium Constants from Experimental Data, Version 3.2. Report 96-01, Department of Chemistry, Oregon State University, Corvallis, Oregon

/2/ Stumm, W. (1992) Chemistry of the solid-water interface. Wiley, New York.

/3/ Sposito, G. (1984) The surface chemistry of Soils. Oxford University Press, New York.

/4/ Sverjensky, D.A. (1994) Zero-point-of-charge prediction from crystal chemistry and solvation theory. Geochimica et Cosmochimica Acta 58, 3123-3129.

/5/ Reich, T., Moll, H., Arnold, T., Denecke, M.A., Hennig, C., Geipel, G., Bernhard, G., Nitsche, H., Allen, P.G., Bucher, J.J., Edelstein, N.M., and Shuh, D.K. (1998) An EXAFS study of uranium(VI) sorption onto silica gel and ferrihydrite. Journal of Electron Spectroscopy and Related Phenomena 96, 237-243.

Workshop programme

Thursday, March 25, 1999

12.30 **Lunch**

13.15 **Opening**

Andreas Bauer, Forschungszentrum Karlsruhe

13.30 **In situ X-ray techniques and related developments in mineral surface analysis**

Roy K. Wogelius, University of Manchester

14.15 **What controls mineral dissolution rates: Surface adsorption or ion exchange reactions ?**

Oleg Pokrovsky, University of Moscow

15.00 Coffee Break

16.00 **A general mechanism for the dissolution of multi oxide solids. Application to basaltic glass**

Eric Oelkers, Université Paul Sabatier, Toulouse

17.00 **Mechanism and affinities of glass alteration close to pseudo-equilibrium**

Bernd Grambow**,** Ecole des Mines de Nantes

18.00 Dinner

19.00 **Poster Session**

Friday, March 26, 1999

8.00 **Breakfast**

9.00 **Effects and catalysts/inhibitors, ionic strength and deviation from equilibrium: Separation of variables in practice and theory**

Jiwchar Ganor, Ben Gurion University of the Negev

10.00 **Nature of surface reactions versus the dissolution rates of alkali-feldspars**

Gilles Berger**,** Université Paul Sabatier, Toulouse

11.00 Coffee Break

11.30 **Kaolinite and smectite dissolution in alkaline solutions**

Andreas Bauer, Forschungszentrum Karlsruhe

12.30 Lunch

13.30 **A microscopic view of crystal growth mechanisms, kinetics and inhibition**

Dirk Bosbach**,** Universität Münster

14.30 **Heterogeneous nucleation and growth kinetics of clays on mineral substrates**

Kathryn L. Nagy**,** University of Colorado at Boulder

15.30 **Closing**

Poster Presentations

High-pH alteration of argillaceous rocks: An experimental and modeling study

M. Adler and U.K. Mäder

Analyses concerning the estimation of the release behaviour heaps of the former mining activities and uranium ore mining

K. Fischer-Appelt, J. Larue, G. Henze and J. Pinka

Polarization dependent XANES of uranium(VI) sorbed onto smectite

M.A. Denecke, A. Bauer, J.I. Kim and H. Moll

The interaction of monosilicic and polysilicic acid with solid surfaces

M. Dietzel

Experimental quantification of permeability change of the Fontainebleau sandstone during mineral dissolution

C.F. Jové, E.H. Oelkers and J. Schott

In-situ distribution of trace metals in a natural aquifer overlying the nuclear repository Morsleben, Germany

H. Geckeis, P. Vejmelka, D. Degering, C. Pohlmann, K. Gompper, J.-I. Kim

Long-term thermodynamic and kinetic study of mineral-soil solutions interactions in an acid brown soil

F. Gérard, J. G. Genon and J. Ranger

Mechanisms limiting the alteration kinetics of R7T7 nuclear glass

S. Gin, C. Jégou and É. Vernaz

Evaluation of the solid solution-aqueous solution equilibrium state for trace metals partitioned in the carbonate – porewater system of a natural sediment

D.A. Kulik and M. Kersten

Distribution of uranium(VI) on biotite surfaces

G. Mainka, T. Zorn, T. Arnold, G. Bernhard

Congruent dissolution of smectite in a flow-through system

V. Metz and J. Ganor

The chemical long-term behaviour of cement based materials in highly salinar solutions

Th. Meyer and H.-J. Herbert

Influence of humic and fulvic acid on the sorption behaviour of Eu(III) on natural hematite

Th. Rabung, H. Geckeis, J.-I. Kim, H.P.Beck

Modification of the sorption behavior of bentonite by hexadecylpyridinium

B. Riebe, S. Dultz, J. Bors

A comparison of different phosphonate growth inhibitors for sulfates: AFM study on barite and celestite

P. Risthaus, D. Bosbach, P.V. Coveney and P. Andrew

Kinetics, steady state or equilibrium ? Reversibility or irreversibility in chemical weathering rate modelling

H. Sverdrup and J. Holmqvist

Experimental investigation of the effect of high pH solutions on the Opalinus shale and the Hammerschmiede smectite

H. Taubald and A. Bauer

Sr uptake during CSH phase formation: Adsorption versus co-precipitation

J. Tits, E. Wieland, C. Poinssot and J. P. Dobler

Modeling the sorption behavior of uranyl onto quartz and albite

T. Zorn, T. Arnold, G. Bernhard